MODIFICATION TO DARCY MODEL FOR HIGH PRESSURE AND HIGH VELOCITY APPLICATIONS AND ASSOCIATED MIXED FINITE ELEMENT FORMULATIONS

A Thesis

Presented to

the Faculty of the Department of Civil and Environmental Engineering

University of Houston

In Partial Fulfillment

of the Requirements for the Degree

Master of Science

in Civil Engineering

by

Justin Chang

May 2013

MODIFICATION TO DARCY MODEL FOR HIGH PRESSURE AND HIGH VELOCITY APPLICATIONS AND ASSOCIATED MIXED FINITE ELEMENT FORMULATIONS

Justin Chang

Approved:

Chair of the Committee
Kalyana Babu Nakshatrala, Assistant Professor
Dept. of Civil & Environmental Engineering

Committee Members:

Kaspar Willam, Distinguished Professor
Dept. of Civil & Environmental Engineering

Keh-Han Wang, Professor
Dept. of Civil & Environmental Engineering

Ralph Metcalfe, Professor
Dept. of Mechanical Engineering

Suresh K. Khator, Associate Dean
Cullen College of Engineering

Kaspar Willam, Professor and Chair
Dept. of Civil and Environmental Engineering

Acknowledgements

First and foremost, I would like to thank my advisor, Dr. Kalyana Babu Nakshatrala, for his guidance throughout my graduate studies here at the University of Houston. Your commitment to working with and teaching your graduate students is unmatched and all of us here at the Computational and Applied Mechanics Laboratory truly appreciate your dedication to furthering our academic careers.

I would also like to thank the University of Houston for providing wonderful facilities and resources. Without this institution, I would not have been able to conduct any of my computer simulations. I also want to thank my fellow office mate, Maruti Mudunuru, for his mentorship and expertise in the field of Computational Mechanics; you have helped me greatly with both my research and course work.

Many thanks go out to my mom, dad, and sister. Thank you for the words of encouragement and prayers. I love you all, and without y'all's unrelenting and unconditional love, I would not be where I am today. And finally, I want to thank my Lord and savior Jesus Christ, because without Him, I am nothing.

MODIFICATION TO DARCY MODEL FOR HIGH PRESSURE AND HIGH VELOCITY APPLICATIONS AND ASSOCIATED MIXED FINITE ELEMENT FORMULATIONS

An Abstract

of a

Thesis

Presented to

the Faculty of the Department of Civil and Environmental Engineering

University of Houston

In Partial Fulfillment

of the Requirements for the Degree

Master of Science

in Civil Engineering

by

Justin Chang

May 2013

Abstract

The Darcy model is based on a plethora of assumptions. One of the most important assumptions is that the Darcy model assumes the drag coefficient to be constant. However, there is irrefutable experimental evidence that viscosities of organic liquids and carbon-dioxide depend on the pressure. Experiments have also shown that the drag varies nonlinearly with respect to the velocity at high flow rates. In important technological applications like enhanced oil recovery and geological carbon-dioxide sequestration, one encounters both high pressures and high flow rates. It should be emphasized that flow characteristics and pressure variation under varying drag are both quantitatively and qualitatively different from that of constant drag. Motivated by experimental evidence, we consider the drag coefficient to depend on both the pressure and velocity. We consider two major modifications to the Darcy model based on the Barus formula and Forchheimer approximation. The proposed modifications to the Darcy model result in nonlinear partial differential equations, which are not amenable to analytical solutions. To this end, we present mixed finite element formulations based on least-squares formalism and variational multiscale formalism for the resulting governing equations. The proposed modifications to the Darcy model and its associated finite element formulations are used to solve realistic problems with relevance to enhanced oil recovery.

Table of Contents

Acknowledgments . . . . . **iv**

Abstract . . . . . **vi**

Table of Contents . . . . . **vii**

List of Figures . . . . . **ix**

List of Tables . . . . . **xii**

Nomenclature . . . . . **ix**

Chapter 1. Introduction & Motivation **1**

1.1 Limitations of Darcy model, and its generalizations 2

1.2 Mixed formulations 3

1.2.1 Variational multi-scale formalism 4

1.2.2 Least-squares formalism 4

1.2.3 Local mass conservation 5

1.3 Enhanced oil recovery 5

1.4 Main contributions of this thesis research 6

1.5 Organization of the thesis 7

Chapter 2. Governing equations: Darcy model and its generalization **8**

2.1 Boundary conditions and well-posedness 9

2.2 Darcy model, experimental evidence, and its generalization 10

2.2.1 Pressure-dependent viscosity 10

2.2.2 High velocity flows and inertial effects 11

2.2.3 Proposed model: Modified Darcy-Forchheimer model 13

Chapter 3. Mixed weak formulations **16**

3.1 A mixed formulation based on least-squares formalism 18

3.2 A mixed formulation based on variational multi-scale formalism 20

Chapter 4. Finite element framework and implementation **22**

4.1 Discretization, Reference elements, and Isoparametric Mapping 22
4.2 Linearized finite element equations 25
4.2.1 Element stiffness matrices and forcing vectors 27
4.3 User input and FEA driver 28
Chapter 5. Numerical benchmark tests 31
5.1 Dimensionless form of equations 31
5.2 One-dimensional problem 32
5.3 Numerical h-convergence 34
5.4 Quarter five-spot problem 42
5.4.1 Least-squares weighting 45
5.4.2 Comparison of beta coefficients, pressure profiles, and linearization types 45
5.4.3 Modified Darcy-Forchheimer numerical results 49
Chapter 6. Enhanced oil recovery applications 52
6.1 Oil reservoir problem 52
6.1.1 Pressure contours 54
6.1.2 Flow rates and local mass balance errors 57
6.2 Multilayer reservoir problem 60
6.3 Flow in a porous media with staggered impervious zones 65
Chapter 7. Concluding remarks & Future work 70
Appendix A. Element-level finite element matrices and vectors 72
A.1 Under least-squares formulation 72
A.2 Under variational multi-scale formulation 74
References 75

List of Figures

Figure 1.1 Simplified depiction of flow through porous media. 1

Figure 1.2 A pictorial description of enhanced oil recovery 6

Figure 4.1 Element types and their respective local node numbering. Clockwise from top left: four-node quadrilateral element (Q4), three-node triangle element (T3), six-node triangle element (T6), and nine-node quadrilateral element (Q9) 23

Figure 4.2 A flowchart of finite element code development for Darcy-type models . 29

Figure 5.1 One dimensional problem: a pictorial description 32

Figure 5.2 One-dimensional problem: pressure profile 34

Figure 5.3 Typical meetings used: a quadrilateral (left) and triangular (right) mesh 35

Figure 5.4 Numerical h-convergence: analytical solutions 35

Figure 5.5 Numerical h-convergence: error slopes for the Darcy (D) model 36

Figure 5.6 Numerical h-convergence: error slopes for the modified Barus (MB) model 37

Figure 5.7 Numerical h-convergence: error slopes for the modified linear (ML) model 38

Figure 5.8 Numerical h-convergence: error slopes for the Darcy-Forchheimer (F) model 39

Figure 5.9 Numerical h-convergence: error slopes for the modified Darcy-Forchheimer Barus (MBF) model 40

Figure 5.10 Numerical h-convergence: error slopes for the modified Darcy-Forchheimer linear (MLF) model 41

Figure 5.11 Quarter five-spot problem: A pictorial description 42

Figure 5.12 Quarter five-spot problem: Q4 solutions for Darcy model 43

Figure 5.13 Quarter five-spot problem: Q9 solutions for Darcy model 44

Figure 5.14 Quarter five-spot problem: pressure profile vs various β_{B} and β_{F} 46

Figure 5.15 Quarter five-spot problem: pressure contours using LS formalism 50

Figure 5.16 Quarter five-spot problem: pressure contours using VMS formalism . . . 51

Figure 6.1 Oil reservoir problem. Top figure is the pictorial description, bottom figure is the idealized computational domain with appropriate boundary conditions 52
Figure 6.2 Oil reservoir problem: qualitative velocity vector field 53
Figure 6.3 Oil reservoir problem: pressure contours using LS formalism 54
Figure 6.4 Oil reservoir problem: pressure contours using VMS formalism 55
Figure 6.5 Oil reservoir problem: comparison of pressure profiles at $y = 1$ 56
Figure 6.6 Oil reservoir problem: comparison of injection pressures vs. flow rates . 57
Figure 6.7 Oil reservoir problem: ratios of local mass balance error over total predicted flux using LS formalism 58
Figure 6.8 Oil reservoir problem: ratios of local mass balance error over total predicted flux using VMS formalism. 59
Figure 6.9 Layered reservoir problem: A pictorial description. 60
Figure 6.10 Layered reservoir problem: qualitative velocity vector field 60
Figure 6.11 Layered reservoir problem: pressure contours using LS formalism 61
Figure 6.12 Layered reservoir problem: pressure contours using VMS formalism . . . 62
Figure 6.13 Layered reservoir problem: ratios of local mass balance error over total predicted flux using LS formalism 63
Figure 6.14 Layered reservoir problem: ratios of local mass balance error over total predicted flux using VMS formalism 64
Figure 6.15 Staggered impervious zones problem: a pictorial description 65
Figure 6.16 Staggered impervious zones problem: qualitative velocity vector field . . 65
Figure 6.17 Staggered impervious zones problem: pressure contours using LS formalism 66
Figure 6.18 Staggered impervious zones problem: pressure contours using VMS formalism 67
Figure 6.19 Staggered impervious zones problem: ratios of local mass balance error over total predicted flux using LS formalism 68

Figure 6.20 Staggered impervious zones problem: ratios of local mass balance error over total predicted flux using VMS formalism 69

List of Tables

Table 5.1 User-defined inputs for the one-dimensional problem 33

Table 5.2 User-defined inputs for the numerical h-convergence problem 38

Table 5.3 Numerical h-convergence slopes for various Darcy models using LS formalism 40

Table 5.4 Numerical h-convergence slopes for various Darcy models using VMS formalism 41

Table 5.5 User-defined inputs for the quarter five-spot problem: Darcy model . . . 43

Table 5.6 Quarter five-spot problem: injection pressure comparison for different LS weightings 45

Table 5.7 Quarter five-spot problem: Picard vs. consistent linearization iteration counts for modified Barus model with $\bar{\beta}_{\mathrm{B}} = 0.6$. The top table corresponds with LS formalism, and the bottom table corresponds with VMS formalism. Q9 elements are used 47

Table 5.8 Quarter five-spot problem: iterations needed vs. $\bar{\beta}$ for Picard ($\vartheta = 0$) and consistent ($\vartheta = 1$) linearization 48

Table 5.9 User-defined inputs for the quarter five-spot problem: all Darcy models . 49

Table 6.1 User-defined inputs for the oil reservoir problem 53

Table 6.2 User-defined inputs for the layered reservoir problem 61

Table 6.3 Layered reservoir problem: flow rates for LS and VMS formalism at $\bar{p}_{\mathrm{enh}} = 1000$ 63

Table 6.4 User-defined inputs for the staggered impervious zones problem 66

Table 6.5 Staggered impervious zones problem: flow rates for LS and VMS formalism at $\bar{p}_{\mathrm{enh}} = 500$ 68

Nomenclature

The following key symbols are used:

α	=	drag coefficient;
β_{B}	=	Barus coefficient;
β_{F}	=	Forchheimer coefficient;
Γ	=	boundary;
μ	=	dynamic viscosity;
Ω	=	domain;
Π	=	minimization functional;
ρ	=	density;
ϑ	=	user-defined parameter for linearization type;
ξ	=	rates of dissipation;
$\boldsymbol{\zeta}$	=	element spatial coordinates;
$\mathbf{A}$	=	least-squares weighting;
$\mathbf{b}$	=	specific body force;
$\mathbf{B}$	=	gradient transformation matrix;
D	=	original Darcy model;
$\mathcal{D}$	=	linearization terms for trial functions;
$\mathbf{DN}$	=	derivative of shape functions;
$\mathbf{f}$	=	forcing vector;
F	=	Darcy-Forchheimer model;
g	=	gravitational constant;
$\mathcal{G}$	=	linearization terms for test functions;
h-size	=	element size;
(i)	=	current iteration number;
$\mathbf{I}$	=	identity matrix;
$\mathbf{J}$	=	Jacobian matrix;
k	=	permeability;

$\mathbf{K}$	=	stiffness matrix;
LS	=	least-squares formalism;
MB	=	modified Darcy Barus model;
MBF	=	modified Darcy-Forchheimer Barus model;
ML	=	modified Darcy linear model;
MLF	=	modified Darcy-Forchheimer linear model;
$\hat{\mathbf{n}}$	=	unit normal vector;
$\mathbf{N}$	=	row vector of shape functions;
nd	=	number of spatial dimensions;
$Nele$	=	total number of elements;
$NumNodes$	=	total number of nodes;
p	=	pressure;
$\mathcal{P}$	=	function space for pressure trial functions;
p-refinement	=	study of element order;
q	=	trial function for pressure;
$\mathcal{Q}$	=	function space for pressure test functions;
$\mathbf{r}$	=	residuals;
$\mathbf{u}$	=	vector of unknowns;
$\mathbf{v}$	=	darcy velocity;
$\mathcal{V}$	=	function space for velocity trial functions;
VMS	=	variational multi-scale formalism;
$\mathcal{W}$	=	function space for velocity test functions;
$\mathbf{w}$	=	trial function for velocity;
$\mathbf{x}$	=	global spatial coordinates;

Chapter 1. Introduction & Motivation

In 1856, Henry Darcy proposed a simple model for the flow of an incompressible fluid in rigid porous media which states that the (Darcy) velocity is linearly proportional to the gradient of the pressure [1]. He obtained the model empirically based on the experiments on the flow of water in sand beds. Darcy's equation has been used in diverse fields (e.g., civil engineering, petroleum engineering, polymer engineering), and in various technological applications like designing filters, enhanced oil recovery, and geological carbon-dioxide sequestration.

Let $\mathbf{v}$, ∇p, μ, k, and α denote fluid velocity, pressure gradient, viscosity, permeability, and drag coefficient respectively. Darcy's equation can be written as follows:

$$\mathbf{v} \propto -\alpha^{-1} \nabla p, \tag{1.1a}$$

$$\alpha = \frac{\mu}{k}. \tag{1.1b}$$

In Figure 1.1, a fluid of velocity $\mathbf{v}$ flows through a medium of high porosity. The connectivity of pores pertains to the permeability k of the medium. Consider a reservoir sitting on top of a porous ground. There is no velocity at the water surface (point A) but at point B, there will be non-zero velocity due to the pressure gradient (induced by hydrostatic forces) and drag. Equation (1.1) is essentially founded on empirical evidence and cannot be derived analytically by performing a momentum balance on a small element of the porous medium. In recent years however, it has been shown that Darcy's model can be achieved

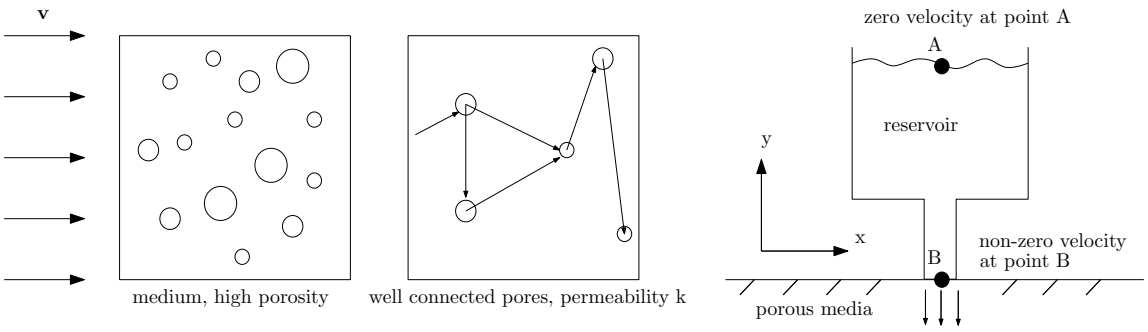

Figure 1.1: Simplified depiction of flow through porous media.

numerically in two possible ways [2]. One method is applying the volume averaging theory on the Navier-Stokes equation, and the other is using mixture theory (also known as the theory of interacting continua). The resulting constitutive model can then be discretized and used to obtain numerical solutions for problems related to heterogeneous flow through porous media.

1.1 LIMITATIONS OF DARCY MODEL, AND ITS GENERALIZATIONS

It is important to note that the Darcy equation is simply an approximation of the balance of linear momentum in the context of theory of interacting continua. Also, it merely predicts flux but cannot predict stresses in solids, so this model cannot be used on deformable solids. Some key assumptions include:

- There is no mass production of individual constituents (i.e., there are no chemical reactions).
- The porous solid is assumed to be rigid. Thus, the balance laws for the solid are trivially satisfied. In particular, the stresses in the solid are what they need to be to ensure that the balance of linear momentum is met.
- The fluid is assumed to be viscous, steady, homogeneous and incompressible.
- The velocity and its gradient are assumed to be small so that the inertial effects can be ignored.
- The partial stress in the fluid is that for an Euler fluid. That is, there is no dissipation of energy between fluid layers.
- The only interaction force is at the fluid and pore boundaries.

For more details, see reference [3, Introduction]. While several generalizations of the standard Darcy model have been proposed in the literature, none of these studies addressed the study undertaken in this thesis research. In particular, the prior studies did not address the combined effect of pressure-dependent viscosity and the inertial effects.

According to Darcy's model, the discharge flux is a function of drag coefficient (which is equal to viscosity over permeability) and pressure gradient. The problem is that the drag coefficient is independent of pressure and velocity, thus assuming drag coefficient to be constant. Experimental studies have shown that the drag coefficient is not constant and varies with pressure and/or velocity. Therefore, Darcy's model as it is may not give us accurate results of flow because it does not take into account pressure and velocity dependence - huge setbacks such as overly estimated discharge fluxes or inaccurate pressure contours may arise if used inappropriately. In order to address this issue, modifications to Darcy's model or more specifically the drag coefficient have been proposed; some well known models include the Forchheimer and Brinkman equations. It will soon be shown that the various modifications to Darcy's model affect the relationship between pressure and velocity both quantitatively and qualitatively.

1.2 MIXED FORMULATIONS

In general, there are two types of finite element methods (FEM): primal (or single-field) and mixed formulations. In a primal formulation, the problem is written in terms of one variable. For example, the Poisson's equation is a primal formulation since it is expressed in terms of some scalar quantity. Darcy's model can also be written in primal formulation if only the pressure term is considered. With the governing equations, one can employ any of the standard numerical methods (for example, the Galerkin finite element formulation) to solve the unknown pressure. The resulting pressure field is then inserted back into the original governing equation and used to solve for the velocity field. However, for low-order finite elements the velocity is poorly approximated because the gradient of the pressure is needed to calculate the velocity. In many situations. such as enhanced oil recovery, velocity is of primary interest so it is important that a numerical formulation yields accurate solutions for any variable of interest. Single-field formulations also do not possess local mass conservation property with respect to the computational grid.

On the other hand, mixed formulations for Darcy's model will take into account both pressure and velocity. This method minimizes the drawbacks of single-field formulations and

is widely used in many numerical simulations. However, it is well known that care should be taken when working with mixed formulations. In order to get stable results, a mixed formulation should either satisfy or circumvent the Ladyzhenskaya-Babuška-Brezzi (LBB) stability condition. More on this can be found in [4]. Several studies as shown in references [5, 6, 7, 8, 9] have proposed various stabilized formulations that provide accurate solutions of Darcy's model through porous media, but this thesis focuses on two formulations: the variational multi-scale (VMS) and least-squares (LS) formalisms.

1.2.1 Variational multi-scale formalism

One of the major finite element groups commonly used is the Galerkin method. This method is based on the weighted residual where suitably chosen test functions are formed for the governing partial differential equations. It is applicable for equations with self adjoint and positive definite operators, but convection dominated flow problems like the Darcy model are of first order thus non-self-adjoint. The consequences include oscillatory and unstable solutions and poor approximation of its derivatives. Consequently neither the Galerkin method nor it's mixed formulation are able to achieve satisfactory results, so various modifications have been proposed in literature. Masud and Hughes [10] have developed a new stabilized mixed finite element formulation known as the VMS formalism which modifies the Galerkin method. In their formulation, the unknown functions are decomposed into coarse and fine scales. The individual terms are then evaluated and substituted, resulting in the addition of stabilization terms (which are based on the residual of the Darcy model). Though this formalism provides amenable pressure and velocity solutions, a subsequent study in [11] has extended the formulation by introducing mesh dependent parameters, and the new numerical solutions have proven to be more accurate. The newer formalism will be used in this thesis' numerical experiments.

1.2.2 Least-squares formalism

The LS finite element method (LSFEM) is based on the minimization of the residuals in a least-squares sense. Its formulation will alway leads to a symmetric positive definite system of algebraic equations, even for non-self-adjoint systems. Unlike the Galerkin method, the

LSFEM has been shown to provide greater accuracy for the derivatives of primal variables and retains all of the properties and advantages of the Rayleigh-Ritz Method in that regions and boundary conditions are easy to manage, the conformity of finite element spaces is sufficient to guarantee stability, and all variables can use a single type of finite element space (see reference [12] for more details). Reddy [13] and other researchers have pointed out through p-refinement studies (i.e., the study of finite element order) that the LSFEM will provide even more accurate results the higher the order used, so comparisons between linear and quadratic elements will be made. For more on the background and derivation of the LSFEM, see reference [14].

1.2.3 Local mass conservation

A draw back to both the VMS and LS formalisms is that neither possess local mass conservation (it should be noted that while it is possible to achieve local mass conservation for the LS formalism, one would no longer be able to attain continuous nodal quantities. See reference [15] for further discussion on this topic). While several independent studies [16, 17, 18] have successfully developed conservative FEM for flow through porous media problems, none of them have been extended to modifications of Darcy's model. Furthermore, in reference [19] the VMS formulation is compared with the locally mass conservative Raviart-Thomas method, and both methods provide similar results for problems related to enhanced oil recovery. This thesis will focus on comparing the VMS with the LS generated solutions. Coupling diffusion equations with Darcy models will place a greater importance on local mass conservation so part of our future work will be to incorporate local mass conservation into our derivations

1.3 ENHANCED OIL RECOVERY

Over the years people have used Darcy's equation beyond its range of applicability. One example of misuse is in modeling enhanced oil recovery (EOR) applications. As illustrated in Figure 1.2 (picture taken from https://www.llnl.gov/str/November01/Kirkendall.html), carbon-dioxide gas is injected into the ground through injection wells. The gases create a

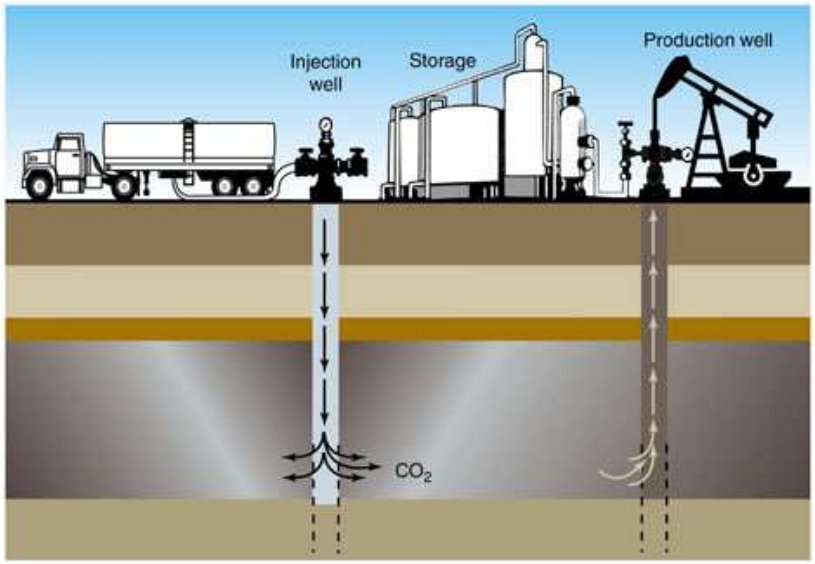

Figure 1.2: A pictorial description of enhanced oil recovery

pressure build up in the ground (i.e., the porous media) and pushes the fluid (i.e., raw oil) out through the production wells. High pressures ranging from $10-100$ MPa are employed, and such high pressures can lead to inaccurate flow estimates or pressure contours if the original Darcy model is used. Oil reservoir simulations are tricky by nature because of the possibility of having varying permeability within layers, impervious zones, non-rigid rock and soil formations, and pockets of natural gases. Seismic imaging and field experimentation may not always return the most accurate data so one must be extremely cautious when providing parameters to run numerical models. Using the right Darcy modification(s) allows one to predict more accurate production rates, help industries determine where to allocate their resources, and prevent environmental damage from unintended cracking in the subsurface.

1.4 MAIN CONTRIBUTIONS OF THIS THESIS RESEARCH

Some of the main contributions of this research are as follows:

1. To consider a generalization of the Darcy model by taking into account both the dependence of viscosity on the pressure and the dependence of drag on the velocity. The classical Darcy-Forchheimer and the modified Darcy model considered in reference [3] will be special cases of the generalized model considered in this paper. The generalization is referred to as modified Darcy-Forchheimer.

2. To develop a linearized LS formulation for modified Darcy-Forchheimer model and study the effect of weighting on the convergence and accuracy of the solutions.

3. To extend the VMS formulation to modified Darcy-Forchheimer model.

4. To compare the numerical performance of variational multiscale mixed formulation and least-squares-based mixed formulations.

5. To document the local mass balance error in both the formalisms.

6. To discuss the implications and applicability of these modified models in numerical simulations of enhanced oil recovery. It will also be show that the pressure profiles of Darcy-Forchheimer are qualitatively and quantitatively different from that of a modification of Darcy model that takes in to account the dependence of viscosity on the pressure.

1.5 ORGANIZATION OF THE THESIS

The remainder of the thesis is organized as follows. In Chapter 2 modifications to Darcy's model using Barus, linear, and Forchheimer terms and their respective equations governing the flow of an incompressible fluid in rigid porous media are presented. In Chapter 3, derivations of mixed finite element formulations based on LS and VMS formalisms are presented. In Chapter 4, the implementation of the FEM unique to this thesis is discussed. In Chapter 5, several representative test problems are solved to show the performance of the proposed LS and VMS formulation and to illustrate the predictive capabilities of modified Darcy-Forchheimer equations. In Chapter 6 some EOR applications are simulated. and solutions from the various models and formalisms are compared. Conclusions are drawn in Chapter 7. Derivations of the finite element matrices and vectors are listed in the appendix.

Chapter 2. Governing equations: Darcy model and its generalization

Let $\Omega \subset \mathbb{R}^{nd}$ be an open and bounded set, where "nd" denotes the number of spatial dimensions. Let $\partial\Omega := \text{cl}(\Omega) - \Omega$ be the boundary (where $\text{cl}(\Omega)$ is the set closure of Ω), which is assumed to be piecewise smooth. A spatial point in $\text{cl}(\Omega)$ is denoted by $\mathbf{x}$. The gradient and divergence operators with respect to $\mathbf{x}$ are, respectively, denoted by grad$[\cdot]$ and div$[\cdot]$. Let $\mathbf{v} : \Omega \to \mathbb{R}^{nd}$ denote the velocity vector field, and $p : \Omega \to \mathbb{R}$ denote the pressure field. The boundary is divided into two parts, denoted by Γ^v and Γ^p, such that $\Gamma^v \cap \Gamma^p = \emptyset$ and $\Gamma^v \cup \Gamma^p = \partial\Omega$. Γ^v is the part of the boundary on which the normal component of the velocity is prescribed, and Γ^p is part of the boundary on which the pressure is prescribed.

We now consider the flow of an incompressible fluid through rigid porous media based on modifications to the standard Darcy model. The governing equations are written as follows:

$$\alpha(\mathbf{v}, p, \mathbf{x})\mathbf{v}(\mathbf{x}) + \text{grad}[p(\mathbf{x})] = \rho\mathbf{b}(\mathbf{x}) \quad \text{in } \Omega, \tag{2.1a}$$

$$\text{div}[\mathbf{v}(\mathbf{x})] = 0 \quad \text{in } \Omega, \tag{2.1b}$$

$$\mathbf{v}(\mathbf{x}) \cdot \hat{\mathbf{n}}(\mathbf{x}) = v_n(\mathbf{x}) \quad \text{on } \Gamma^v, \tag{2.1c}$$

$$p(\mathbf{x}) = p_0(\mathbf{x}) \quad \text{on } \Gamma^p, \tag{2.1d}$$

where α is the drag coefficient (which can depend on the velocity and pressure, and can spatially vary), $v_n(\mathbf{x})$ is the prescribed normal component of the velocity, $p_0(\mathbf{x})$ is the prescribed pressure, ρ is the density of the fluid, $\mathbf{b}(\mathbf{x})$ is the specific body force, and $\hat{\mathbf{n}}(\mathbf{x})$ is the unit outward normal vector to $\partial\Omega$. It can be shown that equation (2.1a) is an approximation to the balance of linear momentum under the framework offered by the theory of interacting continua (e.g., see reference [3, Introduction]). A more thorough discussion on the theory of interacting continua can be found in the several appendices of reference [20], Atkin and Craine [21], and Bowen [22].

2.1 BOUNDARY CONDITIONS AND WELL-POSEDNESS

This section now discusses the well-posedness of the aforementioned boundary value problem in the sense of Hadamard [23]. If $\Gamma^v = \partial\Omega$ (i.e., the normal component of the velocity is prescribed on the entire boundary), one has to meet the following compatibility condition for well-posedness:

$$\int_{\Gamma^v=\partial\Omega} v_n(\mathbf{x})\, \mathrm{d}\Gamma = 0, \tag{2.2}$$

which is a direct consequence of the divergence theorem. To wit,

$$0 = \int_\Omega \mathrm{div}[\mathbf{v}(\mathbf{x})]\, \mathrm{d}\Omega = \int_{\partial\Omega} \mathbf{v}(\mathbf{x}) \cdot \hat{\mathbf{n}}(\mathbf{x})\, \mathrm{d}\Gamma = \int_{\partial\Omega} v_n(\mathrm{x})\, \mathrm{d}\Gamma. \tag{2.3}$$

Moreover, if $\Gamma^p = \emptyset$ (i.e., $\partial\Omega = \Gamma^v$), for uniqueness of the solution, one needs to augment the above equations (2.1a)–(2.1d) with an additional condition. Otherwise, one cannot find the pressure uniquely. In the Mathematics literature, the uniqueness is typically achieved by meeting the condition

$$\int_\Omega p(\mathbf{x})\, \mathrm{d}\Omega = 0, \tag{2.4}$$

which basically fixes the datum for the pressure. However, this approach is seldom used in a computational setting as it is difficult to enforce the above condition numerically. An alternative is to fix the datum for the pressure by prescribing the pressure at a point, which is commonly employed in various computational settings and is also employed in this thesis research.

Remark 1. *It should be noted that the no-slip boundary condition is not compatible with the Darcy model and the generalization that is considered in this thesis research. A simple mathematical explanation can be provided by noting that the inclusion of no-slip boundary condition (in addition to the no-penetration boundary condition) will make the boundary value problem over-determined. Also, it is noteworthy that the governing equations based on Darcy model are first-order in terms of* $\mathbf{v}(\mathbf{x})$ *and* $p(\mathbf{x})$.

2.2 DARCY MODEL, EXPERIMENTAL EVIDENCE, AND ITS GENERALIZATION

The Darcy model assumes that the drag coefficient is independent of the pressure and velocity. In addition, the Darcy model assumes the drag coefficient to be of the form

$$\alpha = \frac{\mu}{k}, \tag{2.5}$$

where μ is the coefficient of viscosity of the fluid, and k is the coefficient of permeability. From the above discussion it is evident that Darcy model cannot be employed for situations in which the viscosity depends on the pressure, permeability depends on the (pore) pressure, or drag does not depend linearly on the velocity of the fluid (i.e., the drag coefficient depends on the velocity). Several experiments have shown unequivocally that these three situations occur in nature, which will now be discussed.

2.2.1 Pressure-dependent viscosity

Bridgman [24] has shown that the viscosity of several organic liquids depend on the pressure, and in fact, the dependence is exponential. Notable scientists such as Andrade [25] and Barus [26] have performed laboratory experiments on liquids to determine the relationship between pressure and viscosity. In recent years, research such as that in [27] has been able to obtain empirical evidence to delineate and confirm the dependency of viscosity on pressure. Furthermore, numerical studies have been performed in references [28, 29] to record the differences these pressure dependent viscosity equations make for several fluid problems like the Navier-Stokes equation.

There are several ways one can generalized the standard Darcy model. For example, one can model the friction between the layers of the fluid, which the standard Darcy model neglects. This is approach taken by Brinkman (see references [30, 31]). The research conducted in this thesis focuses on generalizing the standard Darcy model by modifying the drag to depend on the velocity and the pressure.

To account for the dependence of the viscosity (and hence the drag) on the pressure,

Barus' formula [32] will be used. The drag coefficient based on Barus' formula can be rewritten as

$$\alpha(p, \mathbf{x}) = \frac{\mu(p)}{k(\mathbf{x})} = \frac{\mu_0}{k(\mathbf{x})} \exp[\beta_{\mathrm{B}} p], \tag{2.6}$$

where μ_0 is the fixed viscosity of the fluid and β_{B} is the Barus coefficient that is obtained experimentally. This proposed modification states that the viscosity varies exponentially with pressure, but to further illustrate the effect pressure has on the drag, another modification where viscosity varies linearly with pressure is considered. That is,

$$\alpha(p, \mathbf{x}) = \frac{\mu(p)}{k(\mathbf{x})} = \frac{\mu_0}{k(\mathbf{x})}(1 + \beta_{\mathrm{B}} p). \tag{2.7}$$

Laboratory experimentations have determined the Barus coefficient β_{B} of common organic liquids like Naphthenic mineral oil to be about 23.4 GPa^{-1} at 40° C (see reference [33]). Barus' formula is good for pressure applications of roughly 0.1 GPa, but when pressures reach over 1 GPa, the formula may no longer provide accurate solutions for high coefficients. In such cases, a different and more sophisticated pressure dependent model would be more appropriate.

2.2.2 High velocity flows and inertial effects

It has been experimentally observed that for high velocity flows in porous media, the flux (and hence the flow rate) is not linearly proportional to the gradient of the pressure. This can be explained by noting that inertial effects can play a dominant role for high velocity flows. The standard Darcy model completely ignores inertial effects. To address the non-linear dependence of the flux on the gradient of the pressure for high velocity flows, Philipp Forchheimer, an Austrian scientist (1852–1933), proposed that the drag coefficient to depend on the velocity of the fluid [34]. Herein, the model that is obtained after incorporating Forchheimer's modification will be referred to as the *Darcy-Forchheimer model*.

It is noteworthy that the Darcy-Forchheimer model can be obtained from the Navier-Stokes equations using the volume averaging method [35]. In typical geotechnical and civil

engineering applications, one encounters low velocities so the inertial effects can be disregarded, and the standard Darcy model is adequate. However, in high pressure applications like enhanced oil recovery one may often encounter high velocities so inertial effects must be accounted for. The Darcy-Forchheimer model is written as

$$\alpha(\mathbf{v}, \mathbf{x}) = \frac{\mu_0}{k(\mathbf{x})} + \beta_{\mathrm{F}} \|\mathbf{v}\|, \tag{2.8}$$

where β_{F} is the Forchheimer or inertial coefficient, and $\|\cdot\|$ is the 2-norm. That is,

$$\|\mathbf{v}\| = \sqrt{\mathbf{v} \cdot \mathbf{v}}. \tag{2.9}$$

Several people have proposed their own experimental, theoretical, or computational formulations for the Forchheimer coefficient (see reference [36]). For instance, one way to express β_{F} is

$$\beta_{\mathrm{F}} = \frac{c_{\mathrm{F}} \rho}{\sqrt{k_I}}. \tag{2.10}$$

where c_{F} is a dimensionless form-drag constant and k_I is the inertial permeability, both of which can be obtained experimentally. Successful mixed finite element formulations have been performed on the Darcy-Forchheimer model in references [37, 38], but they all use different variants of the Forchheimer coefficient. For the purpose of this thesis, β_{F} shall remain as a user-defined parameter.

Remark 2. *Some porous solids exhibit strong correlation between permeability and porosity, and studies presented in reference [39] show that the porosity is affected by the (pore) pressure. For these porous solids, one can conclude that the pressure affects the permeability, which in turn will give rise to the dependence of drag coefficient on the pressure. However, in this thesis research, assume that the permeability does not depend on the pressure but is allowed to vary spatially.*

2.2.3 Proposed model: Modified Darcy-Forchheimer model

A major focus of this research will study the effects of incorporating pressure-dependent viscosity into the Darcy-Forchheimer model. The drag coefficient can then be rewritten as

$$\alpha(\mathbf{v}, p, \mathbf{x}) = \frac{\mu(p)}{k(\mathbf{x})} + \beta_{\mathrm{F}}\|\mathbf{v}\|. \tag{2.11}$$

The above model will be referred to as the *modified Darcy-Forchheimer model*. Specifically, the two variants of the pressure dependent viscosities in equation (2.11) can be expressed as follows:

$$\alpha(\mathbf{v}, p, \mathbf{x}) = \frac{\mu_0}{k(\mathbf{x})}(1 + \beta_{\mathrm{B}} p) + \beta_{\mathrm{F}}\|\mathbf{v}\|, \tag{2.12a}$$

$$\alpha(\mathbf{v}, p, \mathbf{x}) = \frac{\mu_0}{k(\mathbf{x})}\exp[\beta_{\mathrm{B}} p] + \beta_{\mathrm{F}}\|\mathbf{v}\|. \tag{2.12b}$$

Equation (2.12a) is the linearized version of the modified Darcy-Forchheimer model, and equation (2.12b) is the modified Darcy-Forchheimer Barus model. The proposed model is suitable for applications like enhanced oil recovery, geological carbon-dioxide sequestration, and filtration process. There terms $\mu(p)$ and $\beta_F\|\mathbf{v}\|$ terms (which are both non-linear) can have competitive effects, and neglecting either of these terms can give erroneous results for these applications.

It will now be shown that the modified Darcy-Forchheimer model is dissipative. That is, the proposed constitutive model satisfies the second law of thermodynamics. Within the context of theory of interacting continua for bodies undergoing isothermal processes [22], the total rate of dissipation ξ_{total} is written as

$$\xi_{\text{total}} = \xi_{\text{solid}} + \xi_{\text{fluid}} + \xi_{\text{interaction}}, \tag{2.13}$$

where ξ_{solid} and ξ_{fluid} are the bulk rates of dissipation within the solid and the fluid, and $\xi_{\text{interaction}}$ is the bulk rate of dissipation due to interaction of the solid and the fluid at their

corresponding interfaces. Since the solid is assumed to be rigid,

$$\xi_{\text{solid}} = 0. \tag{2.14}$$

The fluid is assumed to be perfect (i.e., an Euler fluid), so there is no (internal) dissipation within the fluid. That is,

$$\xi_{\text{fluid}} = 0. \tag{2.15}$$

However, it should be emphasized that there is dissipation at the interface between the solid and fluid, which is due to the drag. Hence the total rate of dissipation is given as

$$\xi_{\text{total}} = \xi_{\text{interaction}} = \alpha(\mathbf{v}, p, \mathbf{x}) \, \|\mathbf{v}(\mathbf{x})\|^2, \tag{2.16}$$

where $\|\cdot\|$ is 2-norm norm and $\mathbf{v}(\mathbf{x})$ is the relative velocity of the fluid with respect to the solid. By ensuring that $\alpha(\mathbf{v}, p, \mathbf{x}) > 0$ one can satisfy the second law of thermodynamics *a priori*. For the modified Darcy-Forchheimer model given by equation (2.12b) $\alpha(\mathbf{v}, p, \mathbf{x}) > 0$, as $\mu_0 > 0, k(\mathbf{x}) > 0$, $\beta_{\text{F}} \geq 0$, $\|\mathbf{v}\| \geq 0$ and $\exp[\cdot] > 0$.

Remark 3. *Before numerical formulations for the proposed model are developed, a remark is warranted on the interpretation(s) of the quantity $p(\mathbf{x})$, which was referred to as the pressure earlier. Within the theory of constraints [40, 41], the quantity $p(\mathbf{x})$ is the undetermined multiplier that arises due to the incompressibility constraint, which is given by equation* (2.1b)*. Note that $p(\mathbf{x})$ is not referred to as a Lagrange multiplier as there are no Lagrange multipliers under the framework of constraints that is outlined in references [40, 41]. Under the theory of interacting continua, the partial (Cauchy) stress in the fluid for Darcy model takes the form*

$$\mathbf{T}^{(f)} = -p(\mathbf{x})\mathbf{I}, \tag{2.17}$$

where $\mathbf{I}$ is the second-order identity tensor. Therefore, under the theory of interacting continua framework, $p(\mathbf{x})$ can be considered as the mechanical pressure in the fluid. Note that

the mechanical pressure is defined as the negative of the mean normal stress (see reference [42]). Therefore, under the modified Darcy-Forchheimer model, $p(\mathbf{x})$ is both the mechanical pressure in the fluid, and the undetermined multiplier to enforce the incompressibility constraint. The above discussion on the precise identity and role of $p(\mathbf{x})$ will be extremely important if one wants to make further generalizations / modifications to the proposed model. In particular, to extend the proposed model to incorporate degradation and fracture of the porous solid, which will be part of our future work.

Chapter 3. Mixed weak formulations

It is, in general, not possible to obtain analytical solutions for the preceding system of equations. Hence, one may have to resort to numerical solutions. One of the main goals of this paper is to present mixed finite element formulations based on the variational multiscale and least-squares formalisms for solving the boundary value problem arising due to the modified Darcy-Forchheimer model. To this end, the following function spaces will be used in the remainder of the thesis:

$$\mathcal{P} := \left\{ p(\mathbf{x}) \in H^1(\Omega) \mid p(\mathbf{x}) = p_0(\mathbf{x}) \text{ on } \Gamma^p \right\}, \tag{3.1a}$$

$$\mathcal{Q} := \left\{ q(\mathbf{x}) \in H^1(\Omega) \mid q(\mathbf{x}) = 0 \text{ on } \Gamma^p \right\}, \tag{3.1b}$$

$$\widetilde{\mathcal{Q}} := \left\{ q(\mathbf{x}) \in H^1(\Omega) \right\}, \tag{3.1c}$$

$$\mathcal{V} := \left\{ \mathbf{v}(\mathbf{x}) \in (L_2(\Omega))^{nd} \mid \operatorname{div}[\mathbf{v}] \in L_2(\Omega),\ \mathbf{v}(\mathbf{x}) \cdot \hat{\mathbf{n}}(\mathbf{x}) = v_n(\mathbf{x}) \text{ on } \Gamma^v \right\}, \tag{3.1d}$$

$$\mathcal{W} := \left\{ \mathbf{w}(\mathbf{x}) \in (L_2(\Omega))^{nd} \mid \operatorname{div}[\mathbf{w}] \in L_2(\Omega),\ \mathbf{w}(\mathbf{x}) \cdot \hat{\mathbf{n}}(\mathbf{x}) = 0 \text{ on } \Gamma^v \right\}, \tag{3.1e}$$

where $L_2(\Omega)$ and $H^1(\Omega)$ are standard Sobolev spaces [4]. Note that two different function spaces are defined for the pressure trial function. If the pressure is prescribed strongly on Γ^p then the function space given in equation (3.1a) will be used for the pressure trial function, and the function space given in equation (3.1b) will be used for the pressure test function (i.e., $q(\mathbf{x})$). If the pressure is prescribed weakly on Γ^p then the function space given in equation (3.1c) will be used for both $p(\mathbf{x})$ and $q(\mathbf{x})$.

It should be emphasized that both $L_2(\Omega)$ and $H^1(\Omega)$ are Hilbert spaces under the standard L_2 inner-product [43]. The standard L_2 inner-product over a set K will be denoted as $(\cdot;\cdot)_K$, and is defined as

$$(a;b)_K := \int_K a \cdot b \, \mathrm{d}K. \tag{3.2}$$

For simplicity, the subscript K will be dropped if $K = \Omega$. Note that for volume integrals $K \subseteq \Omega$ and for surface integrals $K \subseteq \partial\Omega$. In a subsequent chapter on numerical results, the error will be measured in L_2 norm and H^1 seminorm. To this end, the L_2 norm on Ω

is defined as

$$\|a\|_{L_2(\Omega)} := \sqrt{\int_\Omega a \cdot a \, \mathrm{d}\Omega}. \tag{3.3}$$

The H^1 seminorm on Ω is defined as

$$|a|_{H^1(\Omega)} := \sqrt{\int_\Omega \mathrm{grad}[a] \cdot \mathrm{grad}[a] \, \mathrm{d}\Omega}. \tag{3.4}$$

The H^1 norm on Ω can then be defined as

$$\|a\|_{H^1(\Omega)} := \sqrt{\|a\|^2_{L_2(\Omega)} + |a|^2_{H^1(\Omega)}}. \tag{3.5}$$

For further details on inner-product spaces and normed spaces, see references [44, 45].

The aforementioned modifications to the standard Darcy model result in non-linear partial differential equations because the drag coefficient depends on the pressure and/or the velocity. This thesis shall employ a linearized FEM, so to solve the resulting non-linear equations linearization terms will be introduced, and mixed weak formulations using the LS and VMS formalisms shall be constructed.

Let the following linearization functionals be defined as:

$$\mathcal{D}^{(i+1)} := \vartheta \left(\frac{\partial \alpha}{\partial p} \mathbf{v}^{(i)} \right) p^{(i+1)} + \vartheta \left(\frac{\partial \alpha}{\partial \mathbf{v}} \otimes \mathbf{v}^{(i)} \right) \mathbf{v}^{(i+1)}, \tag{3.6}$$

$$\mathcal{D}^{(i)} := \vartheta \left(\frac{\partial \alpha}{\partial p} \mathbf{v}^{(i)} \right) p^{(i)} + \vartheta \left(\frac{\partial \alpha}{\partial \mathbf{v}} \otimes \mathbf{v}^{(i)} \right) \mathbf{v}^{(i)}, \tag{3.7}$$

$$\mathcal{G} := \vartheta \left(\frac{\partial \alpha}{\partial p} \mathbf{v}^{(i)} \right) q + \vartheta \left(\frac{\partial \alpha}{\partial \mathbf{v}} \otimes \mathbf{v}^{(i)} \right) \mathbf{w}, \tag{3.8}$$

where superscripts (i) and $(i+1)$ represent solutions for the current and next iteration respectively, $\otimes$ denotes the tensor product as discussed in reference [46], and $\vartheta \in [0, 1]$ is a user-defined parameter to choose the type of linearization. One can achieve Picard's linearization by choosing $\vartheta = 0$ and consistent linearization by choosing $\vartheta = 1$.

Remark 4. *It should be noted that* $\mathbf{v}$*,* p*,* $\mathbf{w}$*,* q*,* μ*,* $\mathbf{b}$*,* k*, and* $\hat{\mathbf{n}}$ *are functions of* $\mathbf{x}$*. The drag coefficient and its derivatives will be functions of* $p^{(i)}$*,* $\mathbf{v}^{(i)}$ *and* $\mathbf{x}$*.*

3.1 A MIXED FORMULATION BASED ON LEAST-SQUARES FORMALISM

Consider a mathematical problem defined by a set of partial differential equations in the form:

$$\mathbf{Lu} = \mathbf{f} \quad \text{in} \quad \Omega, \tag{3.9}$$

$$\mathbf{Bu} = \mathbf{0} \quad \text{in} \quad \Gamma, \tag{3.10}$$

where $\mathbf{L}$ is the linear differential operator, $\mathbf{B}$ is the boundary operator, $\mathbf{u}$ is the dependent unknown vector, and $\mathbf{f}$ is the forcing vector. For the above model, it seeks the minimizer of the functional

$$\Pi[\mathbf{u}] = \frac{1}{2}\int_{\Omega} \|\mathbf{Lu} - \mathbf{f}\|^2 \, \mathrm{d}\Omega + \frac{1}{2}\int_{\Gamma} \|\mathbf{Bu} - \mathbf{0}\|^2 \, \mathrm{d}\Gamma. \tag{3.11}$$

Definition. *Let* $\Pi : \mathbb{R}^m \to \mathbb{R}^n$. *Given* $\mathbf{u} \in \mathbb{R}^m$ *with* $\mathbf{u} \neq \mathbf{0}$ *define*

$$\delta\Pi[\mathbf{a}, \mathbf{u}] := \lim_{\epsilon \to 0} \frac{\Pi[\mathbf{a} + \epsilon\mathbf{u}] - \Pi[\mathbf{a}]}{\epsilon} \equiv \left[\frac{d}{d\epsilon}\Pi[\mathbf{a} + \epsilon\mathbf{u}]\right]_{\epsilon=0}, \tag{3.12}$$

provided the limit exists. This limit is called the directional derivative of Π *at* $\mathbf{a}$ *with respect to the vector* $\mathbf{u}$. *It is also called the* ***Gâteaux variation****. For more on this, see references [47, 48, 49].*

Studies in [50] have shown that minimizing the problem after linearization produces more accurate results. Also, linearizing a minimized problem can make the formulation of the weak/variational terms extremely difficult, so the former approach shall be employed.

Inserting equation (3.6) and (3.7) into equation (2.1a) yields the following governing equations:

$$\alpha \mathbf{v}^{(i+1)} + \mathcal{D}^{(i+1)} - \mathcal{D}^{(i)} + \text{grad}[p^{(i+1)}] = \rho \mathbf{b} \quad \text{in } \Omega, \tag{3.13a}$$

$$\text{div}[\mathbf{v}^{(i+1)}] = 0 \quad \text{in } \Omega, \tag{3.13b}$$

$$\mathbf{v}^{(i+1)} \cdot \hat{\mathbf{n}} = v_n \quad \text{on } \Gamma^v, \tag{3.13c}$$

$$p^{(i+1)} = p_0 \quad \text{on } \Gamma^p. \tag{3.13d}$$

In reference [51], it has been shown that for the Navier-Stokes equation, an introduction of a mesh dependent variable in the LS formulation greatly improves the accuracy of the solution. Thus for the Darcy modifications, two variants of the LS formulation will be considered by employing the following weights:

$$\mathbf{A} = \begin{cases} \mathbf{I} & \text{weight 1} \\ \alpha \mathbf{I} & \text{weight 2} \end{cases}. \tag{3.14}$$

For all the models considered in this paper, the second-order tensor $\mathbf{A}$ is symmetric and positive definite. This implies that the tensor is invertible. In addition, the square root theorem ensures that its square root exists [52]. Employing the minimization approach on equations (3.13a) and (3.13b) results in the functional

$$\begin{aligned} \Pi[\mathbf{v}^{(i+1)}, p^{(i+1)}] := & \frac{1}{2} \int_\Omega \left\| \mathbf{A}^{-1/2} (\alpha \mathbf{v}^{(i+1)} + \mathcal{D}^{(i+1)} - \mathcal{D}^{(i)} + \text{grad}[p^{(i+1)}] - \rho \mathbf{b}) \right\|^2 \text{d}\Omega \\ & + \frac{1}{2} \int_\Omega \left\| \text{div}[\mathbf{v}^{(i+1)}] \right\|^2 \text{d}\Omega. \end{aligned} \tag{3.15}$$

Let $\mathbf{v}^{(i+1)} \to \mathbf{v}^{(i+1)} + \epsilon \mathbf{w}$ and $p^{(i+1)} \to p^{(i+1)} + \epsilon q$ where $\mathbf{v}^{(i+1)}$ and $\mathbf{w}$ are the velocity trial and test functions respectively and $p^{(i+1)}$ and q are the pressure trial and test functions

respectively. Applying the Gâteaux variation on equation (3.15) results in the functional

$$\begin{aligned}\delta\Pi[\mathbf{v}^{(i+1)}, p^{(i+1)}; \mathbf{w}, q] &= \left[\frac{\mathrm{d}}{\mathrm{d}\epsilon}\Pi[\mathbf{v}^{(i+1)} + \epsilon\mathbf{w}, p^{(i+1)} + \epsilon q]\right]_{\epsilon=0} \\ &:= \int_\Omega (\alpha\mathbf{w} + \mathcal{G} + \mathrm{grad}[q]) \cdot \mathbf{A}^{-1}\left(\alpha\mathbf{v}^{(i+1)} + \mathcal{D}^{(i+1)} - \mathcal{D}^{(i)} + \mathrm{grad}[p^{(i+1)}] - \rho\mathbf{b}\right) \\ &+ \mathrm{div}[\mathbf{w}] \cdot \mathrm{div}[\mathbf{v}^{(i+1)}]\mathrm{d}\Omega, \end{aligned} \tag{3.16}$$

and setting it equal to zero gives the weak/variational form. The final statement for the modified Darcy-Forchheimer model can be rearranged and written as follows: given $\mathbf{v}^{(i)}$ and $p^{(i)}$ find $\mathbf{v}^{(i+1)} \in \mathcal{V}$ and $p^{(i+1)} \in \mathcal{P}$ such that we have

$$\begin{aligned}&\left(\alpha\mathbf{w}; \mathbf{A}^{-1}\alpha\mathbf{v}^{(i+1)}\right) + \left(\alpha\mathbf{w}; \mathbf{A}^{-1}\mathcal{D}^{(i+1)}\right) + \left(\alpha\mathbf{w}; \mathbf{A}^{-1}\mathrm{grad}[p^{(i+1)}]\right) \\ &+ \left(\mathcal{G}; \mathbf{A}^{-1}\alpha\mathbf{v}^{(i+1)}\right) + \left(\mathcal{G}; \mathbf{A}^{-1}\mathcal{D}^{(i+1)}\right) + \left(\mathcal{G}; \mathbf{A}^{-1}\mathrm{grad}[p^{(i+1)}]\right) \\ &+ \left(\mathrm{grad}[q]; \mathbf{A}^{-1}\alpha\mathbf{v}^{(i+1)}\right) + \left(\mathrm{grad}[q]; \mathbf{A}^{-1}\mathcal{D}^{(i+1)}\right) + \left(\mathrm{grad}[q]; \mathbf{A}^{-1}\mathrm{grad}[p^{(i+1)}]\right) \\ &+ \left(\mathrm{div}[\mathbf{w}]; \mathrm{div}[\mathbf{v}^{(i+1)}]\right) = \left(\alpha\mathbf{w}; \mathbf{A}^{-1}\rho\mathbf{b}\right) + \left(\mathcal{G}; \mathbf{A}^{-1}\rho\mathbf{b}\right) + \left(\mathrm{grad}[q]; \mathbf{A}^{-1}\rho\mathbf{b}\right) \\ &+ \left(\alpha\mathbf{w}; \mathbf{A}^{-1}\mathcal{D}^{(i)}\right) + \left(\mathcal{G}; \mathbf{A}^{-1}\mathcal{D}^{(i)}\right) + \left(\mathrm{grad}[q]; \mathbf{A}^{-1}\mathcal{D}^{(i)}\right) \\ &\qquad \forall\mathbf{w} \in \mathcal{W},\ \forall q \in \mathcal{Q}. \end{aligned} \tag{3.17}$$

3.2 A MIXED FORMULATION BASED ON VARIATIONAL MULTI-SCALE FORMALISM

Following the derivation given in reference [11], one can derive a mixed formulation based on VMS formalism. It should be noted that in the previous derivations, the governing equations were not linearized and were solved using a Newton-Raphson approach. Unlike its LS counterpart, the VMS formulation is neither least-squares based nor is it of adjoint-type. Instead, the formulation is residual-based. It should also be noted that the pressure boundary condition is weakly prescribed (i.e., a Neumann boundary condition) and acts normal to the boundary so the function space in equation (3.1c) is utilized.

After incorporating linearization terms into the governing equations, the resulting final weak/variational statement can be written as follows: given $\mathbf{v}^{(i)}$ and $p^{(i)}$ find $\mathbf{v}^{(i+1)} \in \mathcal{V}$

and $p^{(i+1)} \in \mathcal{P}$ such that we have

$$\begin{aligned}
&\left(\mathbf{w}; \alpha \mathbf{v}^{(i+1)}\right) + \left(\mathbf{w}; \mathcal{D}^{(i+1)}\right) - \left(\mathrm{div}[\mathbf{w}]; p^{(i+1)}\right) + \left(\mathbf{w} \cdot \hat{\mathbf{n}}; p_0\right)_{\Gamma^p} - \left(q; \mathrm{div}[\mathbf{v}^{(i+1)}]\right) \\
&\quad \underbrace{-\frac{1}{2}\left(\alpha \mathbf{w} + \mathrm{grad}[q]; \alpha^{-1}\left(\alpha \mathbf{v}^{(i+1)} + \mathcal{D}^{(i+1)} + \mathrm{grad}[p^{(i+1)}]\right)\right)}_{\text{stabilization term}} \\
&\quad = \left(\mathbf{w}; \rho \mathbf{b} + \mathcal{D}^{(i)}\right) \underbrace{-\frac{1}{2}\left(\alpha \mathbf{w} + \mathrm{grad}[q]; \alpha^{-1}\left(\rho \mathbf{b} + \mathcal{D}^{(i)}\right)\right)}_{\text{stabilization term}} \\
&\quad \forall \mathbf{w} \in \mathcal{W},\ \forall q \in \widetilde{\mathcal{Q}}.
\end{aligned} \tag{3.18}$$

Chapter 4. Finite element framework and implementation

In this chapter, the computational framework that has been developed will be discussed. As there are numerous ways of implementing the finite element method, it is important to record the notation that is employed in this thesis research.

4.1 DISCRETIZATION, REFERENCE ELEMENTS, AND ISOPARAMETRIC MAPPING

Evaluation of the integrals presented in the variational/weak problem would be tedious or even impractical due to complexities of the domain Ω. Therefore it is convenient to first divide Ω into a finite number of subdomains (i.e, elements) Ω^e, where e is the element identification. That is,

$$\Omega = \bigcup_{e=1}^{Nele} \Omega^e \quad \text{and} \quad \Omega^i \cap \Omega^j = \emptyset \quad \text{for} \quad i \neq j, \tag{4.1}$$

where $Nele$ is the total number of elements. Then reference elements in $\boldsymbol{\zeta}$ space are used to evaluate the integrals using Gauss-Legendre quadrature. The unknowns will be approximated on each reference element using Lagrange interpolation polynomials. Let

$$\{\mathbf{N}(\boldsymbol{\zeta})\} = \begin{Bmatrix} N_1(\boldsymbol{\zeta}) & N_2(\boldsymbol{\zeta}) & \cdots & N_n(\boldsymbol{\zeta}) \end{Bmatrix}, \tag{4.2}$$

be a row vector comprised of interpolation polynomials at each node (see Figure 4.1 for elemental node arrangement) and $[\mathbf{DN}]$ to be a matrix of size $n \times nd$ such that

$$[\mathbf{DN}(\boldsymbol{\zeta})] = \begin{bmatrix} \frac{\partial N_1(\boldsymbol{\zeta})}{\partial \zeta_1} & \cdots & \frac{\partial N_1(\boldsymbol{\zeta})}{\partial \zeta_{nd}} \\ \vdots & \ddots & \vdots \\ \frac{\partial N_n(\boldsymbol{\zeta})}{\partial \zeta_1} & \cdots & \frac{\partial N_n(\boldsymbol{\zeta})}{\partial \zeta_{nd}} \end{bmatrix}, \tag{4.3}$$

where n is the number of nodes in each element and nd is the number of spatial dimensions.

Remark 5. *Let $\{\square\}$ and $[\square]$ denote vectors and matrices defined in the finite element setting. It should be noted that these differ respectively from first and second ordered tensors*

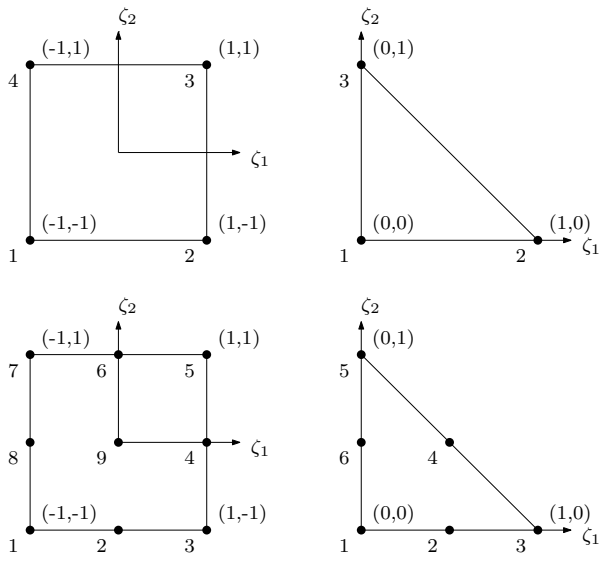

Figure 4.1: Element types and their respective local node numbering. Clockwise from top left: four-node quadrilateral element (Q4), three-node triangle element (T3), six-node triangle element (T6), and nine-node quadrilateral element (Q9)

defined in the continuum setting.

Let the value of unknowns at the nodes of each element Ω^e be $[\hat{\mathbf{u}}]$ which is a matrix of size $n \times dofs$, where $dofs$ denotes the degree-of-freedoms and is equal to $nd + 1$. The unknowns at each point of the reference element can be calculated using the following formula

$$[\hat{\mathbf{u}}]^{\mathrm{T}} \{\mathbf{N}(\boldsymbol{\zeta})\}^{\mathrm{T}}. \tag{4.4}$$

However, the unknowns are sought in the original $\mathbf{x}$ space, so isoparametric mapping can be taken advantage of. Let $\mathbf{x}$ be of the form

$$\mathbf{x}(\boldsymbol{\zeta}) = [\hat{\mathbf{x}}]^{\mathrm{T}} \{\mathbf{N}(\boldsymbol{\zeta})\}^{\mathrm{T}}. \tag{4.5}$$

If the interpolation function of unknown $\mathbf{u}$ can be written as

$$\mathbf{u}(\boldsymbol{\zeta}) = [\hat{\mathbf{u}}]^{\mathrm{T}} \{\mathbf{N}(\boldsymbol{\zeta})\}^{\mathrm{T}}, \tag{4.6}$$

the mapping is said to be isoparametric. Darcy's model requires not a primal formulation

but a mixed formulation as it considers two variables in velocity and pressure. Therefore for each element, unknown $\mathbf{u}$ can be reclassified as a column vector of size $dofs$

$$\mathbf{u} \to \begin{Bmatrix} \mathbf{v} \\ p \end{Bmatrix}. \tag{4.7}$$

First, the nodal unknowns for the velocity and pressure for a given element shall be defined as

$$[\hat{\mathbf{v}}_e] = \begin{bmatrix} v_{1,1} & \cdots & v_{1,nd} \\ \vdots & \ddots & \vdots \\ v_{n,1} & \cdots & v_{n,nd} \end{bmatrix}, \quad \{\hat{\mathbf{p}}_e\} = \begin{Bmatrix} p_1 \\ \vdots \\ p_n \end{Bmatrix}. \tag{4.8}$$

Using isoparametric mappings the unknowns can be approximated in each element as follows:

$$\mathbf{v} = [\hat{\mathbf{v}}_e]^{\mathrm{T}} \{\mathbf{N}\}^{\mathrm{T}}, \tag{4.9a}$$

$$p = \{\hat{\mathbf{p}}_e\}^{\mathrm{T}} \{\mathbf{N}\}^{\mathrm{T}}. \tag{4.9b}$$

Remark 6. *For convenience, assume* $\{\mathbf{N}\}$ *and* $[\mathbf{DN}]$ *to be functions of* $\boldsymbol{\zeta}$.

The finite element approximation of the velocity can be written in an alternate form, which is more helpful and easier to process. Using the definition of the vec[·] operator the nodal velocity unknowns can be expressed as

$$[\hat{\mathbf{v}}_e] \to \mathrm{vec}[\hat{\mathbf{v}}_e^{\mathrm{T}}] = \begin{Bmatrix} v_{1,1} \\ \vdots \\ v_{1,nd} \\ \vdots \\ v_{n,1} \\ \vdots \\ v_{n,nd} \end{Bmatrix}. \tag{4.10}$$

This conversion allows the use of the Kronecker product and makes the implementation of various weak formulations under the FEM more streamlined or systematic. Let $[\mathbf{P}]$ be a $nd \times (n \times nd)$ matrix denoting the Kronecker product of the shape functions row vector $\{\mathbf{N}\}$ and identity matrix $[\mathbf{I}]$ of size $nd \times nd$. Suppose if $nd = 2$, then $[\mathbf{P}]$ can be written as

$$[\mathbf{P}] = [\mathbf{N} \odot \mathbf{I}] = \begin{bmatrix} N_1 & 0 & N_2 & 0 & \cdots & N_n & 0 \\ 0 & N_1 & 0 & N_2 & \cdots & 0 & N_n \end{bmatrix}. \tag{4.11}$$

The following representation for trial and test functions of velocity will be useful:

$$\mathbf{v} = [\mathbf{P}]\text{vec}[\hat{\mathbf{v}}_e^{\mathrm{T}}], \tag{4.12a}$$

$$\mathbf{w} = [\mathbf{P}]\text{vec}[\hat{\mathbf{w}}_e^{\mathrm{T}}]. \tag{4.12b}$$

Other necessary transformations and conversions are listed as follows:

$$[\mathbf{J}] = \frac{\partial \mathbf{x}}{\partial \boldsymbol{\zeta}} = [\hat{\mathbf{x}}]^{\mathrm{T}}[\mathbf{DN}], \tag{4.13a}$$

$$[\mathbf{B}] = [\mathbf{DN}][\mathbf{J}]^{-1}, \tag{4.13b}$$

$$\text{grad}[p] = [\mathbf{B}]^{\mathrm{T}} \left\{\hat{\mathbf{p}}_e\right\}, \tag{4.13c}$$

$$\text{div}[\mathbf{v}] = [\mathbf{B}]^{\mathrm{T}} \cdot [\hat{\mathbf{v}}_e] = \text{vec}[\mathbf{B}^{\mathrm{T}}]^{\mathrm{T}}\text{vec}[\hat{\mathbf{v}}_e^{\mathrm{T}}], \tag{4.13d}$$

where $[\mathbf{J}]$ is the Jacobian matrix and $[\mathbf{B}]$ is the gradient transformation matrix. For more information, see references [53, 54, 55].

4.2 LINEARIZED FINITE ELEMENT EQUATIONS

In a linearized finite element setting, the global stiffness matrix and forcing vector is obtained from the weak/variational form of the governing equations and used to solve for solution $\mathbf{u}^{(i+1)}$. That is,

$$[\mathbf{K}]\left\{\mathbf{u}^{(i+1)}\right\} = \{\mathbf{f}\} \rightarrow \begin{bmatrix} \mathbf{K}_{ff} & \mathbf{K}_{fs} \\ \mathbf{K}_{sf} & \mathbf{K}_{ss} \end{bmatrix} \begin{Bmatrix} \mathbf{u}_f^{(i+1)} \\ \mathbf{u}_s \end{Bmatrix} = \begin{Bmatrix} \mathbf{f}_f \\ \mathbf{f}_s \end{Bmatrix}. \tag{4.14}$$

Equation (4.14) is partitioned into f and s components. Free or f components correspond to unconstrained degrees of freedom, and the supported or s components correspond to strongly prescribed or Dirichlet boundary conditions. It should be noted that $\mathbf{u}_s$ correspond with applied boundary conditions so it remains unchanged; only the free components are updated.

The global terms are obtained by iterating through each element in the domain, obtaining the elemental components of the stiffness matrix and forcing vector, and assembling the quantities based on the degree-of-freedoms. Using the assembly operator A as described in reference [56],

$$[\mathbf{K}] = \mathop{\mathsf{A}}_{e=1}^{Nele} [\mathbf{K}^e], \quad \{\mathbf{f}\} = \mathop{\mathsf{A}}_{e=1}^{Nele} \{\mathbf{f}^e\}\,. \tag{4.15}$$

In a mixed finite element setting, two variables in velocity and pressure are considered. Let subscripts v and p denote the velocity and pressure degree-of-freedoms respectively. At the elemental level, the stiffness matrix and forcing vectors can be expressed as follows:

$$[\mathbf{K}^e] \to \begin{bmatrix} \mathbf{K}^e_{vv} & \mathbf{K}^e_{vp} \\ \mathbf{K}^e_{pv} & \mathbf{K}^e_{pp} \end{bmatrix}, \quad \{\mathbf{f}^e\} \to \begin{Bmatrix} \mathbf{f}^e_v \\ \mathbf{f}^e_p \end{Bmatrix}. \tag{4.16}$$

After obtaining the global stiffness matrices and the global forcing vectors, the global free degree-of-freedoms or unknowns $\mathbf{u}_f^{(i+1)}$ and $\mathbf{f}_s$ can be calculated as

$$\mathbf{u}_f^{(i+1)} = \mathbf{K}_{fs}^{-1}(\mathbf{f}_f - \mathbf{K}_{fs}\mathbf{u}_s), \tag{4.17}$$

$$\mathbf{f}_s = \mathbf{K}_{sf}\mathbf{u}_f^{(i+1)} + \mathbf{K}_{ss}\mathbf{u}_s. \tag{4.18}$$

Following the procedure outlined in reference [56], the partitioned residuals are given by

$$\begin{Bmatrix} \mathbf{r}_f \\ \mathbf{r}_s \end{Bmatrix} = \begin{bmatrix} \mathbf{K}_{ff} & \mathbf{K}_{fs} \\ \mathbf{K}_{sf} & \mathbf{K}_{ss} \end{bmatrix} \begin{Bmatrix} \mathbf{u}_f^{(i)} \\ \mathbf{u}_s \end{Bmatrix} - \begin{Bmatrix} \mathbf{f}_f \\ \mathbf{f}_s \end{Bmatrix}. \tag{4.19}$$

Solving the above systems of equations yields residual $\mathbf{r}$. After attaining all the residuals

and solutions, it is necessary to organize the data to automate of post-processing. Thus,

$$\begin{Bmatrix} \mathbf{r}_f \\ \mathbf{r}_s \end{Bmatrix} \rightarrow \mathbf{r}, \quad \begin{Bmatrix} \mathbf{u}_f^{(i+1)} \\ \mathbf{u}_s \end{Bmatrix} \rightarrow \mathbf{u}. \tag{4.20}$$

Using a Newton-Raphson approach as described in [57], the norm of $\mathbf{r}$ is checked to see if it meets the stopping criterion. In this research, the absolute error is used as the stopping criterion, and ϵ_{TOL} is chosen to be 10^{-9}. If the residuals do not fall below the criterion then $\mathbf{u}_f^{(i)} \leftarrow \mathbf{u}_f^{(i+1)}$, and the FEA is repeated. Otherwise, $\mathbf{u}$ will then be passed to post-processing and visualization routines.

4.2.1 Element stiffness matrices and forcing vectors

Every term in the weak/variational forms of the least-squares and variational multi-scale formulations in Chapter 3 can be partitioned as one of the stiffness matrices or forcing vectors. Assuming Picard's linearization, the corresponding $\mathbf{K}_{vv}^e$ and $\mathbf{K}_{vv}^e$ matrices and $\mathbf{f}_v^e$ vector for equation (3.17) would be:

$$\mathbf{K}_{vv}^e = \int_{\Omega^e} \alpha \mathbf{w} \cdot \mathbf{A}^{-1} \alpha \mathbf{v} \mathrm{d}\Omega + \int_{\Omega^e} (\mathrm{div}[\mathbf{w}])(\mathrm{div}[\mathbf{v}]) \mathrm{d}\Omega, \tag{4.21}$$

$$\mathbf{f}_v^e = \int_{\Omega^e} \alpha \mathbf{w} \cdot \mathbf{A}^{-1} \rho \mathbf{b}. \tag{4.22}$$

Applying the transformation properties from equations (4.12) and (4.13), the above equations can be expressed as follows:

$$\begin{aligned} \mathbf{K}_{vv}^e = \mathrm{vec}[\hat{\mathbf{w}}_e^{\mathrm{T}}]^{\mathrm{T}} \underbrace{\left(\int_{\Omega^e} [\mathbf{P}]^{\mathrm{T}} \alpha [\mathbf{A}]^{-1} \alpha [\mathbf{P}] \mathrm{d}\Omega \right)}_{\text{stiffness matrix}} \mathrm{vec}[\hat{\mathbf{v}}_e^{\mathrm{T}}], \\ + \mathrm{vec}[\hat{\mathbf{w}}_e^{\mathrm{T}}]^{\mathrm{T}} \underbrace{\left(\int_{\Omega^e} \mathrm{vec}[\mathbf{B}^{\mathrm{T}}] \mathrm{vec}[\mathbf{B}^{\mathrm{T}}]^{\mathrm{T}} \mathrm{d}\Omega \right)}_{\text{stiffness matrix}} \mathrm{vec}[\hat{\mathbf{v}}_e^{\mathrm{T}}], \end{aligned} \tag{4.23}$$

$$\mathbf{f}_v^e = \mathrm{vec}[\hat{\mathbf{w}}_e^{\mathrm{T}}]^{\mathrm{T}} \underbrace{\left(\int_{\Omega^e} [\mathbf{P}]^{\mathrm{T}} [\mathbf{A}]^{-1} \rho \mathbf{b} \mathrm{d}\Omega \right)}_{\text{forcing vector}}. \tag{4.24}$$

The remaining stiffness matrices and forcing vectors for Picard's linearization of the least-squares method can be expressed as follows:

$$\mathbf{K}^e_{vp} = \int_{\Omega^e} \alpha \mathbf{w} \cdot \mathbf{A}\text{grad}[p]\text{d}\Omega = \text{vec}[\hat{\mathbf{w}}^{\text{T}}_e]^{\text{T}} \left(\int_{\Omega^e} [\mathbf{P}]^{\text{T}} \alpha [\mathbf{A}]^{-1} [\mathbf{B}]^{\text{T}} \text{d}\Omega \right) \{q_e\}, \tag{4.25}$$

$$\mathbf{K}^e_{pv} = \int_{\Omega^e} \text{grad}[q] \cdot \mathbf{A}\alpha\mathbf{v}\text{d}\Omega = \{q_e\}^{\text{T}} \left(\int_{\Omega^e} [\mathbf{B}] \alpha [\mathbf{A}]^{-1} [\mathbf{P}] \text{d}\Omega \right) \text{vec}[\hat{\mathbf{v}}^{\text{T}}_e], \tag{4.26}$$

$$\mathbf{K}^e_{pp} = \int_{\Omega^e} \text{grad}[q] \cdot \mathbf{A}\text{grad}[p] = \{q_e\}^{\text{T}} \left(\int_{\Omega^e} [\mathbf{B}] [\mathbf{A}]^{-1} [\mathbf{B}]^{\text{T}} \text{d}\Omega \right) \{q_e\}, \tag{4.27}$$

$$\mathbf{f}^e_p = \int_{\Omega^e} \text{grad}[q] \cdot \mathbf{A}\rho\mathbf{b}\text{d}\Omega = \{q_e\}^{\text{T}} \left(\int_{\Omega^e} [\mathbf{B}] [\mathbf{A}]^{-1} \rho \mathbf{b} \text{d}\Omega \right). \tag{4.28}$$

For consistent linearization and/or variational multi-scales terms, see Appendix A.

4.3 USER INPUT AND FEA DRIVER

The entire finite element framework for both the least-squares and variational multi-scale formulations are programmed from scratch. All pre-processing, analysis, and post-processing are handled using MATLAB. As seen in Figure 4.2, the user is responsible for providing the DataFile that contains all necessary information for meshing. Four key data types are required for the user input:

1. Parameters: The parameters in the governing equations are defined here. All possible body forces and/or permeability functions should also be included.

2. Solver Types: These tell the finite element program what weak/variational formulation to use, which Darcy model(s) to employ, and how to linearize the problem(s) if necessary.

3. Meshing: Given the spatial dimensions and node seedings, the final node and element count will be stored. The node numbering and connectivity will be stored as depicted in Figure 4.1.

4. Boundary Conditions: After the connectivity and nodal coordinate matrices have been created, the user will declare either strongly or weakly prescribe boundary conditions along the appropriate boundaries. Depending on the complexity of the domain or prescribed boundary conditions, separate subroutines or algorithms might be necessary.

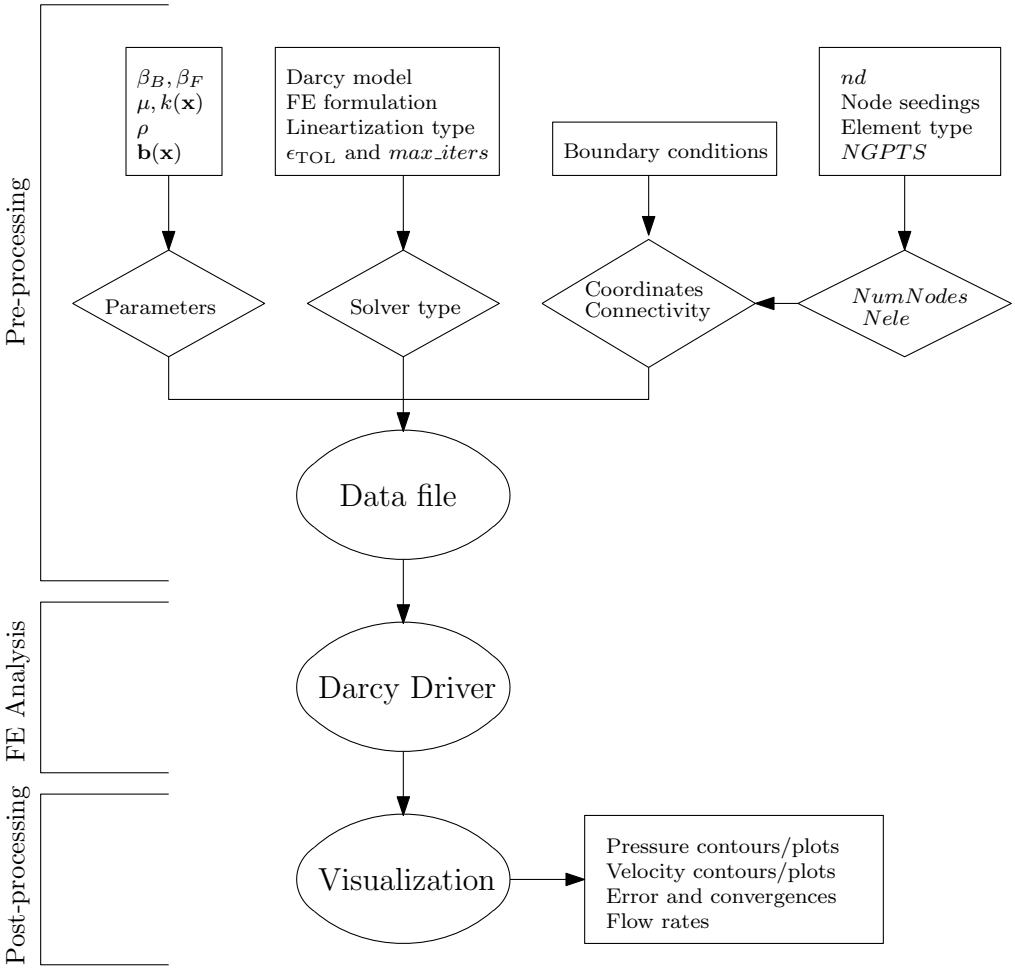

Figure 4.2: A flowchart of finite element code development for Darcy-type models

It is important to note that the meshing algorithms used only handle structured grids. If a complex domain is needed, a pre-processing software will have to be used. Algorithm 1 describes step-by-step the finite element analysis in the driver program.

Algorithm 1 Pseudocode for the finite element analysis driver.

procedure DRIVER ▷ begin finite element analysis
  Read DataFile
  Organize Global dofs by free and prescribed components ▷ for assembly purposes
  Extract Dirichlet Constraints into prescribed components ▷ these remain constant
  Set $(i) = 1$;
  Initialize data $\mathbf{v}^{(i)} = \mathbf{1}$ and $p^{(i)} = 1$ ▷ initialize solution for free components
  while true **do** ▷ non-linear solver
    if $i > max\_iters$ **then**
      break
    end if
    Initialize sparse global stiffness matrices and forcing vectors
    for $e = 1 \rightarrow Nele$ **do** ▷ iterate through each element
      Get $\hat{\mathbf{p}}_e$, $\hat{\mathbf{v}}_e$, and $\hat{\mathbf{x}}_e$ ▷ extracts solutions from iteration (i)
      for $gpt = 1 \rightarrow NGPTS$ **do** ▷ iterate through gauss points
        Get $\{\mathbf{N}\}$ and $[\mathbf{DN}]$
        Get α and $\mathbf{b}$
        Populate local stiffness matrix and local forcing vector
      end for
      Assemble local terms into partitioned global components
    end for
    Solve stiffness equations and obtain $\mathbf{r}$, $\mathbf{v}^{(i+1)}$, and $p^{(i+1)}$
    if $\|\mathbf{r}\| < \epsilon_{\text{TOL}}$ **then**
      break ▷ solution has converged
    else
      $\mathbf{v}^{(i)} \leftarrow \mathbf{v}^{(i+1)}$ and $p^{(i)} \leftarrow p^{(i+1)}$
      $(i) \leftarrow (i + 1)$
    end if
  end while
  Post-processing
end procedure

Chapter 5. Numerical benchmark tests

In this chapter, the FEM developed is employed on several benchmark problems. The upcoming studies will assess the relative performances of the Darcy models and test the robustness of the finite element formalisms.

5.1 DIMENSIONLESS FORM OF EQUATIONS

Numerical studies for subsurface flows like enhanced oil recovery can be displayed in dimensionless form, thus allowing scaling to real flow conditions. The governing equations are non-dimensionalized by choosing primary variables that seem appropriate. This non-dimensional procedure is different from the standard non-dimensionalization procedure for incompressible Navier-Stokes in the choice of primary variables (in the standard non-dimensionalization of Navier-Stokes equations, one employs characteristic velocity v, characteristic length L and density of the fluid ρ as primary variables). Also, the present non-dimensionalization is different and seems more appropriate than the one employed in reference [3] for the chosen applications.

All non-dimensional quantities are denoted using a superposed bar. Let L (reference length in the problem), g (acceleration due to gravity) and p_{atm} (atmospheric pressure) be the reference quantities. The following non-dimensional quantities are then defined:

$$\begin{aligned} &\bar{\mathbf{x}} = \frac{\mathbf{x}}{L},\ \bar{\mathbf{v}} = \frac{\mathbf{v}}{\sqrt{gL}},\ \bar{\mathbf{b}} = \frac{\mathbf{b}}{g},\ \bar{p} = \frac{p}{p_{\text{atm}}},\ \bar{\rho} = \frac{\rho g L}{p_{\text{atm}}},\ \bar{k} = \frac{k}{L^2} \\ &\bar{\beta}_{\text{B}} = \beta_{\text{B}} p_{\text{atm}},\ \bar{\beta}_{\text{F}} = \frac{\beta_{\text{F}} g L^2}{p_{\text{atm}}},\ \bar{\alpha} = \frac{\alpha L}{p_{\text{atm}}},\ \bar{\mu}_0 = \frac{\mu_0 \sqrt{g/L}}{p_{\text{atm}}}. \end{aligned} \tag{5.1}$$

The scaled domain Ω_{scaled} is defined as follows: a point in space with position vector $\bar{\mathbf{x}} \in \Omega_{\text{scaled}}$ corresponds to the same point with position vector given by $\mathbf{x} = \bar{\mathbf{x}} L \in \Omega$. Similarly, one can define the scaled boundaries for Γ^v_{scaled} and Γ^p_{scaled}. Using the above non-dimensionalization procedure, the governing equations (2.1) can be written as follows:

$$\bar{\alpha}(\bar{\mathbf{v}}, \bar{p}, \bar{\mathbf{x}})\bar{\mathbf{v}} + \overline{\mathrm{grad}}[\bar{p}(\bar{\mathbf{x}})] = \bar{\rho}\,\bar{\mathbf{b}}(\bar{\mathbf{x}}) \quad \text{in } \Omega_{\text{scaled}}, \tag{5.2a}$$

$$\overline{\mathrm{div}}[\bar{\mathbf{v}}(\bar{\mathbf{x}})] = 0 \quad \text{in } \Omega_{\text{scaled}}, \tag{5.2b}$$

$$\bar{\mathbf{v}}(\bar{\mathbf{x}}) \cdot \hat{\mathbf{n}}(\bar{\mathbf{x}}) = \bar{v}_0(\bar{\mathbf{x}}) \quad \text{on } \Gamma^v_{\text{scaled}}, \tag{5.2c}$$

$$\bar{p}(\bar{\mathbf{x}}) = \bar{p}_0(\bar{\mathbf{x}}) \quad \text{on } \Gamma^t_{\text{scaled}}. \tag{5.2d}$$

5.2 ONE-DIMENSIONAL PROBLEM

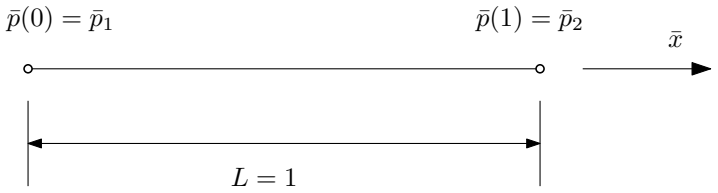

Figure 5.1: One dimensional problem: a pictorial description

First, the proposed mixed formulations presented in Chapter 3 will be tested on a simple one-dimensional problem which is pictorially described in Figure 5.1. Pressures $\bar{p}_1$ and $\bar{p}_2$ are prescribed at the two ends of the unit domain, body force is neglected, and the velocity is constant because of the incompressibility constraint. The governing equations can then be written as:

$$\bar{\alpha}(\bar{p}, \bar{v})\bar{v} + \frac{\mathrm{d}\bar{p}}{\mathrm{d}\bar{x}} = 0 \quad \text{in } (0,1), \tag{5.3a}$$

$$\frac{\mathrm{d}\bar{v}}{\mathrm{d}\bar{x}} = 0 \quad \text{in } (0,1), \tag{5.3b}$$

$$\bar{p}(\bar{x} = 0) = \bar{p}_1, \quad \bar{p}(\bar{x} = 1) = \bar{p}_2. \tag{5.3c}$$

Analytical solutions will be derived using various Darcy models. This problem examines the effect the drag functions of the original Darcy, modified linear, modified Barus, and Darcy-Forchheimer models has on the solutions. Solving the initial value boundary problem for

the respective models results in the following pressure and velocity functions:

$$\bar{\alpha} = \frac{\bar{\mu}_0}{\bar{k}} \begin{cases} \bar{p}(\bar{x}) = (\bar{p}_2 - \bar{p}_1)\bar{x} + \bar{p}_1 \\ \bar{v}(\bar{x}) = -\frac{(\bar{p}_2 - \bar{p}_1)}{\bar{\alpha}} \end{cases} \tag{5.4a}$$

$$\bar{\alpha} = \frac{\bar{\mu}_0}{\bar{k}}(1 + \bar{\beta}_{\mathrm{B}}\bar{p}) \begin{cases} \bar{p}(\bar{x}) = \frac{1}{\bar{\beta}_{\mathrm{B}}}\left[(1 + \bar{\beta}_{\mathrm{B}}\bar{p}_1)^{1-\bar{x}}(1 + \bar{\beta}_{\mathrm{B}}\bar{p}_2)^{\bar{x}} - 1\right] \\ \bar{v}(\bar{x}) = \frac{-1}{\bar{\alpha}\bar{\beta}_{\mathrm{B}}}\ln\left[\frac{1+\bar{\beta}_{\mathrm{B}}\bar{p}_2}{1+\bar{\beta}_{\mathrm{B}}\bar{p}_1}\right] \end{cases} \tag{5.4b}$$

$$\bar{\alpha} = \frac{\bar{\mu}_0}{\bar{k}}\exp[\beta_{\mathrm{B}}\bar{p}] \begin{cases} \bar{p}(\bar{x}) = \frac{-1}{\bar{\beta}_{\mathrm{B}}}\ln\left[(1 - \bar{x})\exp[-\bar{\beta}_{\mathrm{B}}\bar{p}_1] + \bar{x}\exp[-\bar{\beta}_{\mathrm{B}}\bar{p}_2]\right] \\ \bar{v}(\bar{x}) = \frac{1}{\bar{\alpha}\bar{\beta}_{\mathrm{B}}}\exp[-\bar{\beta}_{\mathrm{B}}\bar{p}_2] - \exp[-\bar{\beta}_{\mathrm{B}}\bar{p}_1] \end{cases} \tag{5.4c}$$

$$\bar{\alpha} = \frac{\bar{\mu}_0}{\bar{k}} + \bar{\beta}_{\mathrm{F}}\bar{v} \begin{cases} \bar{p}(\bar{x}) = (\bar{p}_2 - \bar{p}_1)\bar{x} + \bar{p}_1 \\ \bar{v}(\bar{x}) = \frac{-\bar{\alpha} + \sqrt{\bar{\alpha}^2 - 4\bar{\beta}_{\mathrm{F}}(\bar{p}_2 - \bar{p}_1)}}{2\bar{\beta}_{\mathrm{F}}} \end{cases} \tag{5.4d}$$

Figure 5.2 shows the numerical and analytical pressure profiles using the parameters provided in Table 5.1. Numerical solutions show that the proposed finite element formulations of both formalisms perform well. The dependence of viscosity on the pressure results in steep gradients in the pressure near the boundary. The modified linear model does not depict as steep of a pressure gradient as the Barus modification which is expected. Although the Darcy-Forchheimer model is nonlinear, it still gives linear variation of pressure with respect to x. It is seen that the proposed numerical formulations for both formalisms perform well. In cases where velocity is not constant, both the pressure and velocity profiles can differ qualitatively. Therefore, it is important to study the effects of the proposed modifications to the Darcy model on various two dimensional problems.

Table 5.1: User-defined inputs for the one-dimensional problem

Parameter	Value
$\bar{\beta}_{\mathrm{B}}$	0.5
$\bar{\beta}_{\mathrm{F}}$	1
$\bar{k}$	1
$\bar{\mu}_0$	1
$\bar{\rho}$	1
$\bar{\mathbf{b}}$	0
$Nele$	10
$\bar{p}_1$	10
$\bar{p}_2$	1

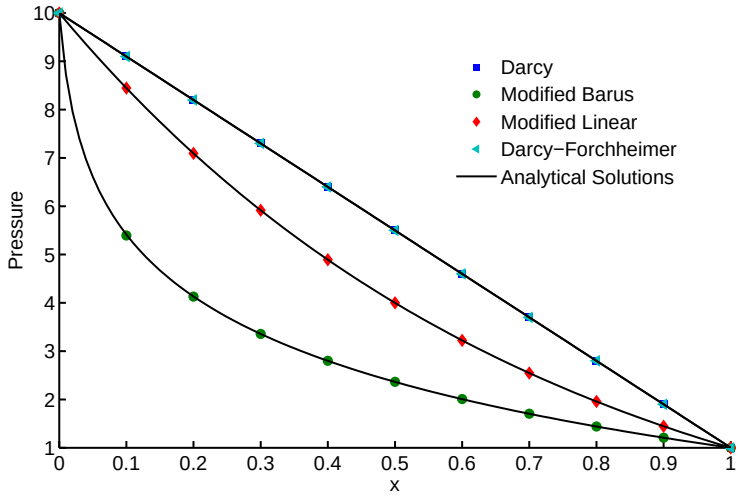

(a) LS formalism

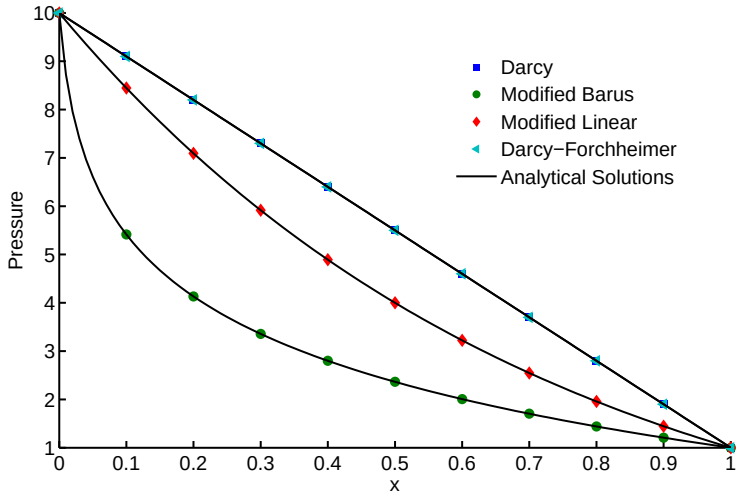

(b) VMS formalism

Figure 5.2: One-dimensional problem: pressure profile

5.3 NUMERICAL H-CONVERGENCE

A finite element formulation is said to be convergent if the numerical solutions tend to the exact solution with mesh refinement. This section will perform an h-convergence analysis on all Darcy models where h is taken to be the edge length for quadrilateral elements and the short-edge length for triangular elements. Consider a unit square as the computational domain. For this and all subsequent numerical studies, the FEM utilizes structured meshes as depicted in Figure 5.3. The velocity and pressure functions for this problem are:

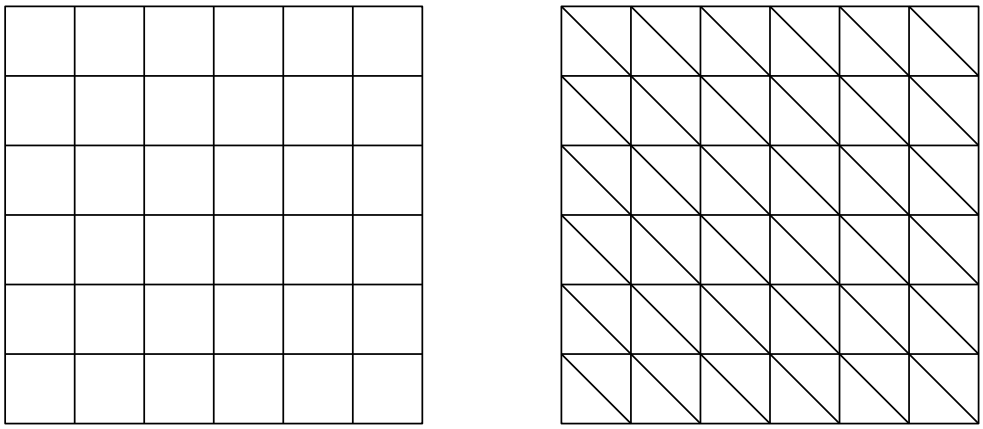

Figure 5.3: Typical meetings used: a quadrilateral (left) and triangular (right) mesh

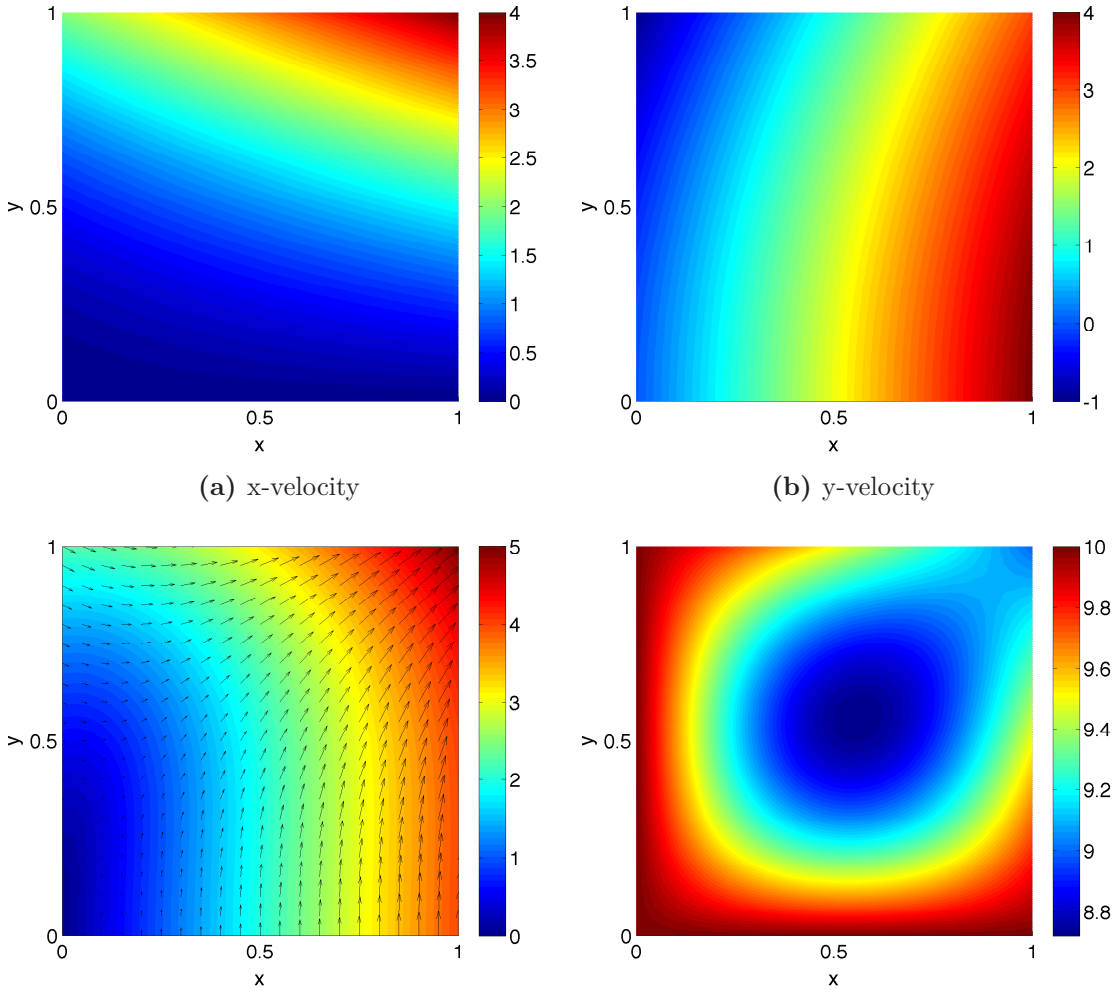

(a) x-velocity **(b)** y-velocity

(c) velocity field **(d)** pressure contour

Figure 5.4: Numerical h-convergence: analytical solutions

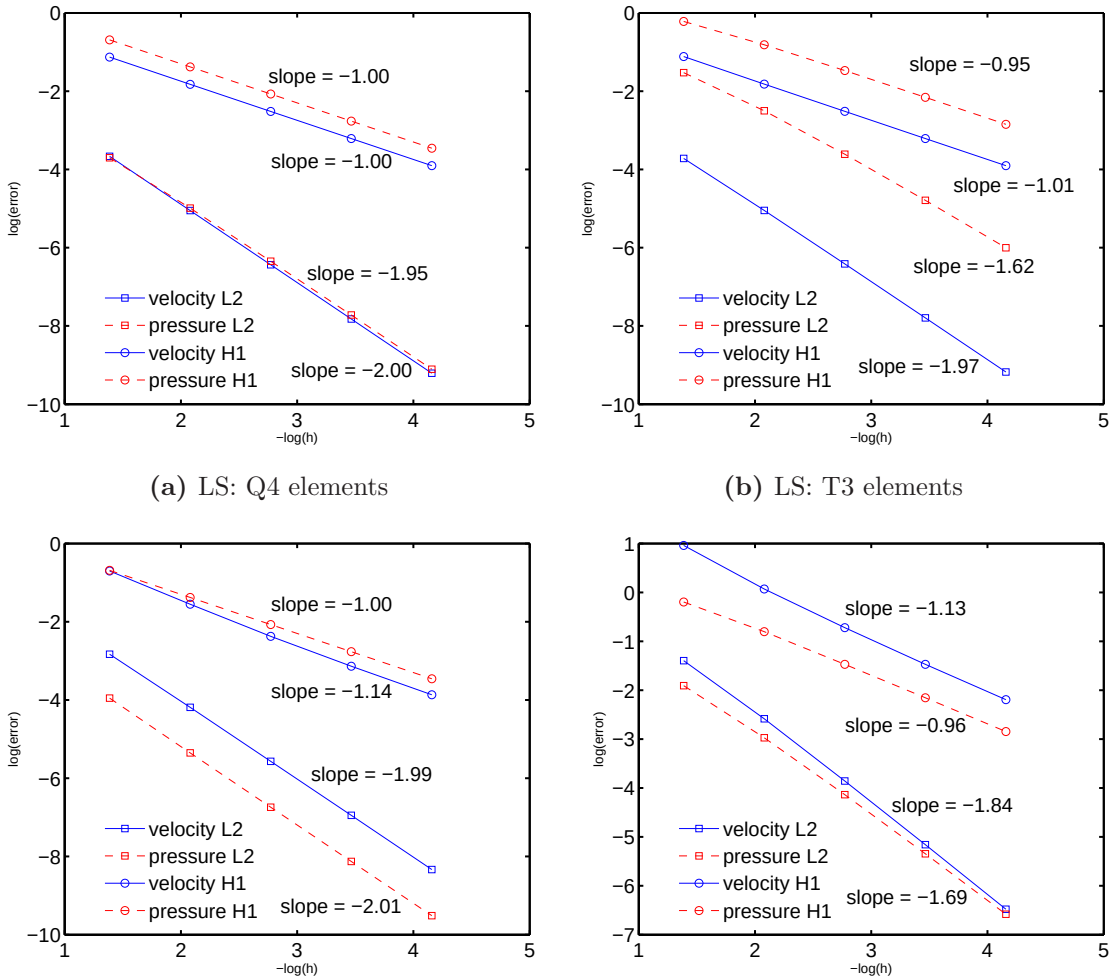

(a) LS: Q4 elements

(b) LS: T3 elements

(c) VMS: Q4 elements

(d) VMS: T3 elements

Figure 5.5: Numerical h-convergence: error slopes for the Darcy (D) model

$$\bar{\mathbf{v}}(x,y) = \begin{Bmatrix} 2y(x+y) \\ 4x - y^2 \end{Bmatrix}, \tag{5.5a}$$

$$\bar{p}(x,y) = 10 - xy - \sin(\pi x)\sin(\pi y). \tag{5.5b}$$

Inserting the velocity and pressure functions back into the Darcy equation results in the following specific body force function

$$\bar{\mathbf{b}}(x,y) = \frac{1}{\bar{\rho}} \begin{Bmatrix} \bar{\alpha} 2y(x+y) - \pi\cos(\pi x)\sin(\pi y) - y \\ \bar{\alpha}(4x - y^2) - \pi\cos(\pi y)\sin(\pi x) - x \end{Bmatrix}. \tag{5.6}$$

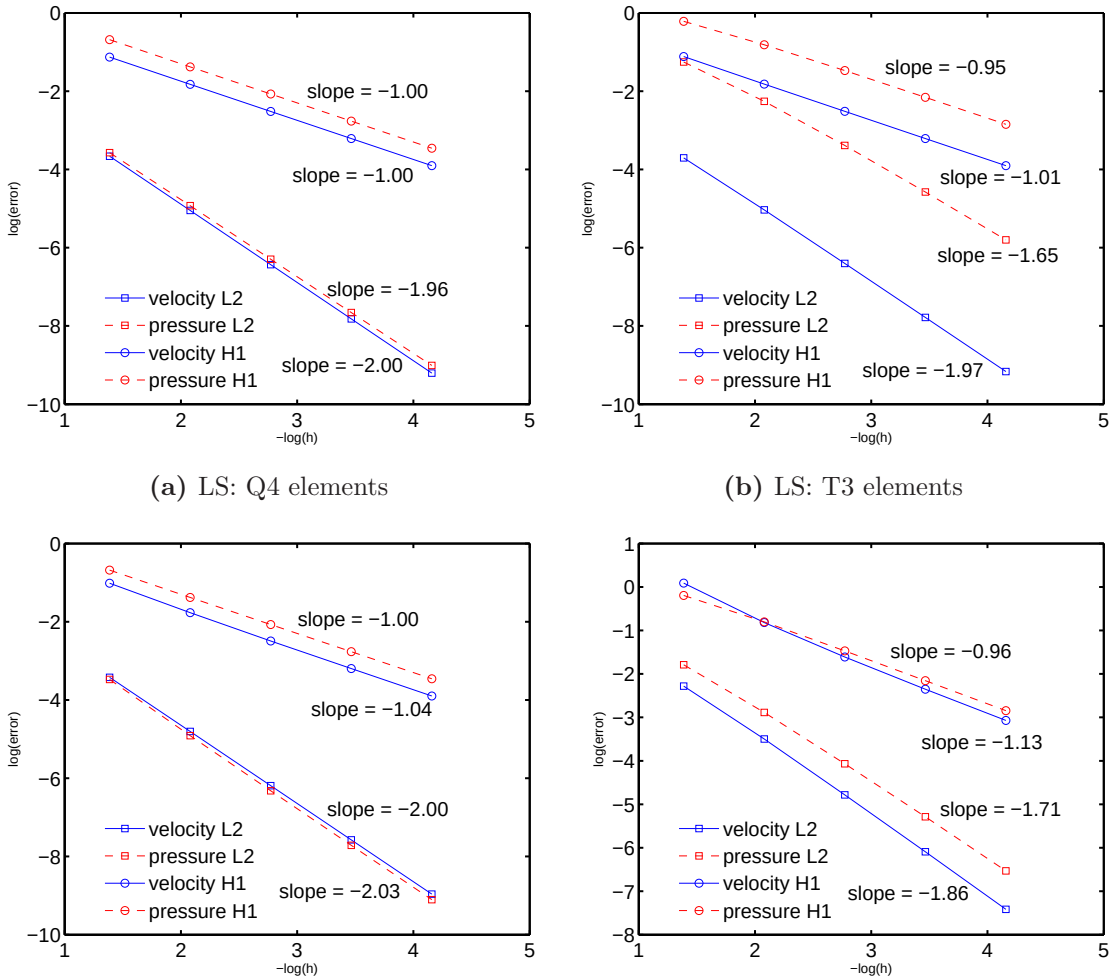

(a) LS: Q4 elements

(b) LS: T3 elements

(c) VMS: Q4 elements

(d) VMS: T3 elements

Figure 5.6: Numerical h-convergence: error slopes for the modified Barus (MB) model

The boundary conditions for equation (5.5) are as follows:

$$\bar{v}_x(x=0,y) = 2y^2, \tag{5.7a}$$

$$\bar{v}_x(x=1,y) = 2y(1+y), \tag{5.7b}$$

$$\bar{v}_y(x,y=0) = 4x, \tag{5.7c}$$

$$\bar{v}_y(x,y=1) = 4x-1, \tag{5.7d}$$

$$\bar{p}(0,0) = 10. \tag{5.7e}$$

Using the parameters listed in Table 5.2, Figure 5.4 depicts the analytical velocity and

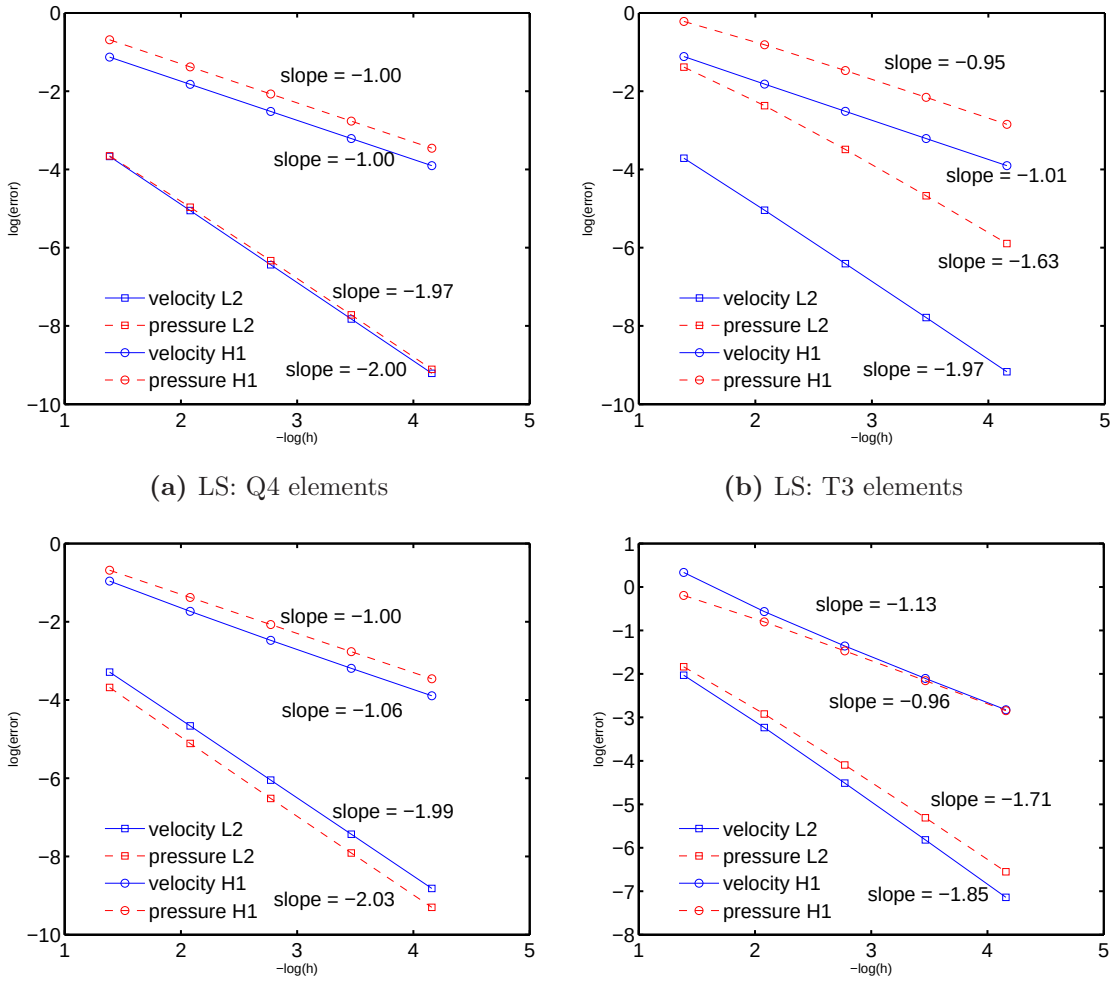

(a) LS: Q4 elements

(b) LS: T3 elements

(c) VMS: Q4 elements

(d) VMS: T3 elements

Figure 5.7: Numerical h-convergence: error slopes for the modified linear (ML) model

pressure solutions to which the finite element solutions shall be compared with. Since neither the pressure nor velocity functions depend on the drag coefficient, only the specific body

Table 5.2: User-defined inputs for the numerical h-convergence problem

Parameter	Value
$\bar{\beta}_{\mathrm{B}}$	0.1
$\bar{\beta}_{\mathrm{F}}$	0.5
$\bar{k}$	1
$\bar{\mu}_0$	1
$\bar{\rho}$	1
ϑ	1
h-sizes	0.250, 0.125, 0.0625, 0.0313, 0.0156

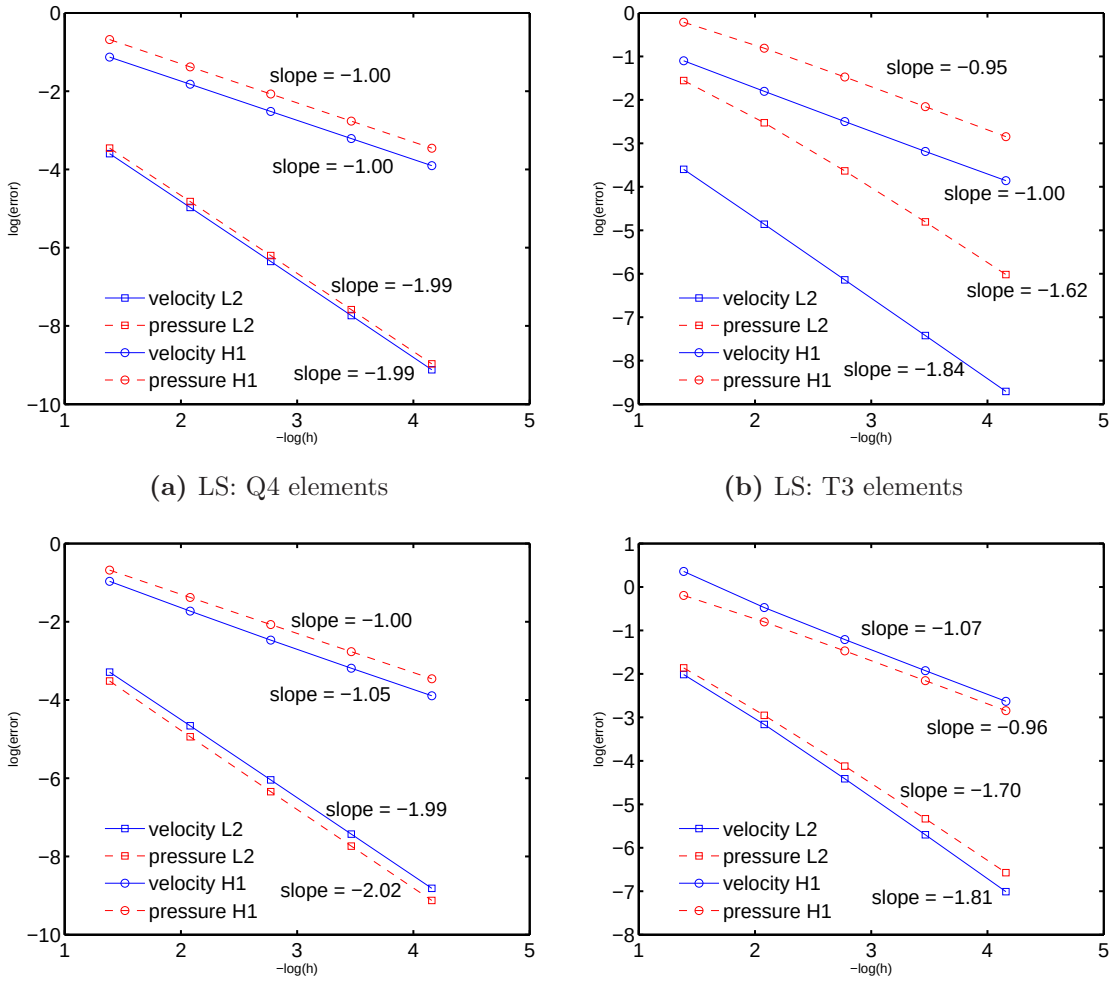

(a) LS: Q4 elements

(b) LS: T3 elements

(c) VMS: Q4 elements

(d) VMS: T3 elements

Figure 5.8: Numerical h-convergence: error slopes for the Darcy-Forchheimer (F) model

force varies with respect to each Darcy model. The six Darcy models used for this problem are: the original Darcy (D), modified Barus (MB), modified linear (ML), Darcy-Forchheimer (F), modified Darcy-Forchheimer Barus (MBF), and the modified Darcy-Forchheimer linear (MLF) models. The L_2 norm and H^1 seminorm error slopes for the respective models are depicted in Figures 5.5, 5.6, 5.7, 5.8, 5.9, and 5.10. Q4 and T3 elements are used to solve the problems, and Tables 5.3 and 5.4 list all the error slopes for the LS and VMS formalisms respectively. It can be seen that the numerical solutions perform well; converged solutions should have error slopes approximately -2.00 and -1.00 for L_2 norm and H^1 seminorm respectively. Quadrilateral elements tend to exhibit faster convergence rates than triangular

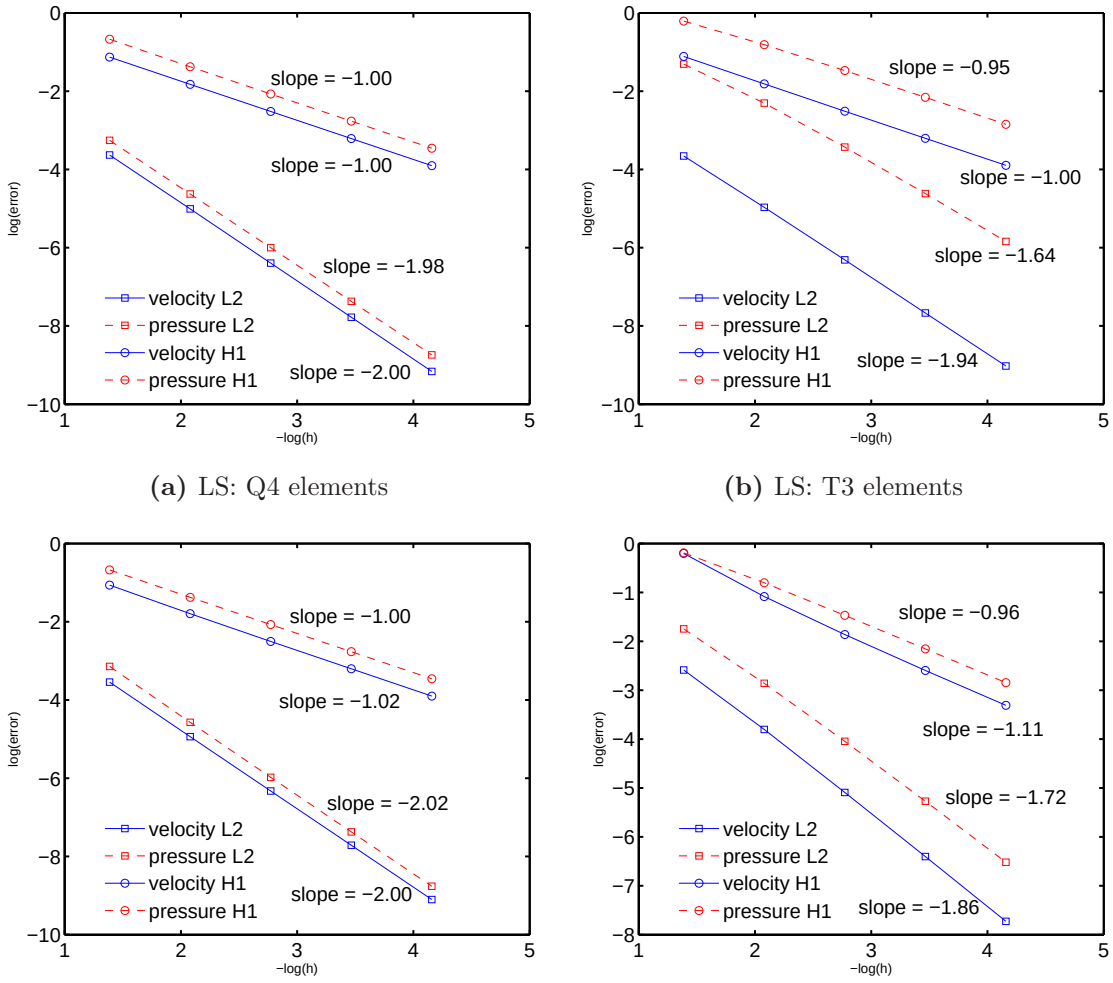

(a) LS: Q4 elements

(b) LS: T3 elements

(c) VMS: Q4 elements

(d) VMS: T3 elements

Figure 5.9: Numerical h-convergence: error slopes for the modified Darcy-Forchheimer Barus (MBF) model

Table 5.3: Numerical h-convergence slopes for various Darcy models using LS formalism

	D	MB	ML	F	MBF	MLF
Q4 elements:						
L_2 error v	-2.00	-2.00	-2.00	-1.99	-2.00	-2.00
H^1 error v	-1.00	-1.00	-1.00	-1.00	-1.00	-1.00
L_2 error p	-1.95	-1.96	-1.97	-1.99	-1.98	-1.99
H^1 error p	-1.00	-1.00	-1.00	-1.00	-1.00	-1.00
T3 elements:						
L_2 error v	- 1.97	-1.97	-1.97	-1.84	-1.94	-1.92
H^1 error v	-1.01	-1.01	-1.01	-1.00	-1.00	-1.00
L_2 error p	-1.62	-1.65	-1.63	-1.62	-1.64	-163
H^1 error p	-0.95	-0.95	-0.95	-0.95	-0.95	-0.95

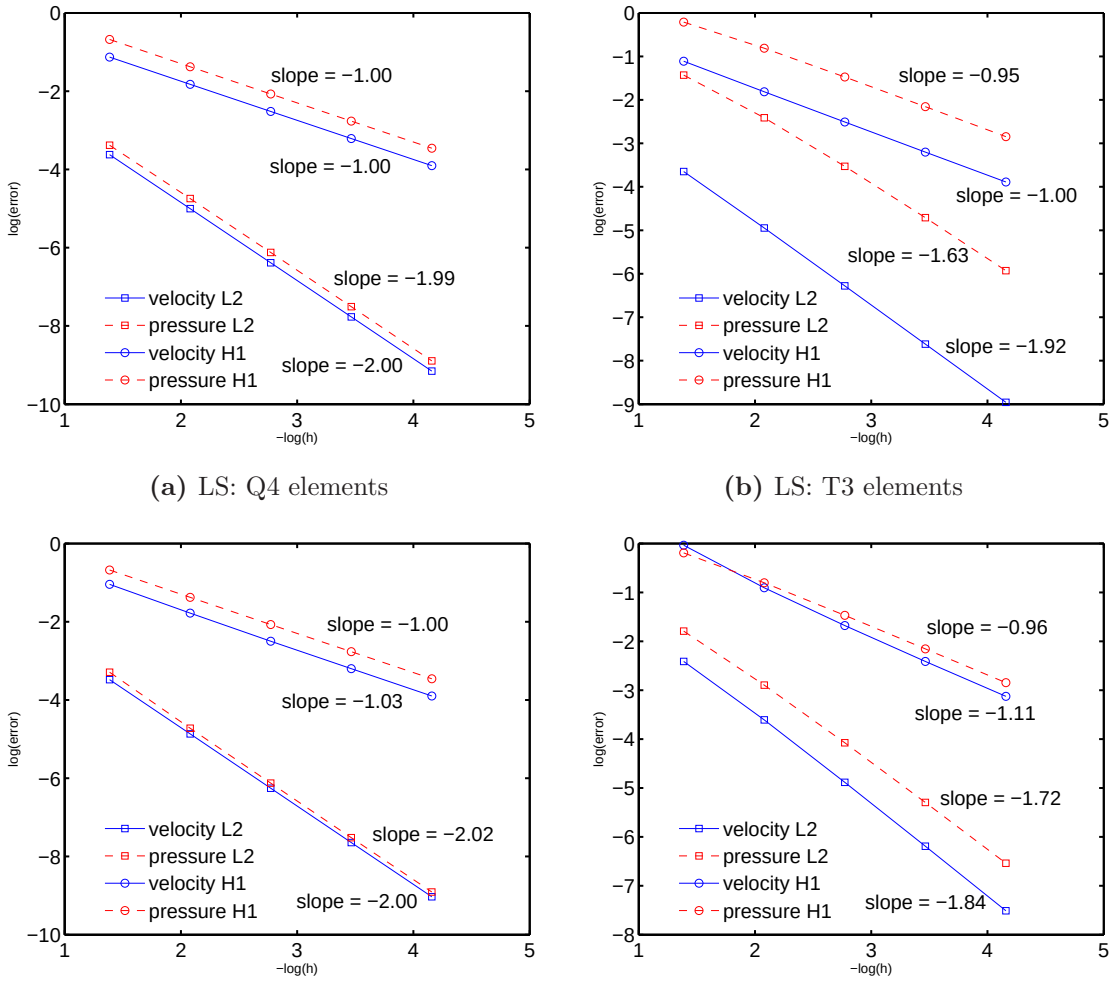

(a) LS: Q4 elements

(b) LS: T3 elements

(c) VMS: Q4 elements

(d) VMS: T3 elements

Figure 5.10: Numerical h-convergence: error slopes for the modified Darcy-Forchheimer linear (MLF) model

Table 5.4: Numerical h-convergence slopes for various Darcy models using VMS formalism

	D	MB	ML	F	MBF	MLF
Q4 elements:						
L_2 error v	-1.99	-2.00	-1.99	-1.99	-2.00	-2.00
H^1 error v	-1.14	-1.04	-1.06	-1.05	-1.02	-1.03
L_2 error p	-2.01	-2.03	-2.03	-2.02	-2.02	-2.02
H^1 error p	-1.00	-1.00	-1.00	-1.00	-1.00	-1.00
T3 elements:						
L_2 error v	-1.84	-1.86	-1.85	-1.81	-1.86	-1.84
H^1 error v	-1.13	-1.13	-1.13	-1.07	-1.11	-1.11
L_2 error p	-1.69	-1.71	-1.71	-1.70	-1.72	-1.72
H^1 error p	-0.96	-0.96	-0.96	-0.96	-0.96	-0.96

elements, and one can expect even faster rates for higher order elements like the Q9 and T6.

5.4 QUARTER FIVE-SPOT PROBLEM

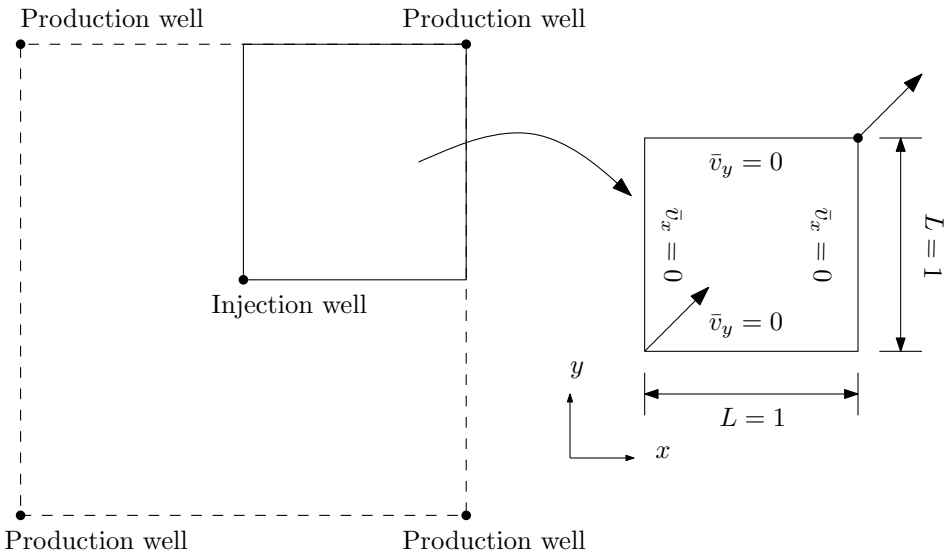

Figure 5.11: Quarter five-spot problem: A pictorial description

This section presents numerical results for a quarter spot problem as depicted in Figure 5.11. In many enhance oil recovery applications, there is an injection well centered around four production wells. When carbon-dioxide is injected into the ground, the pressure build up pushes oil out through the four injection wells. This schematic forms what is often known as the five spot problem. Numerical results will exhibit elliptic singularities near the injection and production wells and provide a good benchmark to test the robustness of the finite element formulations. Due to the symmetric nature of the problem, only the top right quadrant is considered in the analysis. There is no specific body force or volumetric/sink source, and a pressure of $\bar{p}_0 = 1$ is prescribed at the production well or top right node. Since it has been shown in previous sections that the FEM developed performs well for both Q4 and T3 elements, only quadrilateral elements will be used to simulate all proceeding numerical simulations.

Consider a case where there is only $\sqrt{2}$ units of flow through the unit square quadrant. To attain this flow rate, one needs to know the amount of pressure needed at the injection

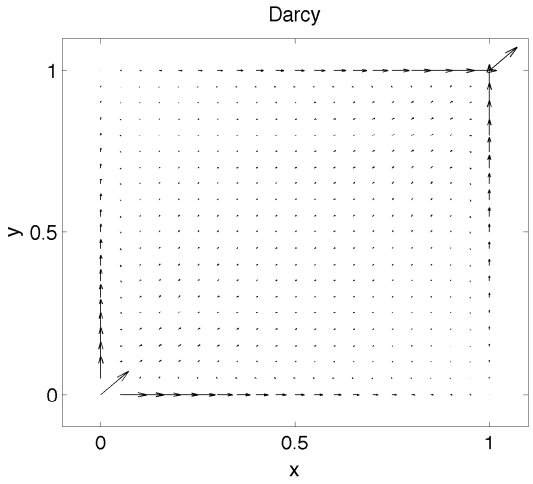

(a) LS velocity vector field

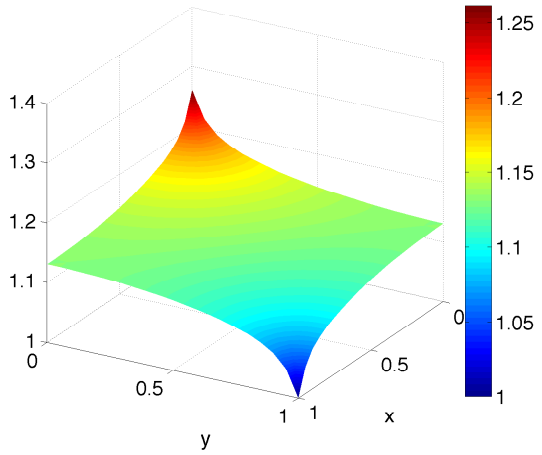

(b) LS pressure contour

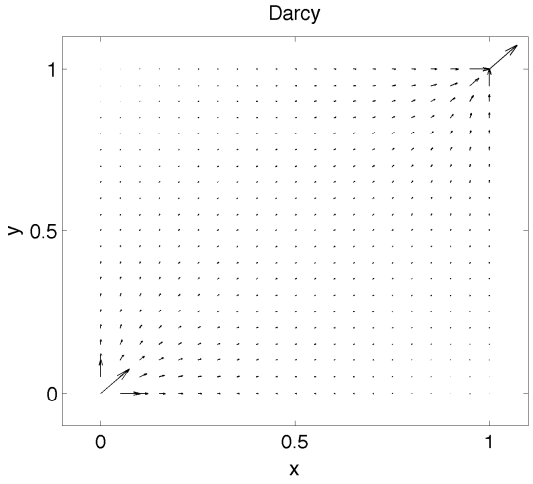

(c) VMS velocity vector field

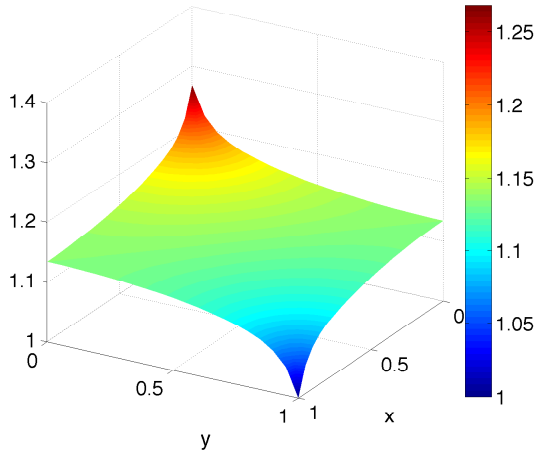

(d) VMS pressure contour

Figure 5.12: Quarter five-spot problem: Q4 solutions for Darcy model

well (i.e., the bottom left node). Using Q4 elements and the parameters listed in Table 5.5,

Table 5.5: User-defined inputs for the quarter five-spot problem: Darcy model

Parameter	Value
$\bar{k}$	1
$\bar{\mu}_0$	1
$\bar{\rho}$	1
$\bar{\mathbf{b}}$	0
$Nele$	400
$\bar{p}(1,1)$	1
$\bar{\mathbf{v}}(0,0)$, $\bar{\mathbf{v}}(1,1)$	$\begin{Bmatrix}1\\1\end{Bmatrix}$

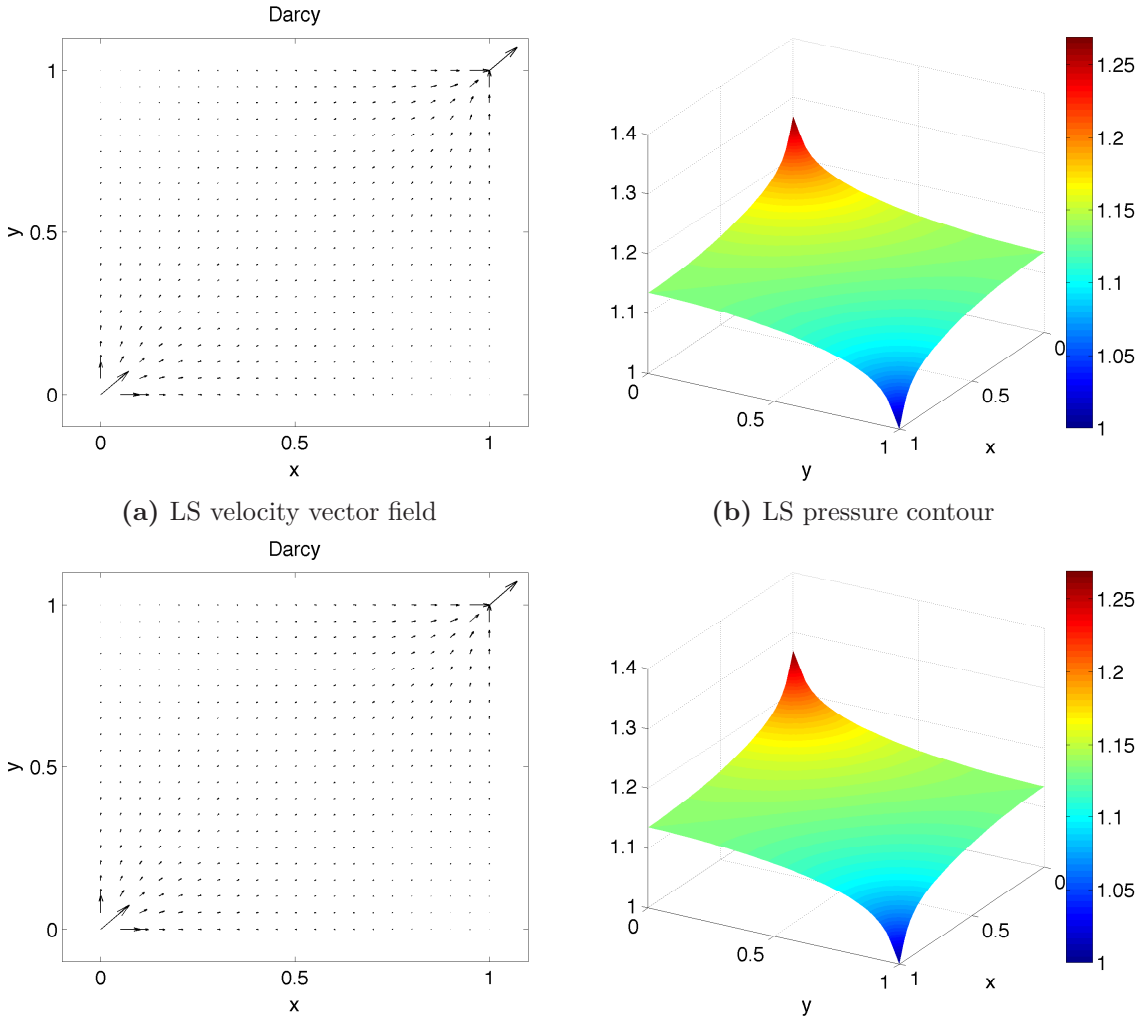

(a) LS velocity vector field

(b) LS pressure contour

(c) VMS velocity vector field

(d) VMS pressure contour

Figure 5.13: Quarter five-spot problem: Q9 solutions for Darcy model

Figure 5.12 depicts the qualitative velocity vector field and the pressure contour. While both formalisms exhibit similar pressure contours, the velocity vector field generated from the LS method exhibits poor dispersion of flow concentration at both wells. Intuitively, the profile of Figure 5.12a makes little to no physical sense so when using the LSFEM, neither Q4 nor any other first order elements can be used to accurately model velocity contours.

However, when higher order elements are used, the LS velocity vector field resembles that of the VMS. Figure 5.13 depicts the results using Q9 elements. It should be noted that the pressure contours remain the same regardless of the element order used. Realistic pressure profiles can be obtained using either formalism or element type, but obtaining

velocity and flow solutions with the LSFEM necessitates the use of Q9 or higher ordered elements.

5.4.1 Least-squares weighting

For all original Darcy model problems up to this point, the non-dimensionalized drag coefficient equals one, so the two possible LS weightings **A** in equation (3.14) would be the same. When $\bar{\alpha}$ no longer equals one, weighting number 2 begins to have a significant impact on the numerical solutions. Herein, the injection pressure shall be obtained using various drag coefficients (all other user-defined parameters are as stated in Table 5.5). The VMS formalism serves as a benchmark for the two LS weightings.

From Table 5.6, it is seen that a divergence in the solutions occurs as the drag coefficient increases. LS formalism using Q9 elements has comparable stiffness to that of VMS formalism using Q4 elements, but as the drag increases, the VMS formalism using Q9 elements requires larger and larger pressures. Nonetheless, all the solutions show a linear relationship between drag and injection pressure. For highly viscous or lowly permeable reservoirs, one has to apply more pressure in order to attain or expect a certain flow. If drag is a function of pressure and/or velocity, one can expect even greater injection pressures.

Table 5.6: Quarter five-spot problem: injection pressure comparison for different LS weightings

$\bar{\alpha}$:	1	20	50	100	250	500	1000
LS weight 1 Q4:	1.26	6.03	12.56	21.57	47.29	91.38	180.57
LS weight 1 Q9:	1.27	6.38	14.44	27.76	67.17	132.63	263.77
LS weight 2 Q4:	1.26	6.19	13.90	26.67	64.43	126.00	244.97
LS weight 2 Q9:	1.27	6.38	14.46	27.92	68.31	135.60	269.37
VMS Q4:	1.27	6.37	14.42	27.84	68.09	135.18	269.37
VMS Q9:	1.27	6.38	14.46	27.93	68.32	135.63	270.27

5.4.2 Comparison of beta coefficients, pressure profiles, and linearization types

This next study shall illustrate the effect the Barus and Forchheimer coefficients have on the pressure profile and convergence of residuals. For pressure dependent viscosities, the Barus coefficient for most oils range between 15 to 35 GPa^{-1} (see reference [58]) which translates to a non-dimensionalized coefficient of roughly 0.001 to 0.004. However, for the

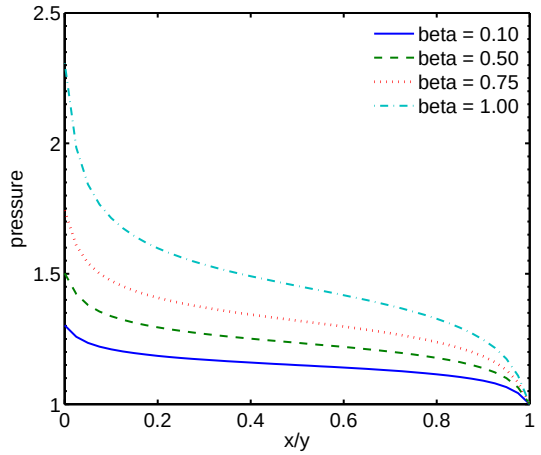

(a) Modified Barus - LS Q9

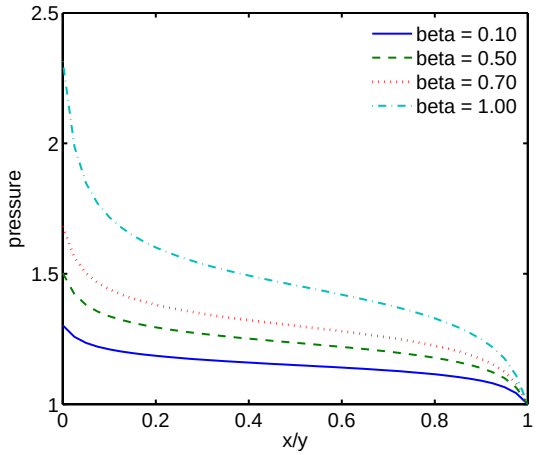

(b) Modified Barus - VMS Q9

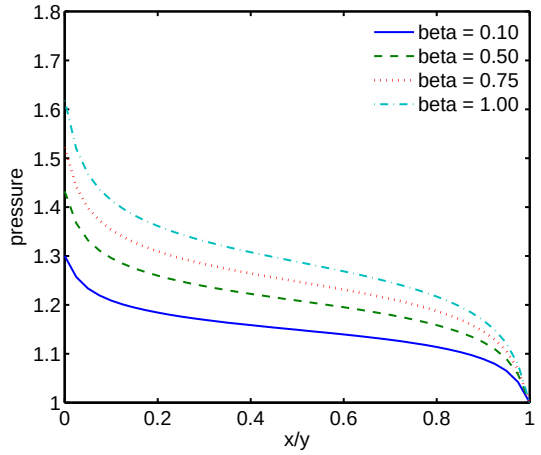

(c) Modified linear - LS Q9

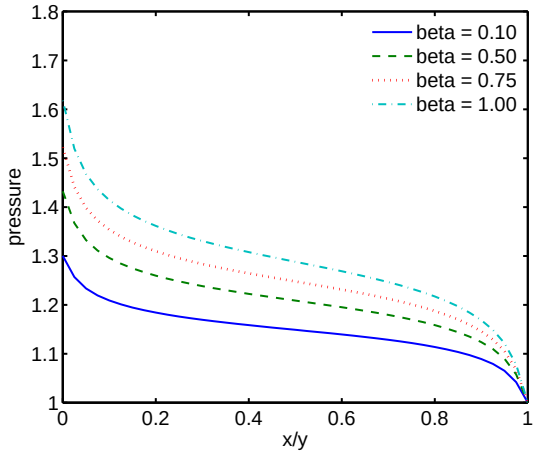

(d) Modified linear - VMS Q9

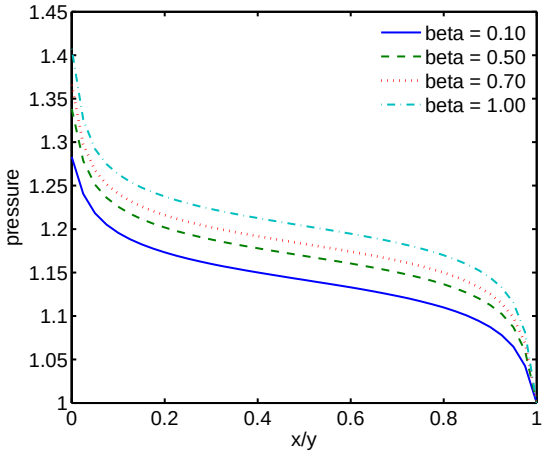

(e) Darcy-Forchheimer - LS Q9

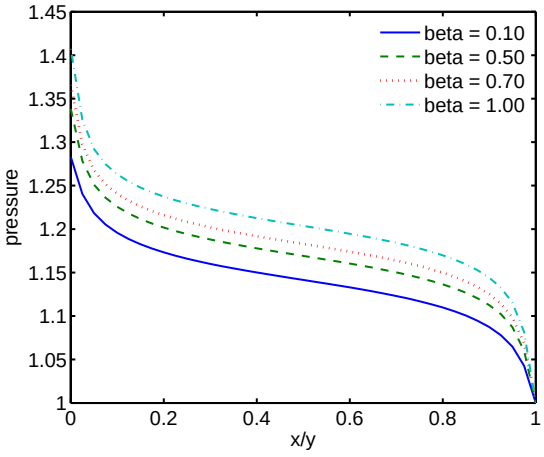

(f) Darcy-Forchheimer - VMS Q9

Figure 5.14: Quarter five-spot problem: pressure profile vs various β_{B} and β_{F}

Table 5.7: Quarter five-spot problem: Picard vs. consistent linearization iteration counts for modified Barus model with $\bar{\beta}_{\mathrm{B}} = 0.6$. The top table corresponds with LS formalism, and the bottom table corresponds with VMS formalism. Q9 elements are used

LS formalism:	Picard's linearization		consistent linearization	
Iteration no. (i)	$\bar{\mathbf{v}}$ residual	$\bar{p}$ residual	$\bar{\mathbf{v}}$ residual	$\bar{p}$ residual
1	1.637285e+01	2.793981e-01	1.637323e+01	2.853694e-01
2	6.735667e-04	6.821094e-03	1.578203e-02	6.444641e-02
3	8.721274e-05	1.096770e-03	7.696835e-04	1.025242e-02
4	8.150045e-06	1.225905e-04	7.976516e-07	2.339612e-05
5	5.881603e-07	1.019954e-05	2.200057e-10	8.554086e-09
6	3.455235e-08	6.755041e-07	5.434345e-14	3.075479e-12
7	1.712434e-09	3.720906e-08		
8	7.340079e-11	1.755375e-09		
9	2.770668e-12	7.240625e-11		

VMS formalism:	Picard's linearization		consistent linearization	
Iteration no. (i)	$\bar{\mathbf{v}}$ residual	$\bar{p}$ residual	$\bar{\mathbf{v}}$ residual	$\bar{p}$ residual
1	6.474444e-02	1.376963e-01	2.086226e-01	1.376963e-01
2	5.513505e-03	3.454112e-03	1.506223e-01	3.675604e-02
3	4.187925e-04	5.555865e-04	4.681837e-03	1.500411e-02
4	2.726750e-05	6.208117e-05	6.326269e-06	9.377515e-05
5	1.551030e-06	5.160684e-06	9.996752e-10	5.528937e-08
6	7.728631e-08	3.412260e-07	1.985333e-13	1.116834e-11
7	3.389569e-09	1.874543e-08		
8	1.318682e-10	8.807571e-10		

purpose of this experiment, much higher Barus coefficients shall be used. The same Barus coefficients used will also be used for the Forchheimer coefficients. The relationship between the coefficients and the number of iterations needed to converge the residuals will also be shown for both linearization types.

Figure 5.14 depicts the pressure profile diagonally across the quarter region. Various beta values were used for the modified Barus, modified linear, and Darcy-Forchheimer models (assume both $\bar{\beta}_{\mathrm{B}}$ and $\bar{\beta}_{\mathrm{F}}$ to be denoted by the same $\bar{\beta}$). Overall the LS and VMS formalisms generate similar results. As the coefficient $\bar{\beta}$ increase, the pressure gradients at the two wells steepen. The modified Barus model exhibits the steepest gradients which is expected. The Darcy-Forchheimer solutions also exhibit increases in the injection pressure, but the qualitative nature of the pressure gradients near the wells are slightly different.

Table 5.8: Quarter five-spot problem: iterations needed vs. $\bar{\beta}$ for Picard ($\vartheta = 0$) and consistent ($\vartheta = 1$) linearization

$\bar{\beta}$:	0.2	0.4	0.6	0.8	1.0
LS Q9 elements:					
MB $\vartheta = 0$	6	7	9	10	13
MB $\vartheta = 1$	4	5	6	6	7
ML $\vartheta = 0$	6	7	7	8	8
ML $\vartheta = 1$	4	4	5	5	5
F $\vartheta = 0$	7	8	9	10	12
F $\vartheta = 1$	5	5	5	5	5
VMS Q9 elements:					
MB $\vartheta = 0$	6	7	8	10	13
MB $\vartheta = 1$	5	5	6	Inf	Inf
ML $\vartheta = 0$	6	7	7	8	8
ML $\vartheta = 1$	4	5	5	5	5
F $\vartheta = 0$	8	10	12	14	16
F $\vartheta = 1$	5	5	5	5	6

Because the modified and Darcy-Forchheimer models rely on two separate non-Darcy coefficients and two different dependent variables, no true comparisons can be drawn. In the next Chapter however, distinction of results from pressure dependent and velocity dependent drag coefficients will become more evident.

It should be noted that the pressure profiles in Figure 5.14 were generated using Picard's linearization (i.e. $\vartheta = 0$). While Picard's and consistent linearization theoretically yield the same results, the residual convergence schemes differ. Table 5.7 contains the iteration count and residual norms for the modified Barus model evaluated at $\bar{\beta}_{\mathrm{B}} = 0.6$. Consistent linearization exhibits terminal quadratic convergence whereas Picard's linearization exhibits terminal linear convergence. For small Barus and Forchheimer coefficients, either linearization type will only require a few iterations but as the non-linearity increases, so does the difference in iteration counts as shown in Table 5.8. If the coefficients are high enough, Picard's linearization may never reach terminal convergence so it is more convenient to use consistent linearization.

However, for VMS formalism the modified Barus model consistent linearization fails to converge for $\bar{\beta}_{\mathrm{B}}$ coefficients of 0.6 and higher. It should also be noted that neither Picard's linearization nor the LS formalism have this problem. In previous literature it has been well established that high $\bar{\beta}_{\mathrm{B}}$ coefficients or pressures may render the Barus formula useless so

one must be well aware of all the conditions and parameters needed to run any simulation. One can avoid ill-condition stiffness matrices and improve residual convergence schemes by precondition the resulting linear equations at each iteration. Employing a finer mesh will also help avoid singularities in the finite element analysis.

5.4.3 Modified Darcy-Forchheimer numerical results

So far it has been established in this chapter that quadratic elements and LS weight 2 are preferred for the LS formalism. Numerical simulations have also shown that high Barus and Forchheimer coefficients yield results that differ quantitatively from the original Darcy model. This next example shall study the effects of combining the Darcy models and employs a finer mesh.

Table 5.9: User-defined inputs for the quarter five-spot problem: all Darcy models

Parameter	Value
$\bar{\beta}_{\mathrm{B}}$	0.5
$\bar{\beta}_{\mathrm{F}}$	0.5
$\bar{k}$	1
$\bar{\mu}_0$	1
$\bar{\rho}$	1
$\bar{\mathbf{b}}$	0
Element type	Q9
$Nele$	900
$\bar{p}(1,1)$	1
$\bar{\mathbf{v}}(0,0)$, $\bar{\mathbf{v}}(1,1)$	$\begin{Bmatrix} 1 \\ 1 \end{Bmatrix}$

Using the parameters given in Table 5.9, the pressure contours for both the LS and VMS formalisms are shown in Figures 5.15 and 5.16 respectively. Comparing the Darcy model pressure contours with the ones in Figure 5.13, it can be seen that refining the mesh lowers the required injection pressure. For problems where flow quantities are fixed, coarse meshes over predict the injection pressure needed. The Barus, linear, and Forchheimer models all predict pressures greater than that of the original Darcy model, but when one employs the modified Darcy-Forchheimer models, even higher pressures are depicted. The original Darcy model under predicts the amount of pressure required so it is important to use the modified Darcy-Forchheimer models to visualize the pressure contours.

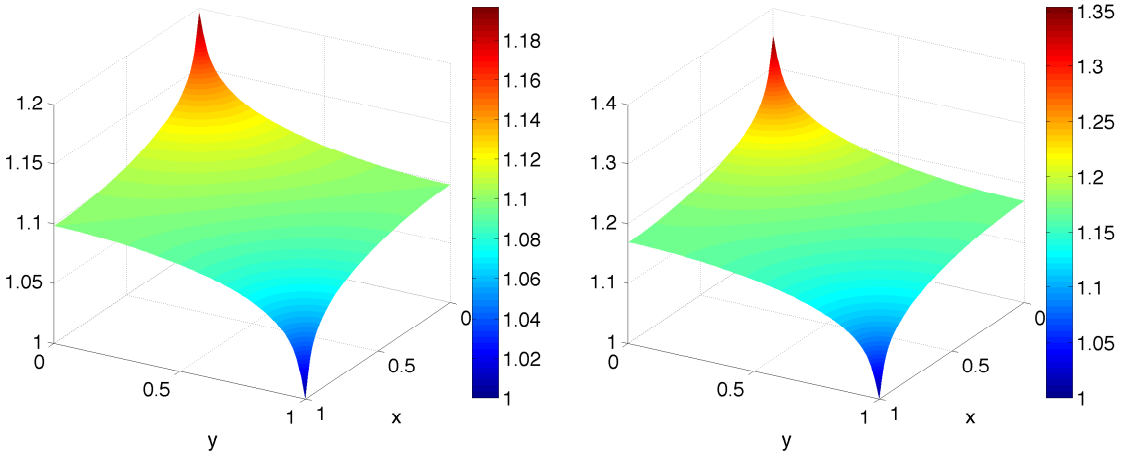

(a) Darcy model

(b) Modified Barus

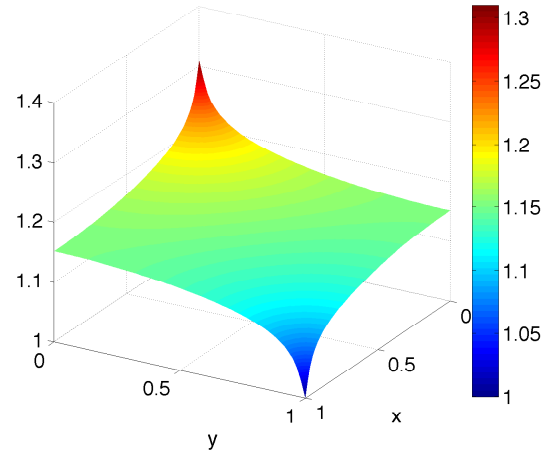

(c) Modified linear

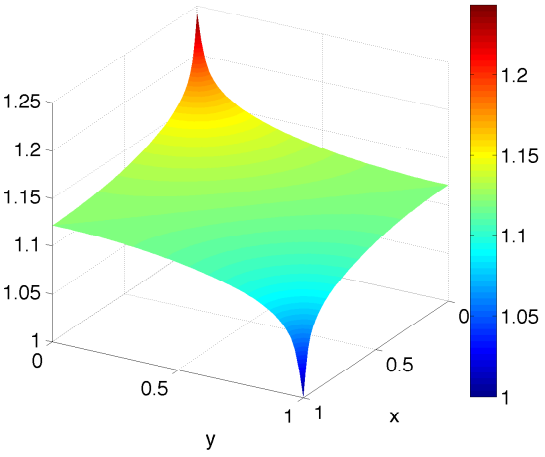

(d) Darcy-Forchheimer

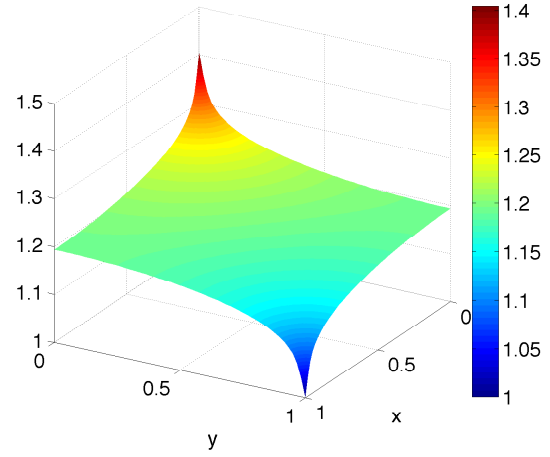

(e) Modified Darcy-Forchheimer Barus

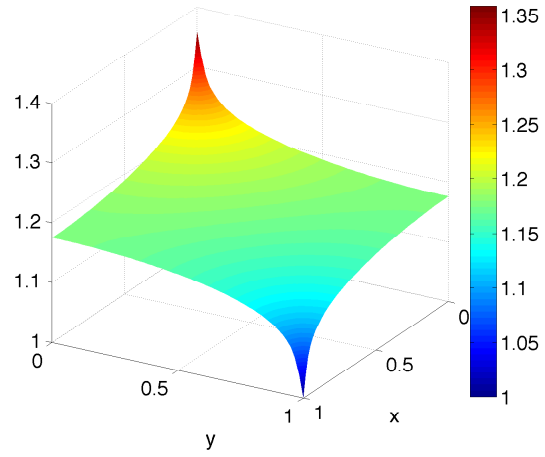

(f) Modified Darcy-Forchheimer linear

Figure 5.15: Quarter five-spot problem: pressure contours using LS formalism

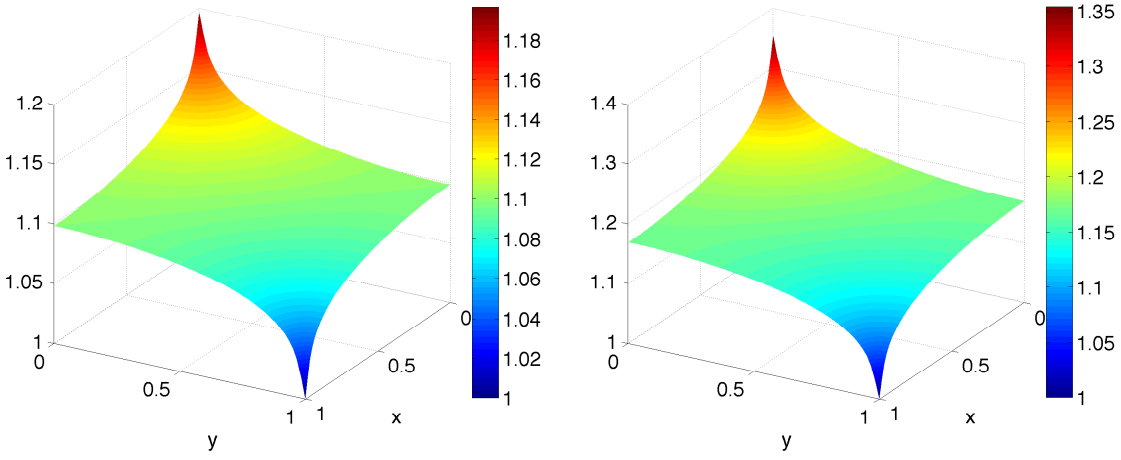

(a) Darcy model

(b) Modified Barus

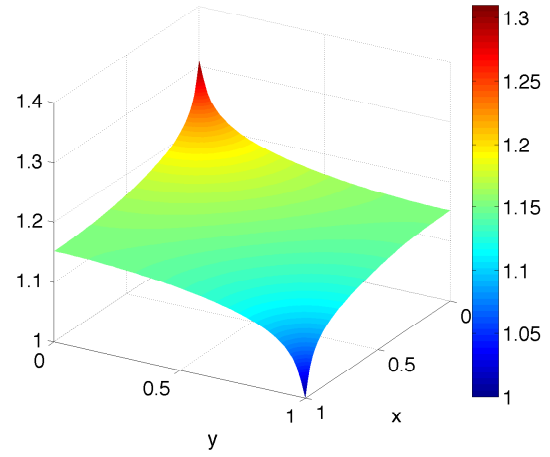

(c) Modified linear

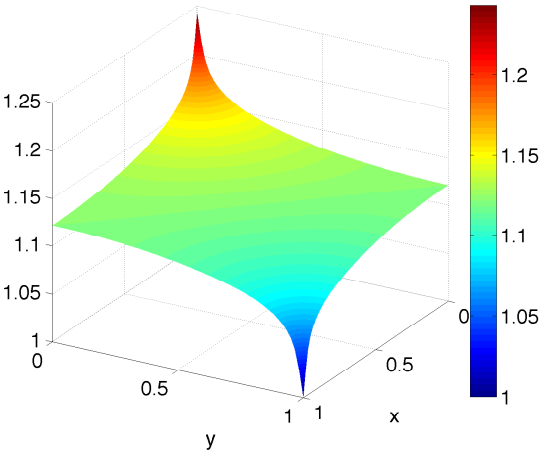

(d) Darcy-Forchheimer

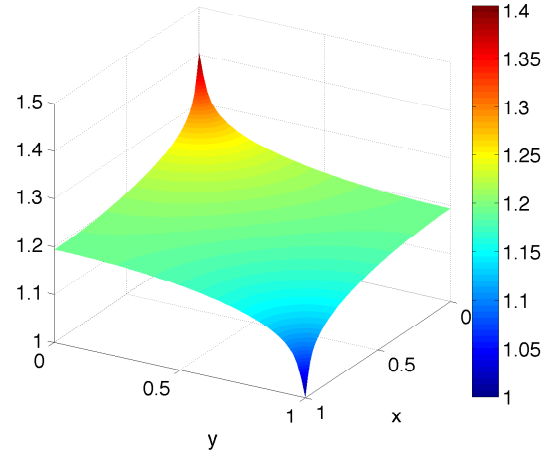

(e) Modified Darcy-Forchheimer Barus

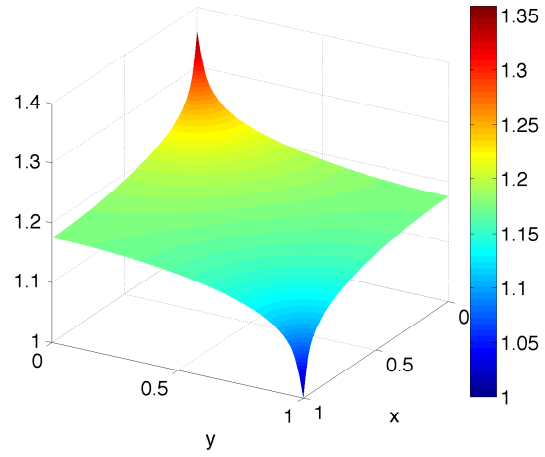

(f) Modified Darcy-Forchheimer linear

Figure 5.16: Quarter five-spot problem: pressure contours using VMS formalism

Chapter 6. Enhanced oil recovery applications

It has been shown in the previous chapter that the FEM performs well for the benchmark tests and that various modifications to the Darcy model have a significant impact on the results. This chapter focuses on relevant enhanced oil recovery applications which are more complex by nature. Pressure contours of the reservoirs, flow rates from the production wells, and errors in the local mass balance shall be presented.

6.1 OIL RESERVOIR PROBLEM

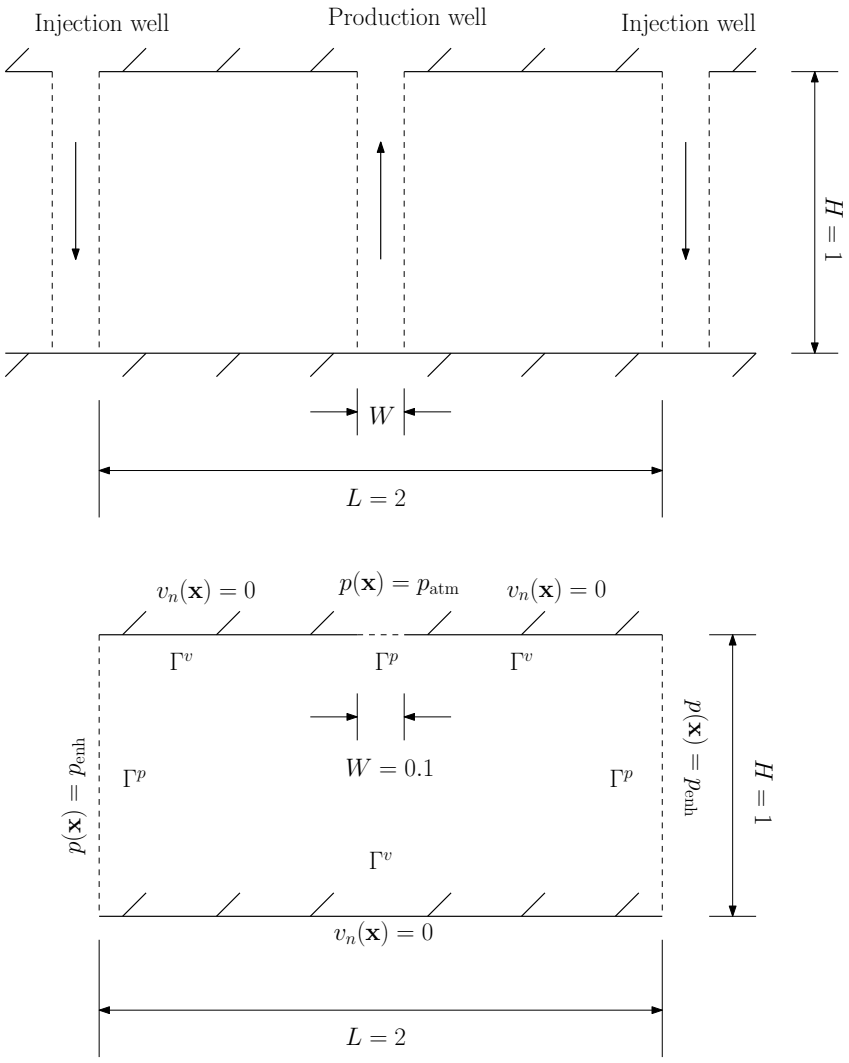

Figure 6.1: Oil reservoir problem. Top figure is the pictorial description, bottom figure is the idealized computational domain with appropriate boundary conditions

For high pressure applications like enhanced oil recovery, one is interested in the quantitative and qualitative nature of the pressure contours and velocities within the oil reservoir. The pictorial description of a typical oil reservoir is depicted in Figure 6.1. Injection wells are located on either side the production well, and carbon- dioxide is pumped into the reservoir to ease the extraction of raw oil through the production well. The parameters used for this study are listed in Table 6.1. All Darcy models and finite element formulations are expected to yield differing flows, but the general qualitative velocity vector can be depicted in Figure 6.2. As the oil fluid nears the production well, the Darcy velocities increases.

Table 6.1: User-defined inputs for the oil reservoir problem

Parameter	Value
$\bar{\beta}_{\mathrm{B}}$	0.005
$\bar{\beta}_{\mathrm{F}}$	0.01
$\bar{k}$	1
$\bar{\mu}_0$	1
$\bar{\rho}$	1
ϑ	1
$\bar{\mathbf{b}}(\mathbf{x})$	$\begin{Bmatrix} 0 \\ -1 \end{Bmatrix}$
Element type	Q9
$Nele$	1600
$\bar{p}_{\mathrm{enh}}$	1000

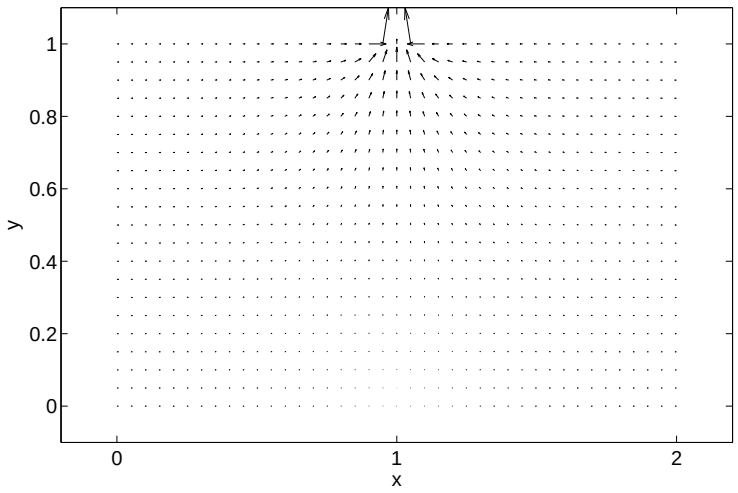

Figure 6.2: Oil reservoir problem: qualitative velocity vector field

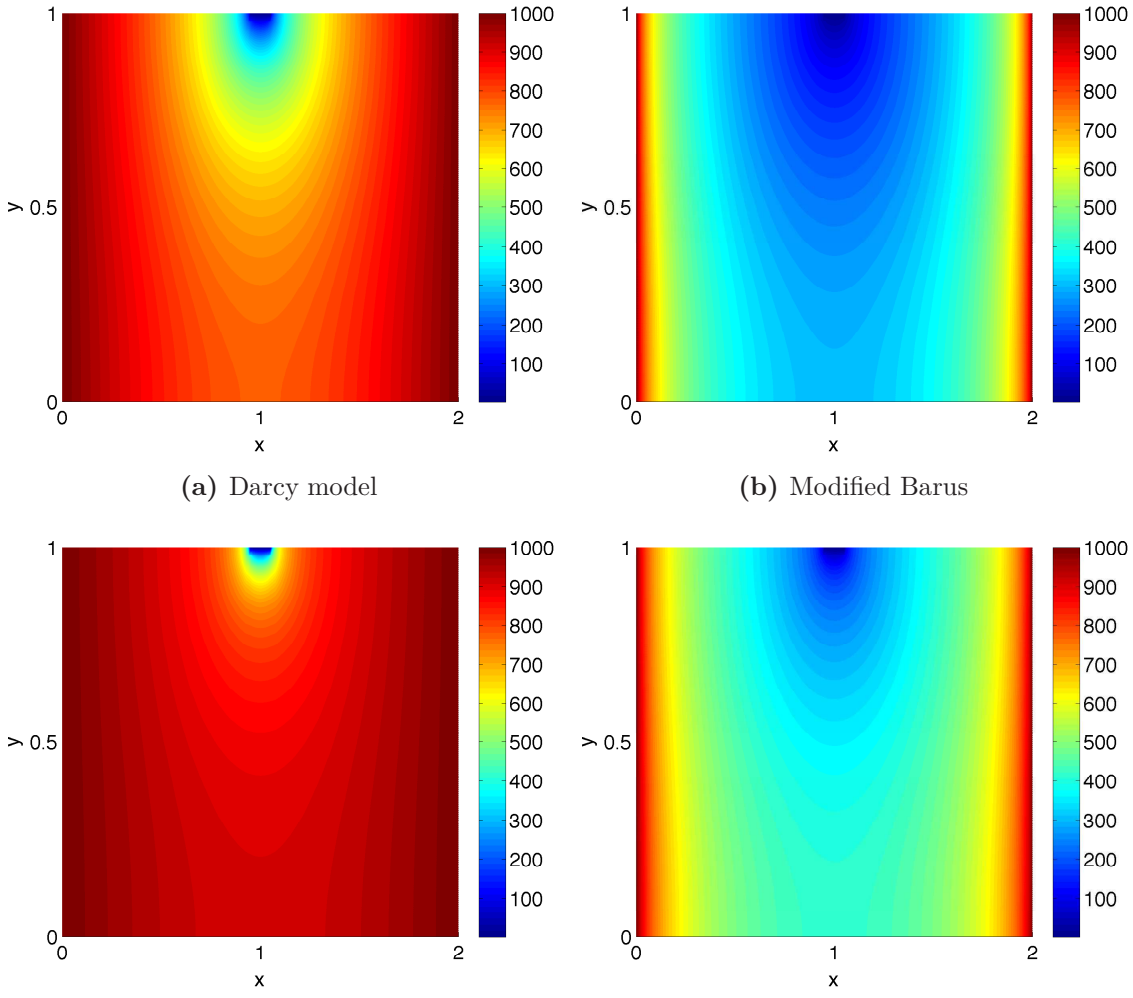

(a) Darcy model

(b) Modified Barus

(c) Darcy-Forchheimer

(d) Modified Darcy-Forchheimer Barus

Figure 6.3: Oil reservoir problem: pressure contours using LS formalism

6.1.1 Pressure contours

Pressure contours within the oil reservoirs are important to know because high pressures can result in cracking of the solid. Figures 6.3 and 6.4 contain the pressure contours using the LS and VMS formalisms respectively. The Darcy models used throughout this chapter are: original Darcy, modified Barus, Darcy-Forchheimer, and modified Darcy-Forchheimer. It can be seen from each model that the pressure contours within the reservoirs vary both qualitatively and quantitatively. For the Barus model, there are steep pressure gradients near the injection well, and the pressures within the reservoir are generally smaller than that of the Darcy model. However, the Darcy-Forchheimer models

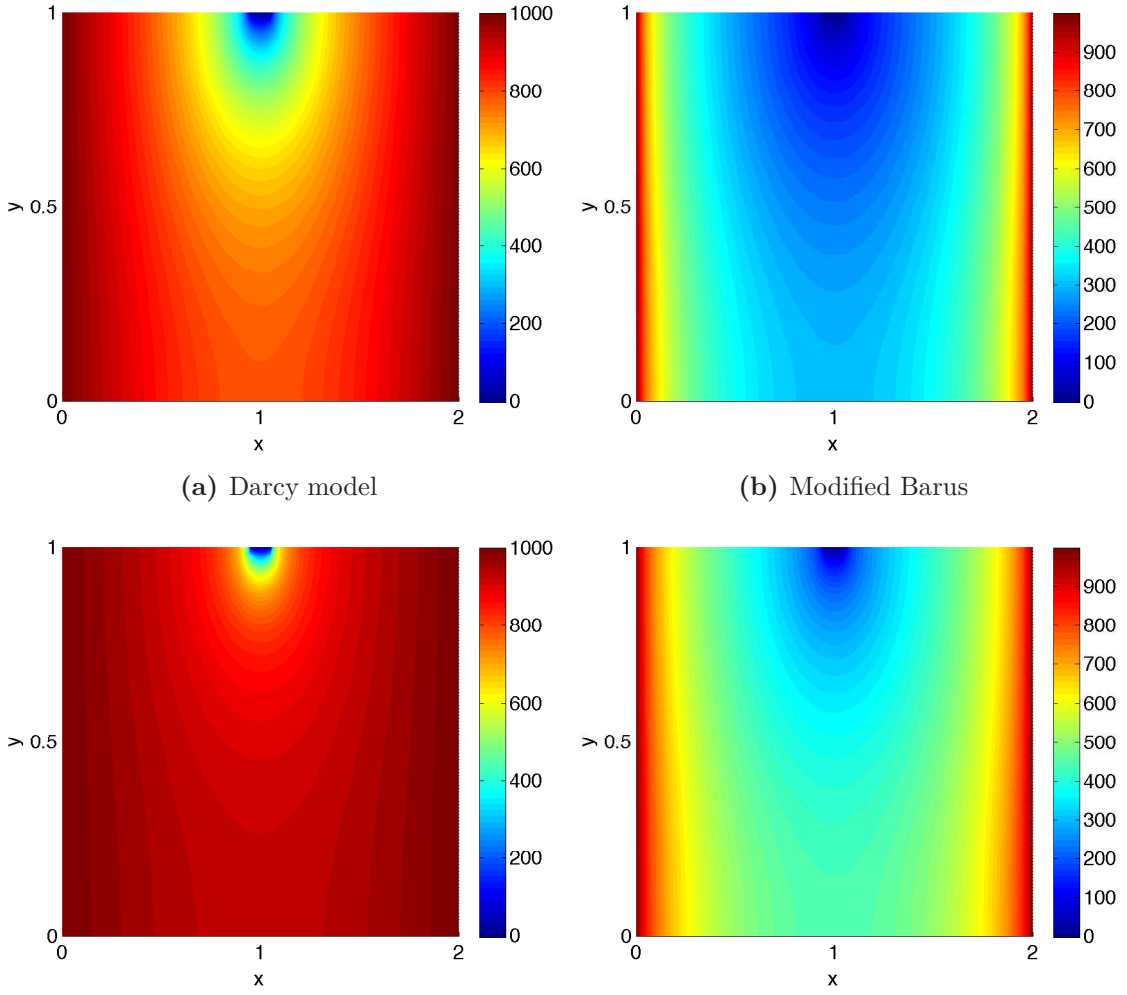

(a) Darcy model

(b) Modified Barus

(c) Darcy-Forchheimer

(d) Modified Darcy-Forchheimer Barus

Figure 6.4: Oil reservoir problem: pressure contours using VMS formalism

exhibits steep pressure gradients near the production well, thus predicting higher pressures throughout the reservoir. While pressure dependent viscosity may yield favorable pressure contours, one has to account for increases in pressure due to inertial effects, so combining the Barus and Forchheimer models should yield the most accurate results. Figure 6.5 depicts the pressure profiles of all models and formalisms at the top most interface of the reservoir.

It should be noted that there are some minor differences in the pressure profiles between the LS and VMS formalisms. While both formalisms have strongly prescribed velocity boundary conditions, the VMS boundary condition for pressures are weakly prescribed and

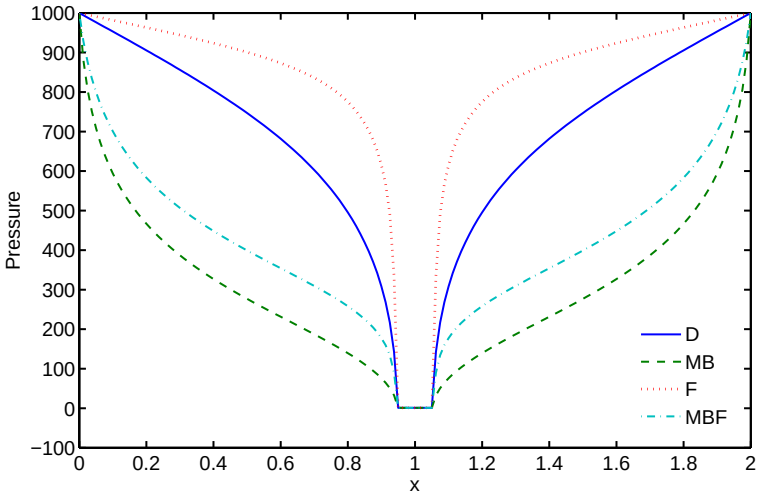

(a) LS formalism

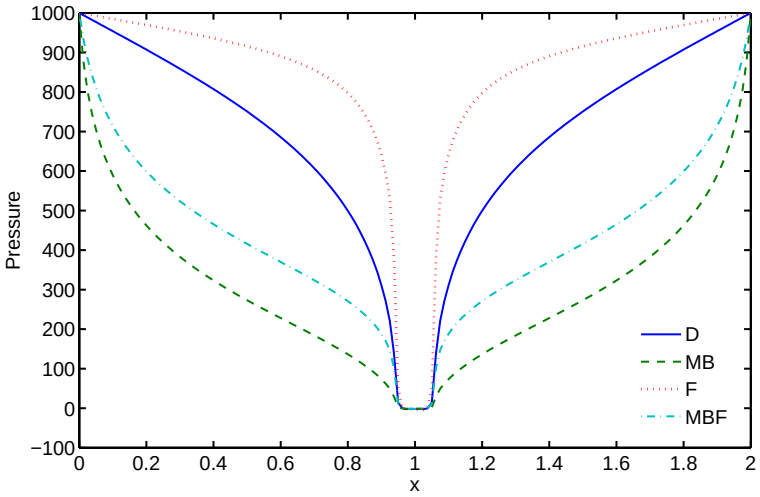

(b) VMS formalism

Figure 6.5: Oil reservoir problem: comparison of pressure profiles at $y = 1$

consequently exhibit some oscillations. The oscillations diminish with mesh refinement, but one must recognize the potential ramifications oscillatory boundary conditions may have on the solutions, especially for more complex prescribed pressures.

6.1.2 Flow rates and local mass balance errors

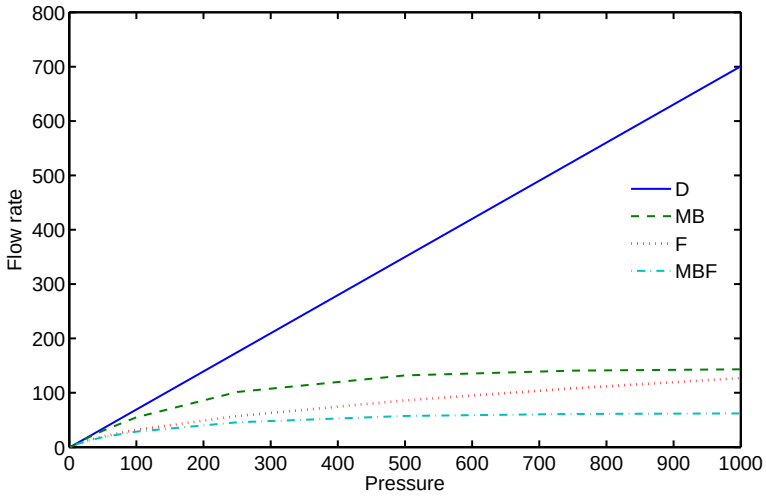

(a) LS formalism

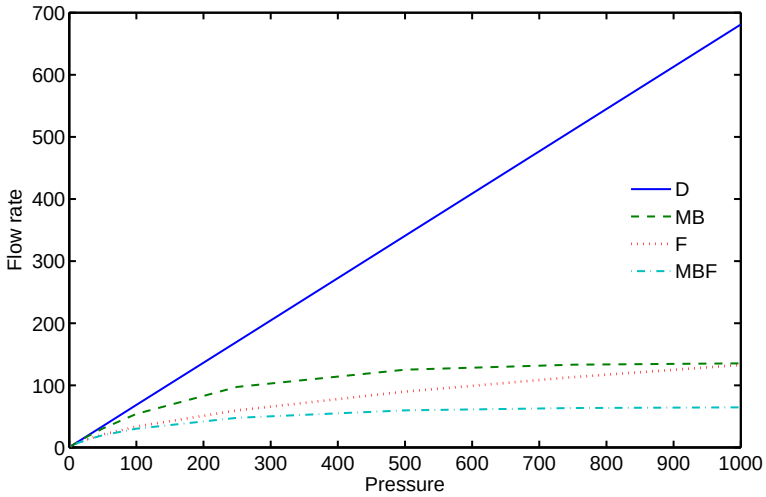

(b) VMS formalism

Figure 6.6: Oil reservoir problem: comparison of injection pressures vs. flow rates

In reservoir simulations, another quantity of interest is the outflow of raw oil. The flow rate or total flux at the production well is calculated using

$$\int_{\Gamma^p} \bar{\mathbf{v}} \cdot \hat{\mathbf{n}} \, \mathrm{d}\Gamma, \tag{6.1}$$

where Γ^p corresponds with the prescribed atmospheric pressure boundary. In Figure 6.6, a comparison of flow rates versus prescribed pressures is shown for both formalisms. The

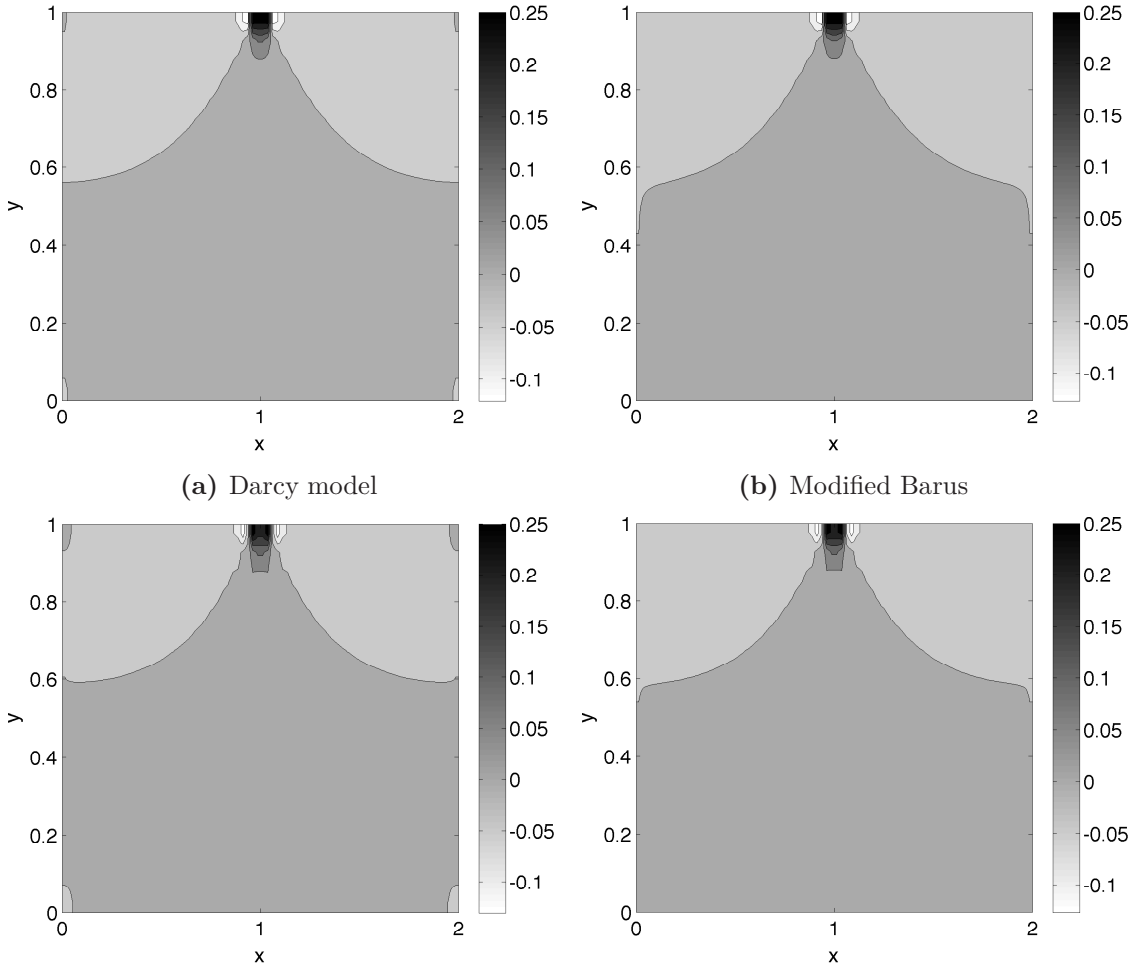

(a) Darcy model

(b) Modified Barus

(c) Darcy-Forchheimer

(d) Modified Darcy-Forchheimer Barus

Figure 6.7: Oil reservoir problem: ratios of local mass balance error over total predicted flux using LS formalism

original Darcy models predict a linear relationship between prescribed pressures and flow rates but the non-linear Darcy models exhibit ceiling fluxes. As the pressure increases, the original Darcy models becomes increasingly unreliable as it over predicts the amount of oil production one can expect. It is interesting to note that for both the Darcy and Barus models, the LS formalism predicts higher flows for a fixed injection pressure whereas the VMS formalism predicts higher Forchheimer flow rates. Nevertheless, the ceiling fluxes for the Barus and Forchheimer models differ for various betas, but combining the two models will always yield smaller flow rates.

As stated in Chapter 1, neither the LS nor VMS formalisms have local mass conservation. The ratios of local mass balance errors over the total predicted flux for LS and

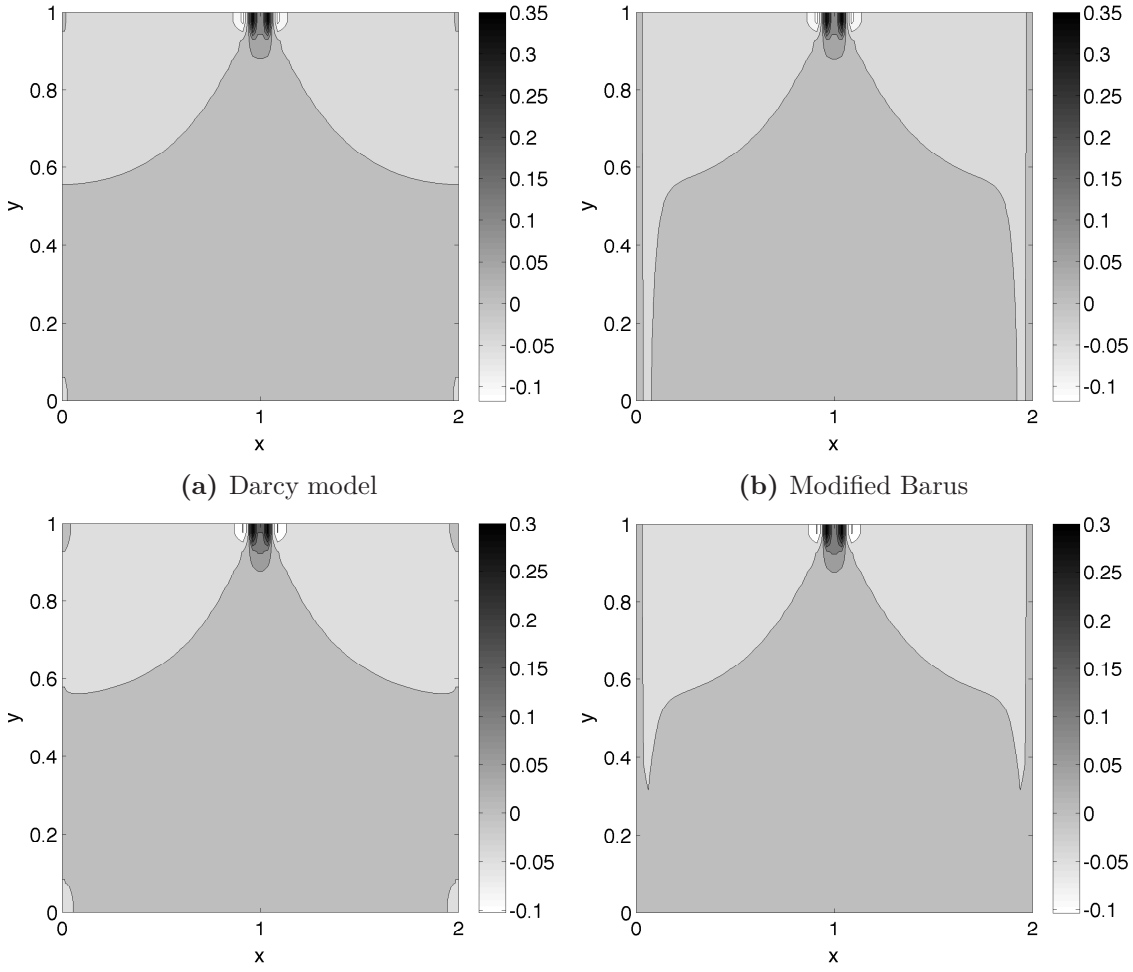

(a) Darcy model

(b) Modified Barus

(c) Darcy-Forchheimer

(d) Modified Darcy-Forchheimer Barus

Figure 6.8: Oil reservoir problem: ratios of local mass balance error over total predicted flux using VMS formalism.

VMS formalisms are shown in Figures 6.7 and 6.8 respectively. While the ratios are approximately the same for all models, it should be noted that the greater the velocities, the greater the local mass balancing error. The results show that all models exhibit the greatest errors near the production wells. It is interesting to note that while both formalisms predict roughly the same velocity flow rates, the VMS formalism shows greater local mass balancing error. Ratios of 0.25-0.35 are considered quite large, but for lower pressure and velocity applications, the ratios should be much smaller.

6.2 MULTILAYER RESERVOIR PROBLEM

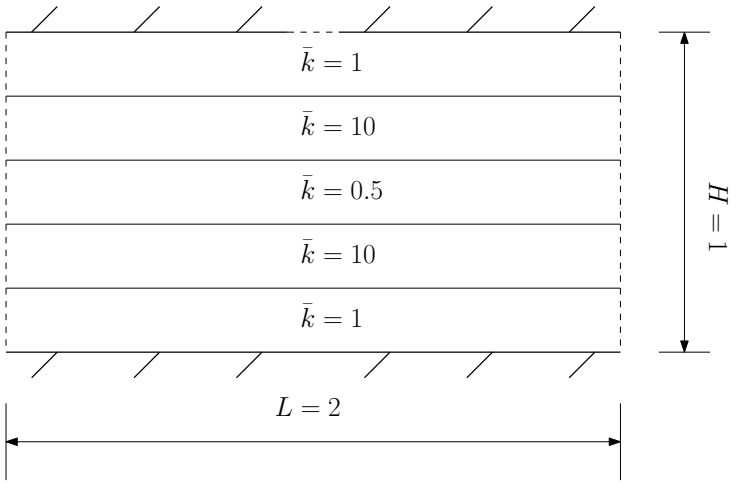

Figure 6.9: Layered reservoir problem: A pictorial description.

One may not always encounter constant permeability within the subsurface. Some layers within the oil reservoir may consist of coarse sands while others may consist of less permeable material. This numerical experiment shall study the effect varying permeability regions has on the pressure contours, flow rates, and local mass balance errors. Consider the domain depicted in Figure 6.9 with the same boundary conditions as that in Figure 6.1. Regions with higher permeability have larger velocities as depicted in Figure 6.10. The parameters used for this problem are listed in Table 6.2, and the pressure contours for LS and VMS formalisms are depicted in Figures 6.11 and 6.12 respectively.

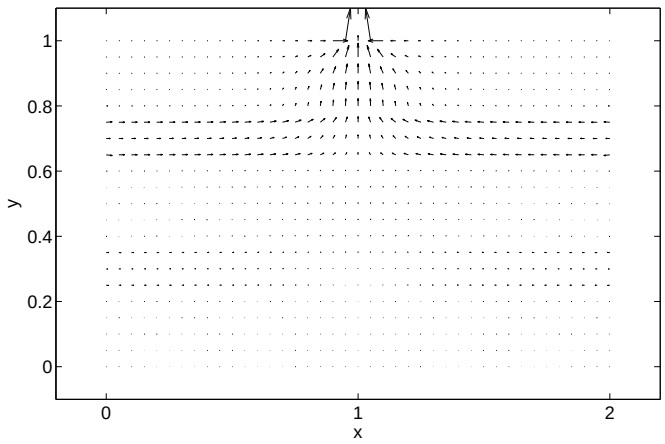

Figure 6.10: Layered reservoir problem: qualitative velocity vector field

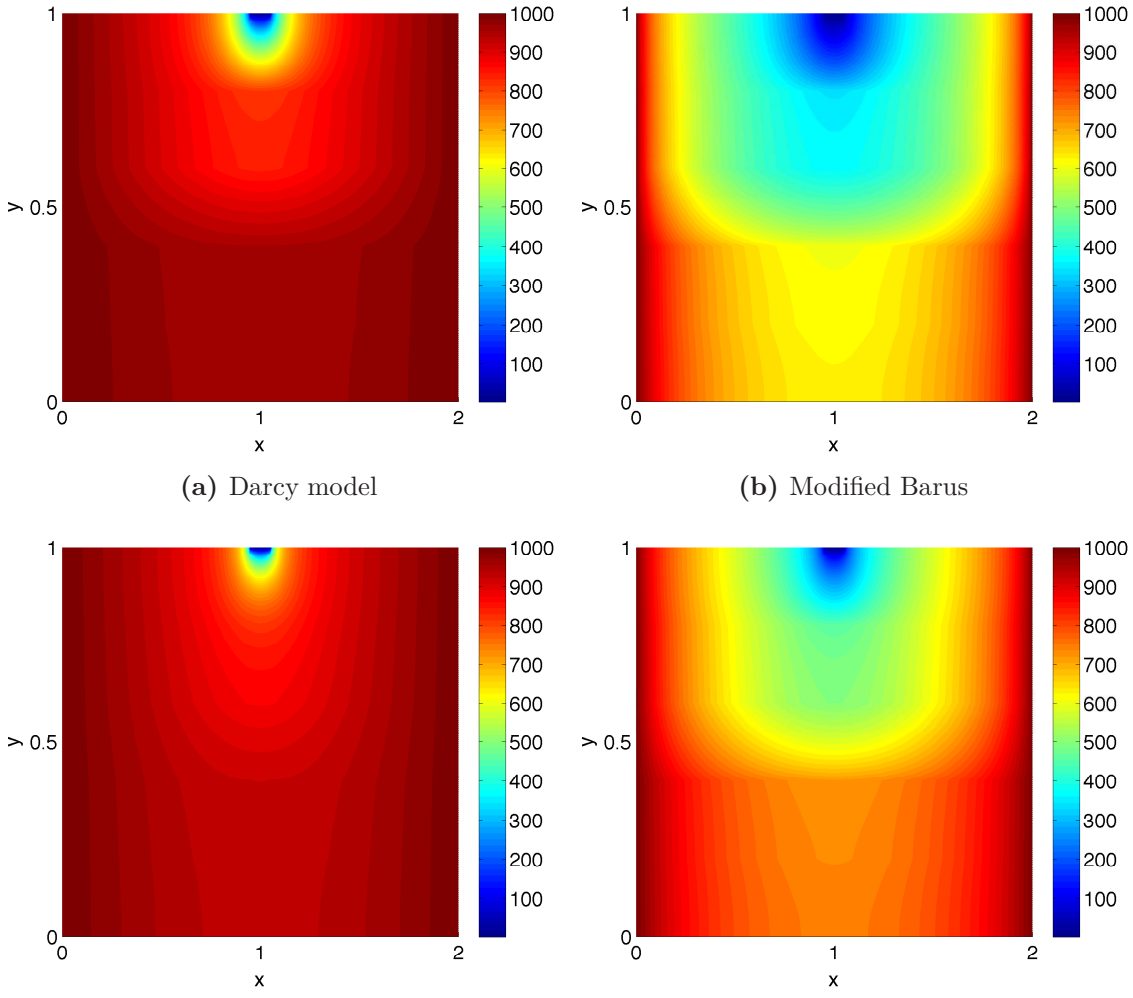

(a) Darcy model

(b) Modified Barus

(c) Darcy-Forchheimer

(d) Modified Darcy-Forchheimer Barus

Figure 6.11: Layered reservoir problem: pressure contours using LS formalism

Table 6.2: User-defined inputs for the layered reservoir problem

Parameter	Value
$\bar{\beta}_{\mathrm{B}}$	0.005
$\bar{\beta}_{\mathrm{F}}$	0.01
$\bar{k}$	varies
$\bar{\mu}_0$	1
$\bar{\rho}$	1
ϑ	1
$\bar{\mathbf{b}}(\mathbf{x})$	$\{0; -1\}$
Element type	Q9
$Nele$	3200
$\bar{p}_{\mathrm{enh}}$	1000

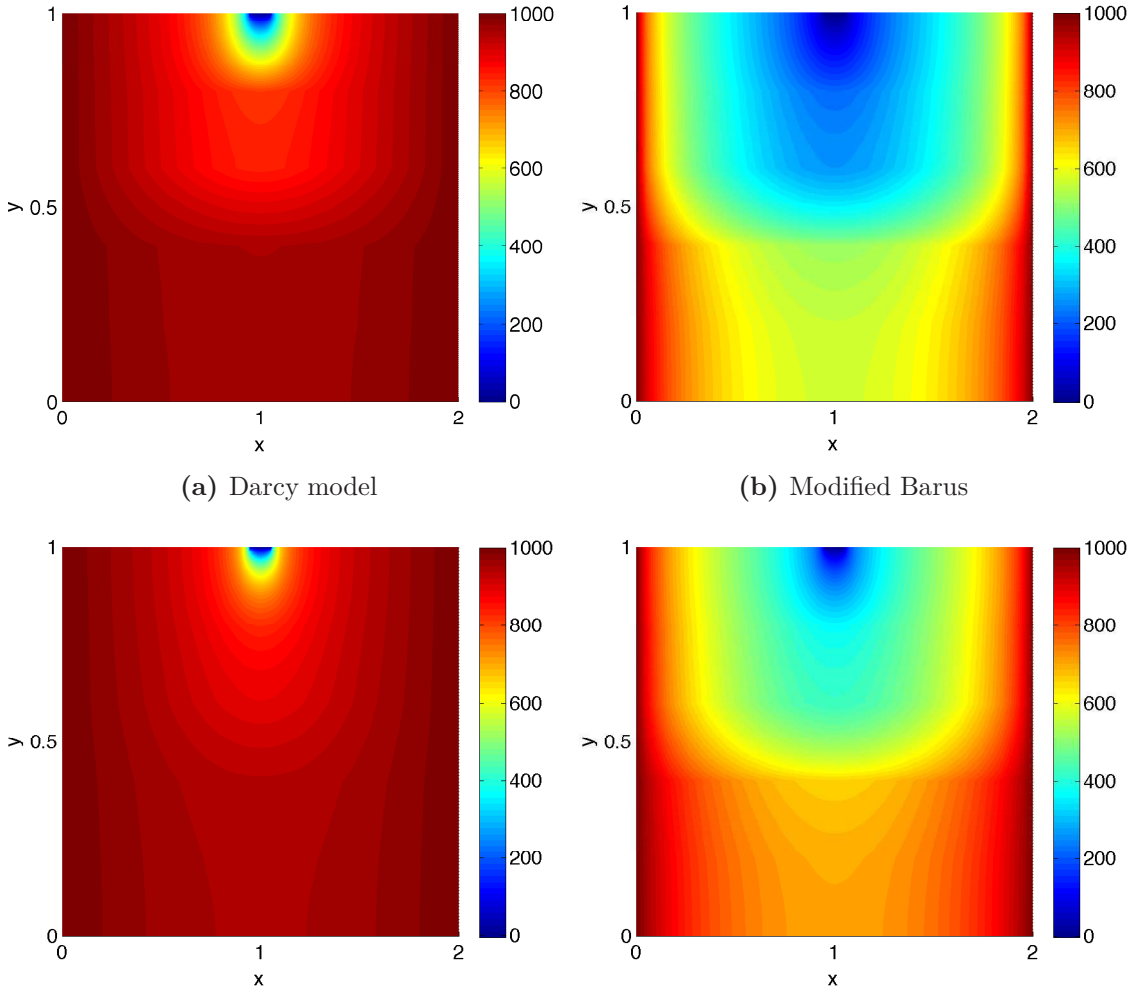

(a) Darcy model

(b) Modified Barus

(c) Darcy-Forchheimer

(d) Modified Darcy-Forchheimer Barus

Figure 6.12: Layered reservoir problem: pressure contours using VMS formalism

It can be seen that layers with higher permeability contain higher pressures and that steep gradients occur at the interfaces between the layers. The LS formalism predicts higher pressures for all Darcy models but also yields larger flow rates as seen from Table 6.3. Like with the previous oil reservoir problem, the VMS formalism also predicts higher fluxes for the Darcy-Forchheimer model. The ratio of local mass balance errors and total predicted fluxes are depicted in Figures 6.13 and 6.14. While the VMS formalisms still have slightly higher errors, the overall error ratios for this problem are smaller despite having larger flow rates

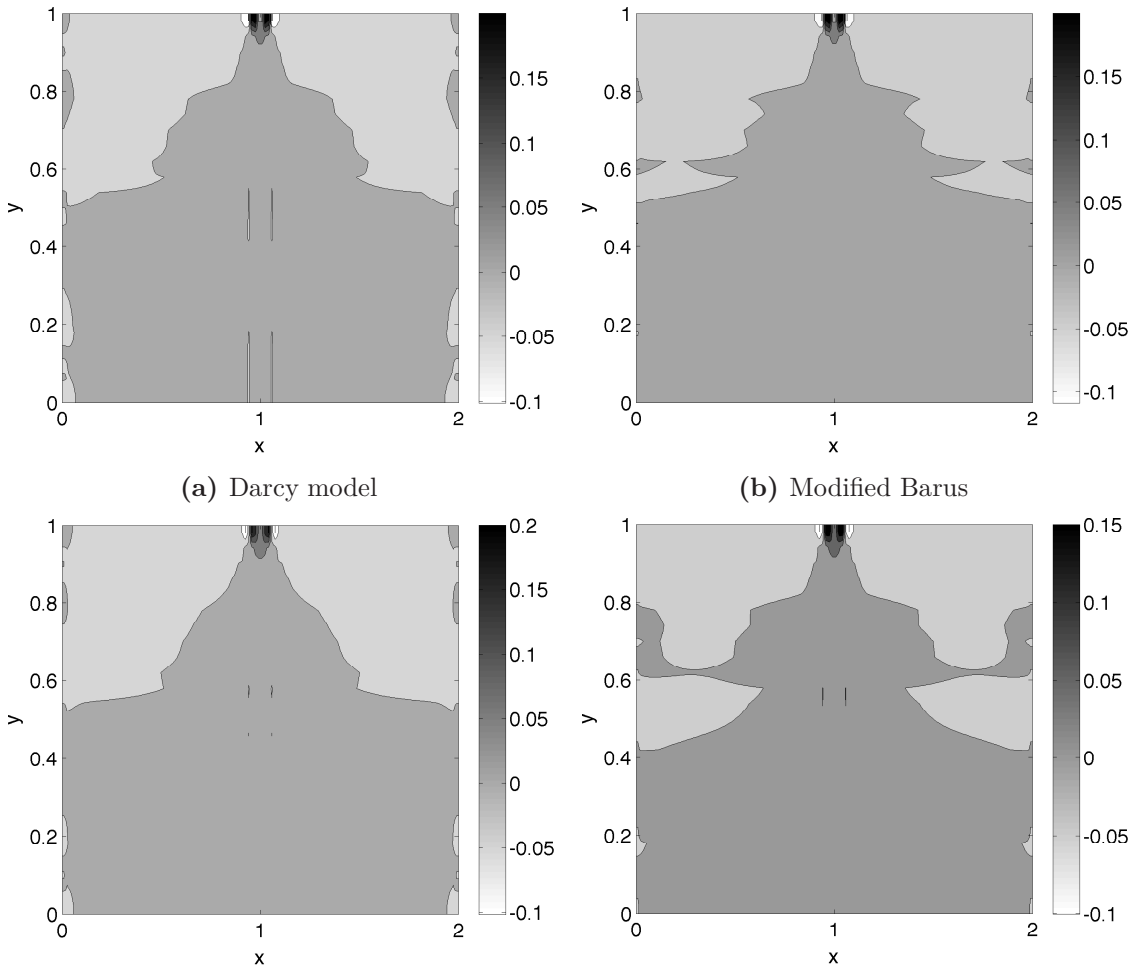

(a) Darcy model

(b) Modified Barus

(c) Darcy-Forchheimer

(d) Modified Darcy-Forchheimer Barus

Figure 6.13: Layered reservoir problem: ratios of local mass balance error over total predicted flux using LS formalism

Table 6.3: Layered reservoir problem: flow rates for LS and VMS formalism at $\bar{p}_{\text{enh}} = 1000$

Darcy models:	D	MB	F	MBF
LS	1038	210	133	75
VMS	1025	204	137	77

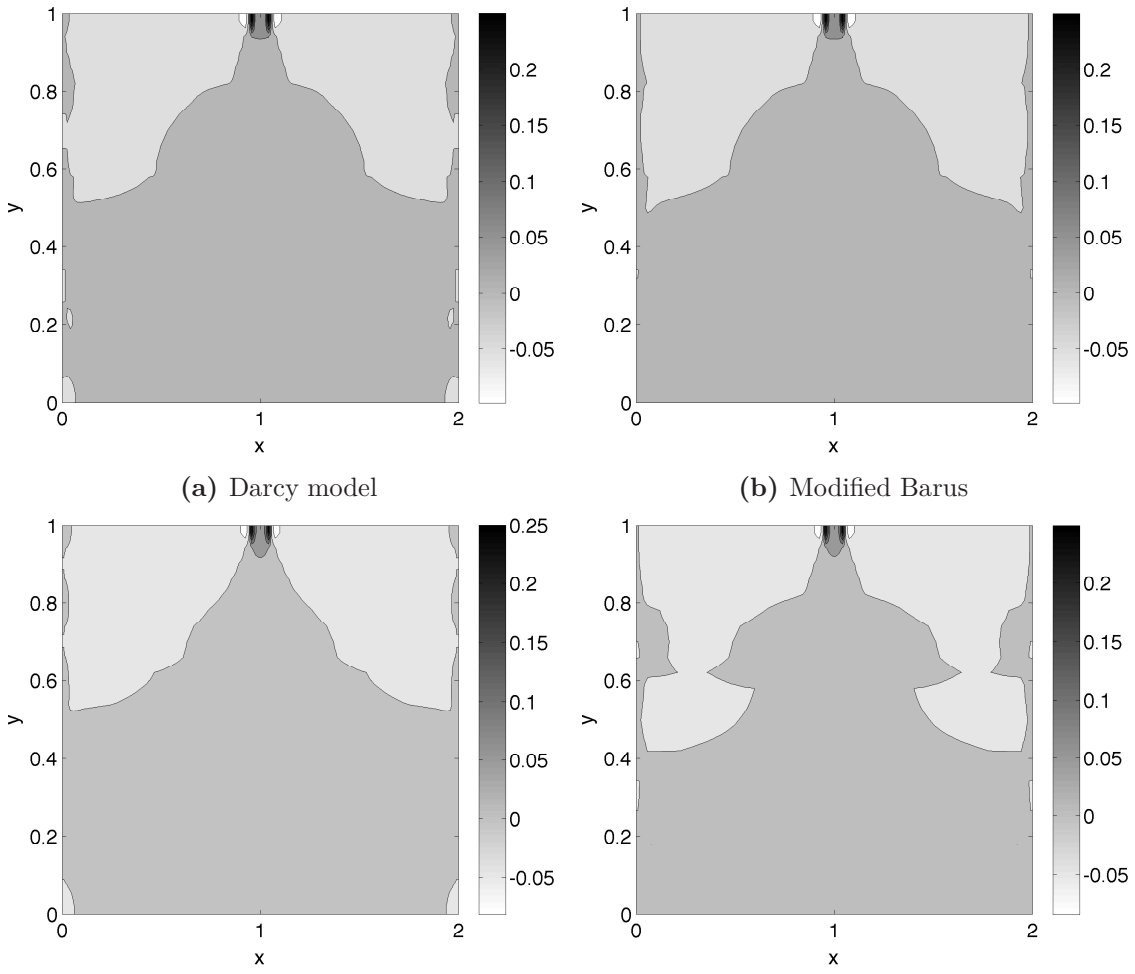

(a) Darcy model

(b) Modified Barus

(c) Darcy-Forchheimer

(d) Modified Darcy-Forchheimer Barus

Figure 6.14: Layered reservoir problem: ratios of local mass balance error over total predicted flux using VMS formalism

6.3 FLOW IN A POROUS MEDIA WITH STAGGERED IMPERVIOUS ZONES

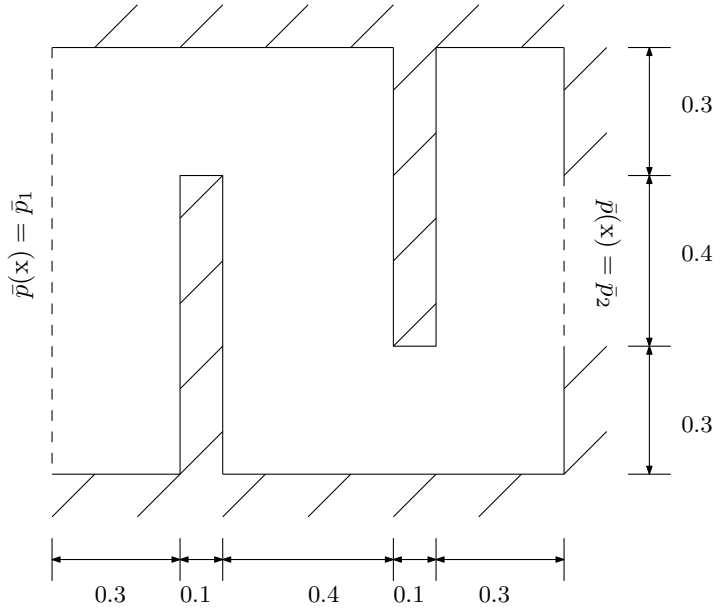

Figure 6.15: Staggered impervious zones problem: a pictorial description

Consider flow through a region with staggered impervious zones in Figure 6.15. In any heterogeneous flow through porous media applications, one may encounter domains where oil must flow through a complex domain with many impervious regions. The qualitative velocity vector field in Figure 6.16 indicates that higher flows occur around the sharp bends.

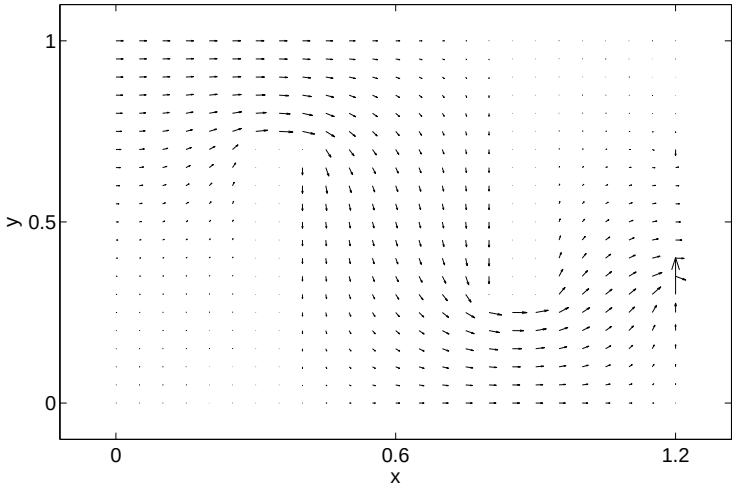

Figure 6.16: Staggered impervious zones problem: qualitative velocity vector field

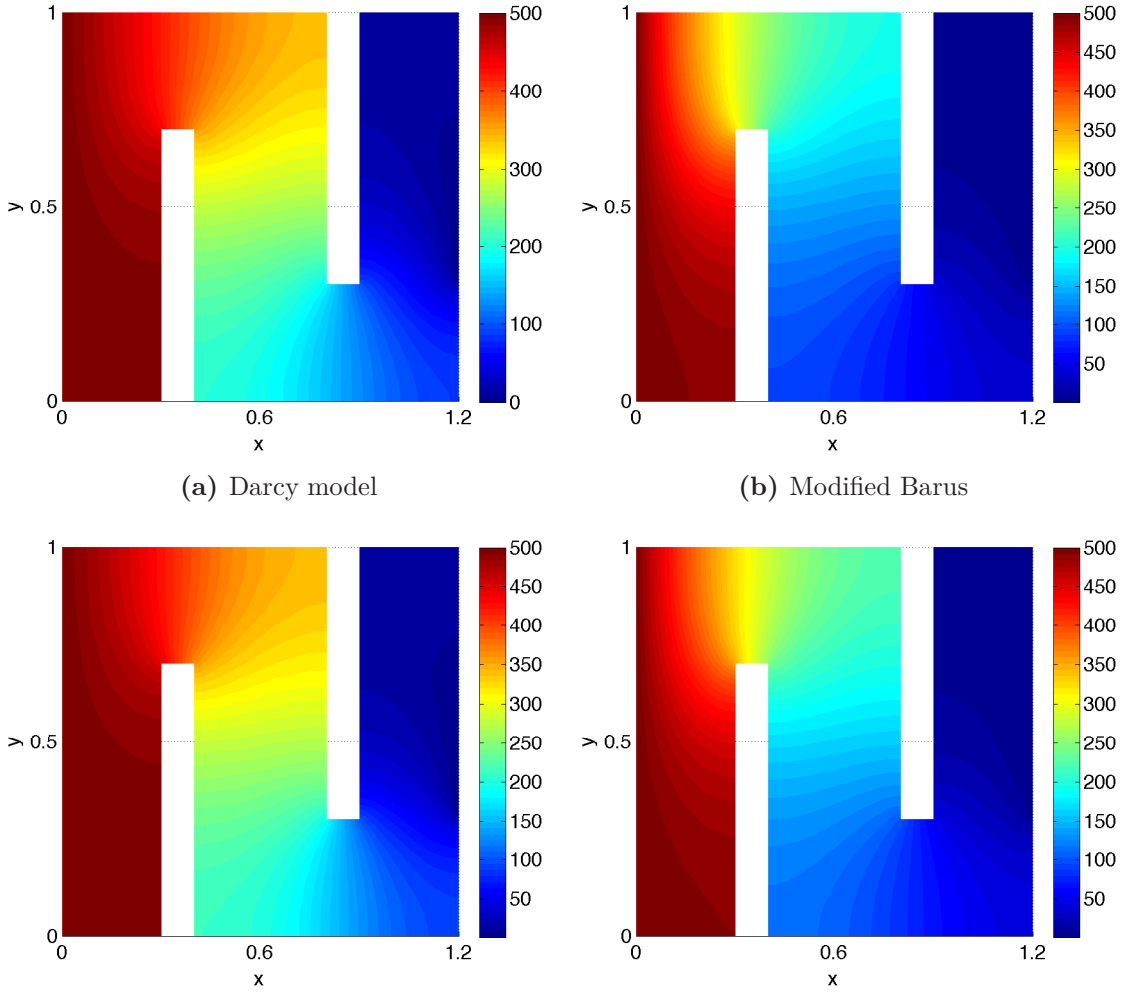

(a) Darcy model

(b) Modified Barus

(c) Darcy-Forchheimer

(d) Modified Darcy-Forchheimer Barus

Figure 6.17: Staggered impervious zones problem: pressure contours using LS formalism

Table 6.4: User-defined inputs for the staggered impervious zones problem

Parameter	Value
β_{B}	0.005
$\bar{\beta}_{\mathrm{F}}$	0.01
$\bar{k}$	1
$\bar{\mu}_0$	1
$\bar{\rho}$	1
ϑ	1
$\bar{\mathbf{b}}$	0
Element type	Q9
$Nele$	1696
$\bar{p}_{\mathrm{enh}}$	500

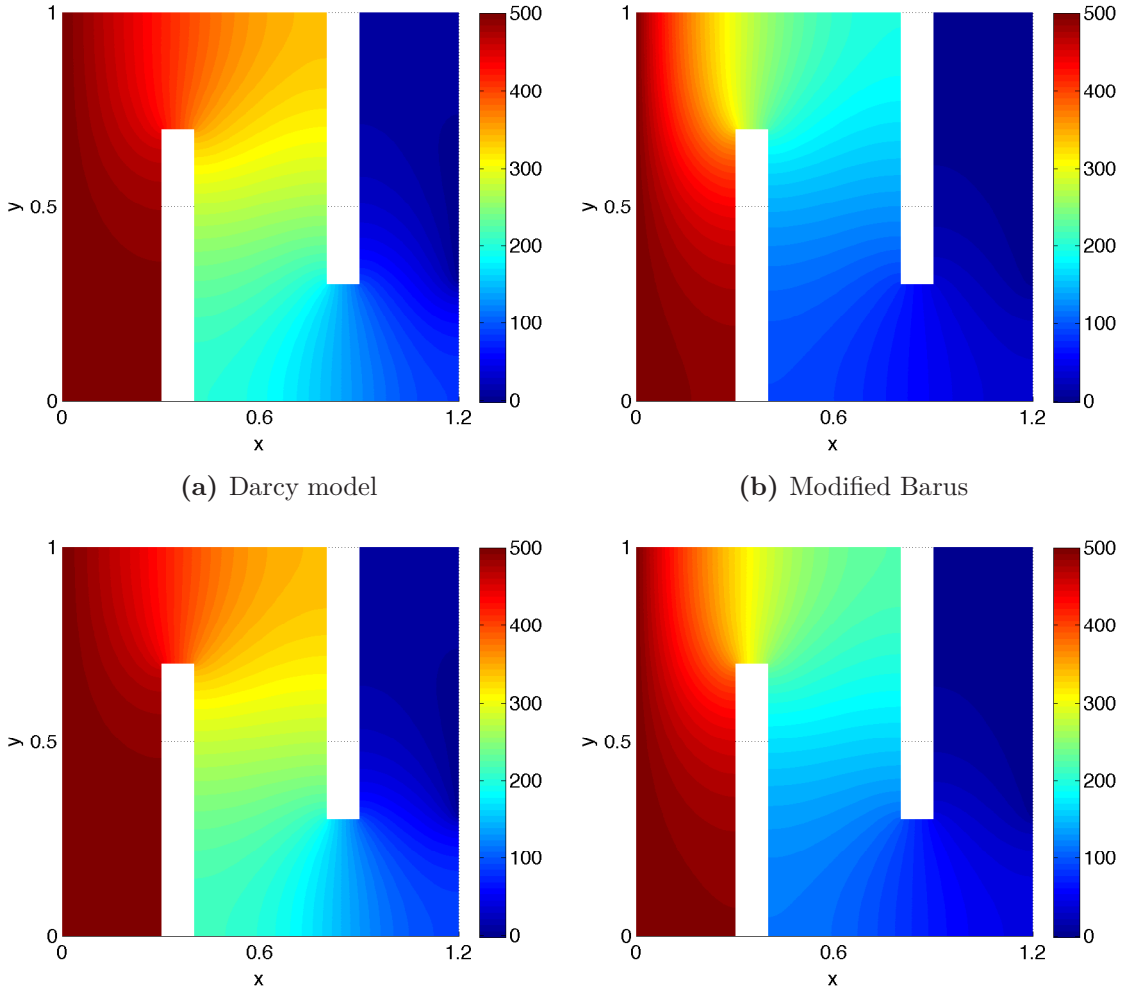

(a) Darcy model

(b) Modified Barus

(c) Darcy-Forchheimer

(d) Modified Darcy-Forchheimer Barus

Figure 6.18: Staggered impervious zones problem: pressure contours using VMS formalism

The pressure contours are depicted in Figures 6.17 and 6.18. While a smaller pressure has been prescribed for this problem (see Table 6.4 for key parameters used in this problem), it can still be seen that the different Darcy models make an impact on the qualitative nature of the pressure contours. It should also be noted that unlike in the layered reservoir problem, the VMS formalism yields higher pressures throughout the domain but predicts smaller fluxes as seen in Table 6.5. Errors in the local mass balance tend to be greatest in regions with high velocities (i.e., the sharp bends around the impervious layers). Figures 6.19 and 6.20 denote the errors using the LS and VMS formalisms.

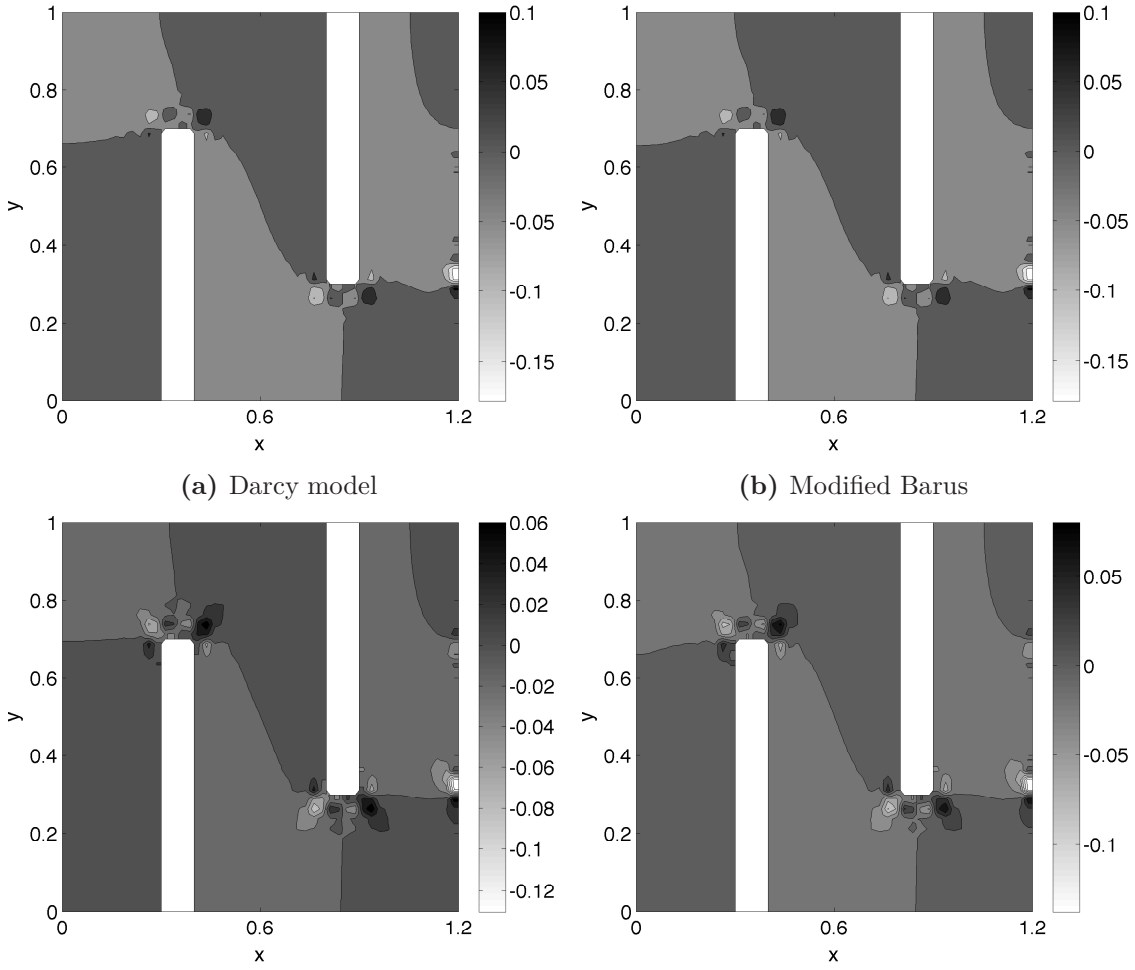

(a) Darcy model

(b) Modified Barus

(c) Darcy-Forchheimer

(d) Modified Darcy-Forchheimer Barus

Figure 6.19: Staggered impervious zones problem: ratios of local mass balance error over total predicted flux using LS formalism

Table 6.5: Staggered impervious zones problem: flow rates for LS and VMS formalism at $\bar{p}_{\text{enh}} = 500$

Darcy models:	D	MB	F	MBF
LS	75.2	27.5	33.7	20.0
VMS	65.8	24.5	31.1	18.7

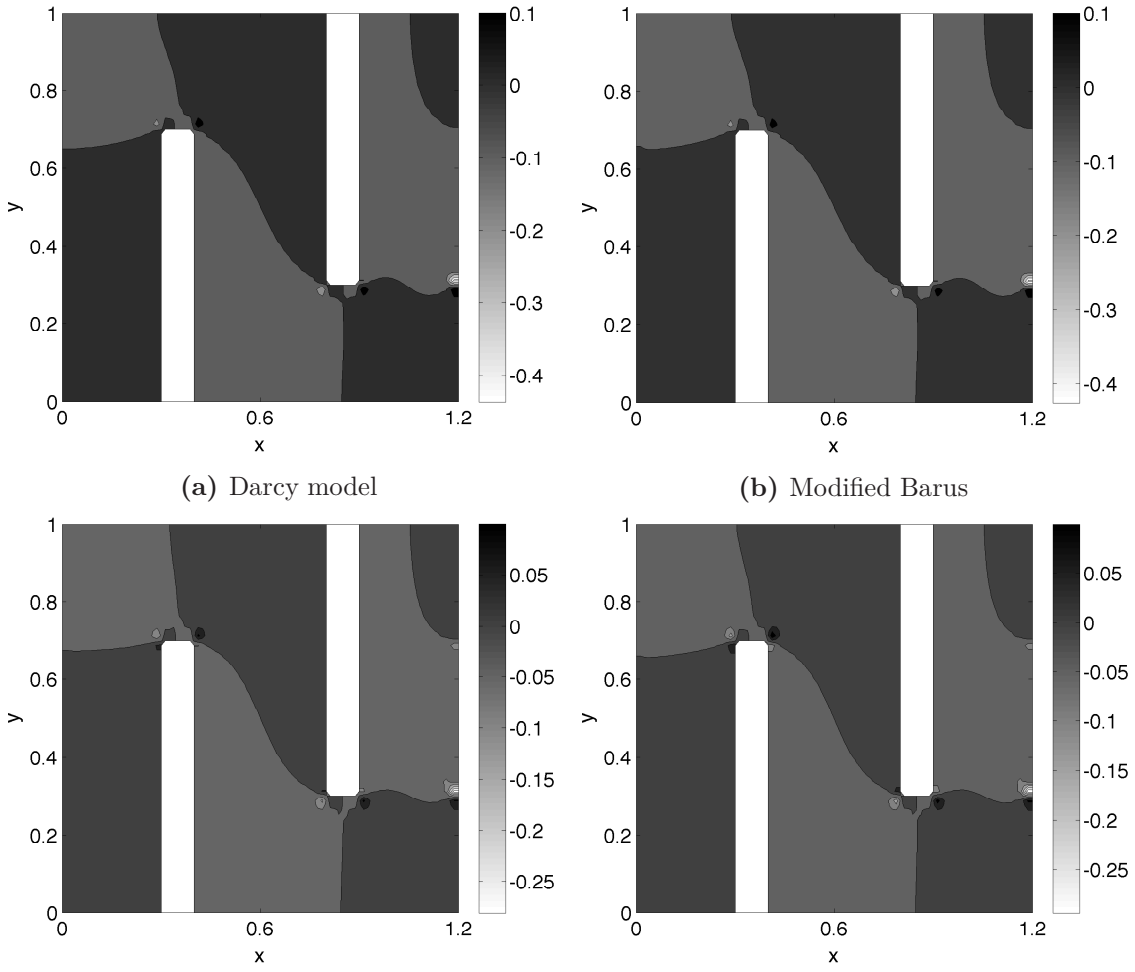

(a) Darcy model

(b) Modified Barus

(c) Darcy-Forchheimer

(d) Modified Darcy-Forchheimer Barus

Figure 6.20: Staggered impervious zones problem: ratios of local mass balance error over total predicted flux using VMS formalism

Chapter 7. Concluding remarks & Future work

The work in this thesis proposes a modification to the standard Darcy model that takes into account both the dependence of the viscosity on the pressure and the inertial effects, which have been observed in many physical experiments. The current models in the literature consider either of the effects but not both. The proposed model will be particularly important for predictive simulations of applications involving high pressures and high velocities (e.g., enhanced oil recovery). This modification has been referred to as the *modified Darcy-Forchheimer model*. It has been shown numerically that the results obtained by taking into account the dependence of drag coefficient on the pressure and on the velocity are both qualitatively and quantitatively different from that the results obtained using the standard Darcy model, Darcy-Forchheimer equation (which neglects the dependence of drag coefficient and viscosity on the pressure) or modified Darcy model [3, 59] (which neglects the dependence of the drag coefficient on the velocity).

This thesis has also developed stable mixed finite element formulations for the resulting governing equations using two different approaches: VMS formalism and LS formalism. Using numerical experiments, we have compared their merits and demerits.

The LS formulation has more terms to evaluate than the VMS formulation, and hence the LS formulation is slightly more computationally expensive than the VMS formulation. However, it should be emphasized that this is not significant in a parallel setting as element-level calculations are embarrassingly parallel. It is also observed that the LS formulation with p-refinement produces accurate results. Another point that is worth mentioning is that the VMS formalism weakly prescribes pressure boundary conditions, and it has been shown that minor oscillations occur when meshes are not adequately refined. The error in element-wise / local mass balance for various Darcy-type models is also quantified, and the error becomes significant when there are large pressures and velocities.

There are several ways one can extend the research work presented in this thesis. *On the modeling front*, a good but difficult research problem is to develop mathematical models that couple deformation and damage of the porous solid with the flow aspects and reactive

transport across several spatial and temporal scales. The following are some possible future works *on the numerical front*:

(a) Develop mixed finite element formulations with better local mass balance property under equal-order interpolation for the pressure and the velocity.

(b) Develop multi-scale models by coupling continuum / macro-scale flow models with meso-scale models (e.g., lattice Boltzmann models). The advantage is that meso-scale models can easily handle complex pore structure, which may not computationally feasible if one uses only a macro-scale model.

(c) Another important but difficult problem is to develop numerical upscaling techniques for heterogeneous porous media. In layman terms, numerical upscaling captures fine-scale features on coarse computational grids.

(d) Develop stable and accurate coupling algorithms for coupling flow, deformation and transport aspects.

On the computer implementation front, a possible work is to implement the mixed formulations taking the advantage of GPU processors, and implementing on heterogeneous parallel computing environment.

Appendix A. Element-level finite element matrices and vectors

For completeness, we provide the partitioned element-level finite element matrices and vectors. These expressions will be handy during a computer implementation of the proposed mixed formulations.

A.1 UNDER LEAST-SQUARES FORMULATION

Picard's linearization

$$\mathbf{K}^e_{vv} = \int_{\Omega^e} [\mathbf{P}]^{\mathrm{T}} \alpha [\mathbf{A}]^{-1} \alpha [\mathbf{P}] + \mathrm{vec}[\mathbf{B}^{\mathrm{T}}] \mathrm{vec}[\mathbf{B}^{\mathrm{T}}]^{\mathrm{T}} \mathrm{d}\Omega, \tag{A.1}$$

$$\mathbf{K}^e_{vp} = \int_{\Omega^e} [\mathbf{P}]^{\mathrm{T}} \alpha [\mathbf{A}]^{-1} [\mathbf{B}]^{\mathrm{T}} \mathrm{d}\Omega, \tag{A.2}$$

$$\mathbf{K}^e_{pv} = \int_{\Omega^e} [\mathbf{B}] \alpha [\mathbf{A}]^{-1} [\mathbf{P}] \mathrm{d}\Omega, \tag{A.3}$$

$$\mathbf{K}^e_{pp} = \int_{\Omega^e} [\mathbf{B}] [\mathbf{A}]^{-1} [\mathbf{B}]^{\mathrm{T}} \mathrm{d}\Omega, \tag{A.4}$$

$$\mathbf{f}^e_{v} = \int_{\Omega^e} [\mathbf{P}]^{\mathrm{T}} \alpha [\mathbf{A}]^{-1} \rho \mathbf{b} \mathrm{d}\Omega, \tag{A.5}$$

$$\mathbf{f}^e_{p} = \int_{\Omega^e} [\mathbf{B}] [\mathbf{A}]^{-1} \rho \mathbf{b} \mathrm{d}\Omega. \tag{A.6}$$

Consistent linearization of modified Darcy

$$\mathbf{K}^e_{vp} = \int_{\Omega^e} [\mathbf{P}]^{\mathrm{T}} \alpha [\mathbf{A}]^{-1} \frac{\partial \alpha}{\partial p} \mathbf{v}^{(i)} \{\mathbf{N}\} \, \mathrm{d}\Omega, \tag{A.7}$$

$$\mathbf{K}^e_{pv} = \int_{\Omega^e} \{\mathbf{N}\}^{\mathrm{T}} \mathbf{v}^{(i)\mathrm{T}} \frac{\partial \alpha}{\partial p} [\mathbf{A}]^{-1} \alpha [\mathbf{P}] \mathrm{d}\Omega, \tag{A.8}$$

$$\begin{aligned} \mathbf{K}^e_{pp} = \int_{\Omega^e} & \{\mathbf{N}\}^{\mathrm{T}} \mathbf{v}^{(i)\mathrm{T}} \frac{\partial \alpha}{\partial p} [\mathbf{A}]^{-1} \frac{\partial \alpha}{\partial p} \mathbf{v}^{(i)} \{\mathbf{N}\} + \{\mathbf{N}\}^{\mathrm{T}} \mathbf{v}^{(i)\mathrm{T}} \frac{\partial \alpha}{\partial p} [\mathbf{A}]^{-1} [\mathbf{B}]^{\mathrm{T}} \\ & + [\mathbf{B}] [\mathbf{A}]^{-1} \frac{\partial \alpha}{\partial p} \mathbf{v}^{(i)} \{\mathbf{N}\} \, \mathrm{d}\Omega, \end{aligned} \tag{A.9}$$

$$\mathbf{f}^e_{v} = \int_{\Omega^e} [\mathbf{P}]^{\mathrm{T}} \alpha [\mathbf{A}]^{-1} \frac{\partial \alpha}{\partial p} \mathbf{v}^{(i)} p^{(i)} \mathrm{d}\Omega, \tag{A.10}$$

$$\begin{aligned} \mathbf{f}^e_{p} = \int_{\Omega^e} & \{\mathbf{N}\}^{\mathrm{T}} \mathbf{v}^{(i)\mathrm{T}} \frac{\partial \alpha}{\partial p} [\mathbf{A}]^{-1} \frac{\partial \alpha}{\partial p} \mathbf{v}^{(i)} p^{(i)} + \{\mathbf{N}\}^{\mathrm{T}} \mathbf{v}^{(i)\mathrm{T}} \frac{\partial \alpha}{\partial p} [\mathbf{A}]^{-1} \rho \mathbf{b} \\ & + [\mathbf{B}]^{\mathrm{T}} [\mathbf{A}]^{-1} \frac{\partial \alpha}{\partial p} \mathbf{v}^{(i)} p^{(i)} \mathrm{d}\Omega. \end{aligned} \tag{A.11}$$

Consistent linearization of Darcy-Forchheimer

$$\mathbf{K}^e_{vv} = \int_{\Omega^e} [\mathbf{P}]^{\mathrm{T}} \alpha [\mathbf{A}]^{-1} \left[\frac{\partial \alpha}{\partial \mathbf{v}} \otimes \mathbf{v}^{(i)} \right] [\mathbf{P}] + [\mathbf{P}]^{\mathrm{T}} \left[\mathbf{v}^{(i)} \otimes \frac{\partial \alpha}{\partial \mathbf{v}} \right] A^{-1} \alpha [\mathbf{P}] + [\mathbf{P}]^{\mathrm{T}} \left[\mathbf{v}^{(i)} \otimes \frac{\partial \alpha}{\partial \mathbf{v}} \right] A^{-1} \left[\frac{\partial \alpha}{\partial \mathbf{v}} \otimes \mathbf{v}^{(i)} \right] [\mathbf{P}] \mathrm{d}\Omega, \tag{A.12}$$

$$\mathbf{K}^e_{vp} = \int_{\Omega^e} [\mathbf{P}]^{\mathrm{T}} \left[\mathbf{v}^{(i)} \otimes \frac{\partial \alpha}{\partial \mathbf{v}} \right] A^{-1} [\mathbf{B}]^{\mathrm{T}} \mathrm{d}\Omega, \tag{A.13}$$

$$\mathbf{K}^e_{pv} = \int_{\Omega^e} [\mathbf{B}] [\mathbf{A}]^{-1} \left[\frac{\partial \alpha}{\partial \mathbf{v}} \otimes \mathbf{v}^{(i)} \right] [\mathbf{P}] \mathrm{d}\Omega, \tag{A.14}$$

$$\mathbf{f}^e_v = \int_{\Omega^e} [\mathbf{P}]^{\mathrm{T}} \alpha [\mathbf{A}]^{-1} \left[\frac{\partial \alpha}{\partial \mathbf{v}} \otimes \mathbf{v}^{(i)} \right] \mathbf{v}^{(i)} + [\mathbf{P}]^{\mathrm{T}} \left[\mathbf{v}^{(i)} \otimes \frac{\partial \alpha}{\partial \mathbf{v}} \right] [\mathbf{A}]^{-1} \left[\frac{\partial \alpha}{\partial \mathbf{v}} \otimes \mathbf{v}^{(i)} \right] \mathbf{v}^{(i)} + [\mathbf{P}]^{\mathrm{T}} \left[\mathbf{v}^{(i)} \otimes \frac{\partial \alpha}{\partial \mathbf{v}} \right] [\mathbf{A}]^{-1} \rho \mathbf{b} \mathrm{d}\Omega, \tag{A.15}$$

$$\mathbf{f}^e_p = \int_{\Omega^e} [\mathbf{B}] [\mathbf{A}]^{-1} \left[\frac{\partial \alpha}{\partial \mathbf{v}} \otimes \mathbf{v}^{(i)} \right] \mathbf{v}^{(i)} \mathrm{d}\Omega. \tag{A.16}$$

Consistent linearization for modified Darcy-Forchheimer:

$$\mathbf{K}^e_{vp} = \int_{\Omega^e} [\mathbf{P}]^{\mathrm{T}} \left[\mathbf{v}^{(i)} \otimes \frac{\partial \alpha}{\partial \mathbf{v}} \right] [\mathbf{A}]^{-1} \frac{\partial \alpha}{\partial p} \mathbf{v}^{(i)} \{\mathbf{N}\} \, \mathrm{d}\Omega, \tag{A.17}$$

$$\mathbf{K}^e_{pv} = \int_{\Omega^e} \{\mathbf{N}\}^{\mathrm{T}} \mathbf{v}^{(i)\mathrm{T}} \frac{\partial \alpha}{\partial p} [\mathbf{A}]^{-1} \left[\frac{\partial \alpha}{\partial \mathbf{v}} \otimes \mathbf{v}^{(i)} \right] [\mathbf{P}] \mathrm{d}\Omega, \tag{A.18}$$

$$\mathbf{f}^e_v = \int_{\Omega^e} [\mathbf{P}]^{\mathrm{T}} \left[\mathbf{v}^{(i)} \otimes \frac{\partial \alpha}{\partial \mathbf{v}} \right] [\mathbf{A}]^{-1} \frac{\partial \alpha}{\partial p} \mathbf{v}^{(i)} p^{(i)} \mathrm{d}\Omega, \tag{A.19}$$

$$\mathbf{f}^e_p = \int_{\Omega^e} \{\mathbf{N}\}^{\mathrm{T}} \mathbf{v}^{(i)\mathrm{T}} \frac{\partial \alpha}{\partial p} [\mathbf{A}]^{-1} \left[\frac{\partial \alpha}{\partial \mathbf{v}} \otimes \mathbf{v}^{(i)} \right] \mathbf{v}^{(i)} \mathrm{d}\Omega. \tag{A.20}$$

A.2 UNDER VARIATIONAL MULTI-SCALE FORMULATION

Picard's linearization

$$\mathbf{K}_{vv}^{e} = \int_{\Omega^e} [\mathbf{P}]^{\mathrm{T}} \alpha [\mathbf{P}] - \frac{1}{2} [\mathbf{P}]^{\mathrm{T}} \alpha [\mathbf{P}] \mathrm{d}\Omega, \tag{A.21}$$

$$\mathbf{K}_{vp}^{e} = \int_{\Omega^e} -\mathrm{vec}[[\mathbf{B}]^{\mathrm{T}}] \{\mathbf{N}\} - \frac{1}{2} [\mathbf{P}]^{\mathrm{T}} [\mathbf{B}]^{\mathrm{T}} \mathrm{d}\Omega, \tag{A.22}$$

$$\mathbf{K}_{pv}^{e} = \int_{\Omega^e} -\{\mathbf{N}\}^{\mathrm{T}} \mathrm{vec}[[\mathbf{B}]^{\mathrm{T}}]^{\mathrm{T}} - \frac{1}{2} [\mathbf{B}][\mathbf{P}] \mathrm{d}\Omega, \tag{A.23}$$

$$\mathbf{K}_{pp}^{e} = \int_{\Omega^e} -\frac{1}{2} [\mathbf{B}] \alpha^{-1} [\mathbf{B}]^{\mathrm{T}} \mathrm{d}\Omega, \tag{A.24}$$

$$\mathbf{f}_{v}^{e} = \int_{\Omega^e} \frac{1}{2} [\mathbf{P}]^{\mathrm{T}} \rho \mathbf{b} \mathrm{d}\Omega, \tag{A.25}$$

$$\mathbf{f}_{p}^{e} = \int_{\Omega^e} -\frac{1}{2} [\mathbf{B}] \alpha^{-1} \rho \mathbf{b} \mathrm{d}\Omega. \tag{A.26}$$

Consistent linearization of modified Darcy

$$\mathbf{K}_{vp}^{e} = \int_{\Omega^e} [\mathbf{P}]^{\mathrm{T}} \frac{\partial \alpha}{\partial p} \mathbf{v}^{(i)} \{\mathbf{N}\} - \frac{1}{2} [\mathbf{P}]^{\mathrm{T}} \frac{\partial \alpha}{\partial p} \mathbf{v}^{(i)} \{\mathbf{N}\} \mathrm{d}\Omega, \tag{A.27}$$

$$\mathbf{K}_{pp}^{e} = \int_{\Omega^e} -\frac{1}{2} [\mathbf{B}] \alpha^{-1} \frac{\partial \alpha}{\partial p} \mathbf{v}^{(i)} \{\mathbf{N}\} \mathrm{d}\Omega, \tag{A.28}$$

$$\mathbf{f}_{v}^{e} = \int_{\Omega^e} [\mathbf{P}]^{\mathrm{T}} \frac{\partial \alpha}{\partial p} \mathbf{v}^{(i)} p^{(i)} - \frac{1}{2} [\mathbf{P}]^{\mathrm{T}} \frac{\partial \alpha}{\partial p} \mathbf{v}^{(i)} p^{(i)} \mathrm{d}\Omega, \tag{A.29}$$

$$\mathbf{f}_{p}^{e} = \int_{\Omega^e} -\frac{1}{2} [\mathbf{B}] \alpha^{-1} \frac{\partial \alpha}{\partial p} \mathbf{v}^{(i)} p^{(i)} \mathrm{d}\Omega. \tag{A.30}$$

Consistent linearization of Darcy-Forchheimer

$$\mathbf{K}_{vv}^{e} = \int_{\Omega^e} [\mathbf{P}]^{\mathrm{T}} \left[\frac{\partial \alpha}{\partial \mathbf{v}} \otimes \mathbf{v}^{(i)} \right] [\mathbf{P}] - \frac{1}{2} [\mathbf{P}]^{\mathrm{T}} \left[\frac{\partial \alpha}{\partial \mathbf{v}} \otimes \mathbf{v}^{(i)} \right] [\mathbf{P}] \mathrm{d}\Omega, \tag{A.31}$$

$$\mathbf{K}_{pv}^{e} = \int_{\Omega^e} -\frac{1}{2} [\mathbf{B}] \alpha^{-1} \left[\frac{\partial \alpha}{\partial \mathbf{v}} \otimes \mathbf{v}^{(i)} \right] [\mathbf{P}] \mathrm{d}\Omega, \tag{A.32}$$

$$\mathbf{f}_{v}^{e} = \int_{\Omega^e} [\mathbf{P}]^{\mathrm{T}} \left[\frac{\partial \alpha}{\partial \mathbf{v}} \otimes \mathbf{v}^{(i)} \right] \mathbf{v}^{(i)} - \frac{1}{2} [\mathbf{P}]^{\mathrm{T}} \left[\frac{\partial \alpha}{\partial \mathbf{v}} \otimes \mathbf{v}^{(i)} \right] \mathbf{v}^{(i)} \mathrm{d}\Omega, \tag{A.33}$$

$$\mathbf{f}_{p}^{e} = \int_{\Omega^e} -\frac{1}{2} [\mathbf{B}] \alpha^{-1} \left[\frac{\partial \alpha}{\partial \mathbf{v}} \otimes \mathbf{v}^{(i)} \right] \mathbf{v}^{(i)} \mathrm{d}\Omega. \tag{A.34}$$

References

[1] H. Darcy. Les Fontaines Publiques de la Ville de Dijon. *Victor Dalmont, Paris*, 1856.

[2] S. P. Neuman. Theoretical derivation of Darcy's law. *Acta Mechanica*, 25:153–170, 1977.

[3] K. B. Nakshatrala and K. R. Rajagopal. A numerical study of fluids with pressure dependent viscosity flowing through a rigid porous medium. *International Journal for Numerical Methods in Fluids*, 67:342–368, 2011.

[4] F. Brezzi and M. Fortin. *Mixed and Hybrid Finite Element Methods, volume 15 of Springer Series in Computational Mathematics*. Springer-Verlag, New York, USA, 1991.

[5] K. A. Mardal, X. C. Tai, and R. Winther. A robust finite element method for Darcy-Stokes flow. *SIAM Journal of Numerical Analysis*, 40:1605–1631, 2002.

[6] A. Masud. A stabilized mixed finite element method for Darcy-Stokes flow. *International Journal for Numerical Methods in Fluids*, 54:665–681, 2007.

[7] O. Iliev, R. Lazarov, and J. Willems. Variational multiscale finite element method for flows in highly porous media. *Multiscale Modeling and Simulation*, 9:1350–1372, 2011.

[8] M. R. Correa and A. F. D. Loula. Stabilized velocity post-processings for Darcy flow in heterogeneous porous media. *Communications in Numerical Methods in Engineering*, 23:461–489, 2007.

[9] J. M. Urquiza, D. N. Dri, A. Garon, and M. C. Delfour. A numerical study of primal mixed finite element approximations of Darcy equations. *Communications in Numerical Methods in Engineering*, 22:901–915, 2006.

[10] A. Masud and T. J. R. Hughes. A stabilized mixed finite element method for Darcy flow. *Computer Methods in Applied Mechanics and Engineering*, 191:4341–4370, 2002.

[11] K. B. Nakshatrala, D. Z. Turner, K. D. Hjelmstad, and A. Masud. A stabilized mixed finite element formulation for Darcy flow based on a multiscale decomposition of the solution. *Computer Methods in Applied Mechanics and Engineering*, 195:4036–4049, 2006.

[12] P. B. Bochev and M. D. Gunzburger. Finite element methods of least-squares type. *Society for Industrial and Applied Mathematics*, 40:789–837, 1998.

[13] J. N. Reddy. *An Introduction to Nonlinear Finite Element Analysis*. Oxford University Press, New York, USA, 2004.

[14] B. Jiang. *The Least-Squares Finite Element Method: Theory and Applications in Computational Fluid Dynamics and Electromagnetics*. Springer-Verlag, New York, USA, 1998.

[15] P. B. Bochev and M. D. Gunzburger. A locally conservative least-squares method for Darcy flows. *Communications in Numerical Methods in Engineering*, 24:97–110, 2008.

[16] G. R. Barrenechea, L. P. Franca, and F. Valentin. A Petrov-Galerkin enriched method: A mass conservative finite element method for the Darcy equation. *Computer Methods in Applied Mechanics and Engineering*, 197:2449–2464, 2007.

[17] S. Sun and J. Liu. A locally conservative finite element method based on piecewise constant enrichment of the continuous Galerkin method. *SIAM Journal of Scientific Computing*, 31:2528–2548, 2009.

[18] J. Liu and X. Ye. A comparative study of locally conservative numerical methods for Darcy's flows. *Procedia Computer Science*, 4:974–983, 2011.

[19] D. Z. Turner, K. B. Nakshatrala, M. J. Martinez, and P. K. Notz. Modeling subsurface water resource systems involving heterogeneous porous media using the variational multiscale formulation. *Journal of Hydrology*, 428-429:1–14, 2011.

[20] C. Truesdell. *Rational Thermodynamics*. Springer, New York, USA, 1984.

[21] R. J. Atkin and R. E. Craine. Continuum theories of mixtures: Basic theory and historical development. *The Quaterly Journal of Mechanics and Applied Mathematics*, 29:209–244, 1976.

[22] R. M. Bowen. Theory of mixtures. In A. C. Eringen, editor, *Continuum Physics*, volume III. Academic Press, New York, 1976.

[23] R. McOwen. *Partial Differential Equations: Methods and Applications*. Prentice Hall, New Jersey, USA, 1996.

[24] P. W. Bridgman. *The Physics of High Pressure*. MacMillan Company, New York, USA, 1931.

[25] E. C. Andrade. Viscosity of liquids. *Nature*, 125:109–141, 1930.

[26] C. Barus. Isotherms, isopiestics and isometrics relative to viscosity. *American Journal of Science*, 45:87–96, 1893.

[27] H. J. van Leewen. The determination of the pressure viscosity coefficient of a lubricant through an accurate film thickness formula and accurate film thickness measurements. *Journal of Engineering Tribology*, 223:1143–1163, 2009.

[28] M. Franta, J. Malek, and K. R. Rajagopal. On steady flows of fluids with pressure- and shear-dependent viscosities. *Proceedings: Mathematical, Physical and Engineering Sciences*, 461:651–670, 2005.

[29] A. Him, M. Lanzendoerfer, and J. Stebel. Finite element approximation of flow of fluids with shear-rate- and pressure-dependent viscosity. *IMA Journal of Numerical Analysis*, 32:1604–1634, 2012.

[30] H. C. Brinkman. A calculation of the viscous force exerted by a flowing fluid on a dense swarm of particles. *Applied Scientific Research*, A1:27–34, 1947.

[31] S. Srinivasan and K. B. Nakshatrala. A stabilized mixed formulation for unsteady Brinkman equation based on the method of horizontal lines. *International Journal for Numerical Methods in Fluids*, 68:642–670, 2011.

[32] A. Z. Szeri. *Fluid Film Lubrication: Theory and Design*. Cambridge University Press, Cambridge, UK, 2005.

[33] E. Höglund. Influence of lubricant properties on elastohydrodynamic lubrication. *Wear*, 232:176–184, 1999.

[34] P. Forchheimer. Wasserbewegung durch Boden. *Zeitschrift des Vereines Deutscher Ingeneieure*, 45:1782–1788, 1901.

[35] S. Whitaker. The Forchheimer equation: A theoretical development. *Transport in Porous Media*, 25:27–61, 1996.

[36] W. Sobieski and A. Trykozko. Sensitivity aspects of Forchheimer's approximation. *Transport in Porous Media*, 89:155–164, 2011.

[37] E. J. Park. Mixed finite element methods for generalized Forchheimer flow in porous media. *Numerical Methods for Partial Differential Equations*, 21:213–228, 2005.

[38] H. Pan and H. Rui. Mixed element method for two-dimensional Darcy-Forchheimer model. *Journal of Scientific Computing*, 52:563–587, 2012.

[39] B. Martin, K. J. Michael, and S. Harvey. Simulation and theory of two-phase flow in porous media. *Physics Review A*, 46:7680–7699, 1992.

[40] D. E. Carlson, E. Fried, and D. A. Tortorelli. Geometrically-based consequences of internal constraints. *Journal of Elasticity*, 70:101–109, 2003.

[41] O. M. O'Reilly and A. R. Srinivasa. On a decomposition of generalized constraint forces. *Proceedings of the Royal Society of London, Series A*, 457:1307–1313, 2001.

[42] G. K. Batchelor. *An Introduction to Fluid Dynamics*. Cambridge University Press, New York, USA, 2000.

[43] L. C. Evans. *Partial Differential Equations*. American Mathematical Society, Providence, Rhode Island, USA, 1998.

[44] B. D. Reddy. *Introductory Functional Analysis: With Applications to Boundary Value Problems and Finite Elements*. Springer-Verlag, New York, USA, 1998.

[45] J. T. Oden and L. F. Demkowicz. *Applied Functional Analysis*. CRC Press, Boca Raton, Florida, USA, second edition, 2010.

[46] P. Chadwick. *Continuum Mechanics: Concise Theory and Problems*. Dover Publications, Inc., Minealo, New York, 1999.

[47] M. Spivak. *Calculus on Manifolds: A Modern Approach to Classical Theorems of Advanced Calculus*. Westview Press, Massachusetts, USA, 1997.

[48] G. A. Holzapfel. *Nonlinear Solid Mechanics: A Continuum Approach for Engineering*. John Wiley, New York, USA, 2000.

[49] R. Glowinski. *Numerical Methods for Nonlinear Variational Problems*. Springer-Verlag, Leipzig, Germany, 2008.

[50] G. S. Payette and J. N. Reddy. On the roles of minimization and linearization in least-squares finite element models of nonlinear boundary-value problems. *Journal of Computational Physics*, 230:3589–3613, 2011.

[51] J. M. Deang and M. D. Gunzburger. Issues related to least-squares finite element methods for the Stokes equations. *SIAM Journal on Scientific Computing*, 20:878–906, 1999.

[52] M. E. Gurtin. *An Introduction to Continuum Mechanics*. Academic Press, San Diego, USA, 1981.

[53] A. Graham. *Kronecker Products and Matrix Calculus: With Applications*. Halsted Press, Chichester, UK, 1981.

[54] A. L. Laub. *Matrix Analysis for Scientists and Engineers*. Society for Industrial and Applied Mathematics, Philadelphia, Pennsylvania, USA, 2004.

[55] D. W. Nicholson. *Finite Element Analysis: Thermomechanics of Solids*. CRC Press, Boca Raton, Florida, USA, 2003.

[56] O. C. Zienkiewicz, R. L. Taylor, and J. Z. Zhu. *The Finite Element Methods: Its Basis and Fundamentals*. Elsevier Ltd., Burlington, Massachusetts, 2006.

[57] S. C. Chapra. *Numerical Methods for Engineers*. McGraw-Hill, New York, USA, sixth edition, 2006.

[58] G. Stachowiak and A. W. Batchelor. *Engineering Tribology*. Elsevier Science, Burlington, MA, third edition, 2011.

[59] K. B. Nakshatrala and D. Z. Turner. A mixed formulation for a modification to Darcy equation based on Picard linearization and numerical solutions to large-scale realistic problems. *Available on arXiv: http://arxiv.org/abs/1105.0706*, 2013.